



**HAL**  
open science

## Design and Simulation of Next-Generation High-Power, High-Brightness Laser Diodes

Jun Lim, Slawomir Sujecki, Lei Lang, Zhichao Zhang, David Pabœuf, Gilles Pauliat, Gaëlle Lucas-Leclin, Patrick Georges, Roderick Mackenzie, Stephen Bull, et al.

► **To cite this version:**

Jun Lim, Slawomir Sujecki, Lei Lang, Zhichao Zhang, David Pabœuf, et al.. Design and Simulation of Next-Generation High-Power, High-Brightness Laser Diodes. IEEE Journal of Selected Topics in Quantum Electronics, 2009, 15 (3), pp.993-1008. hal-00528924

**HAL Id: hal-00528924**

**<https://iogs.hal.science/hal-00528924v1>**

Submitted on 22 Oct 2010

**HAL** is a multi-disciplinary open access archive for the deposit and dissemination of scientific research documents, whether they are published or not. The documents may come from teaching and research institutions in France or abroad, or from public or private research centers.

L'archive ouverte pluridisciplinaire **HAL**, est destinée au dépôt et à la diffusion de documents scientifiques de niveau recherche, publiés ou non, émanant des établissements d'enseignement et de recherche français ou étrangers, des laboratoires publics ou privés.

# Design and Simulation of Next-Generation High-Power, High-Brightness Laser Diodes

Jun Jun Lim, *Member, IEEE*, Slawomir Sujecki, Lei Lang, *Student Member, IEEE*, Zhichao Zhang, *Member, IEEE*, David Paboeuf, Gilles Pauliat, Gaëlle Lucas-Leclin, Patrick Georges, Roderick C. I. MacKenzie, Philip Bream, Stephen Bull, *Member, IEEE*, Karl-Heinz Hasler, Bernd Sumpf, Hans Wenzel, Götz Erbert, *Member, IEEE*, Birgitte Thestrup, Paul Michael Petersen, Nicolas Michel, Michel Krakowski, and Eric C. Larkins

(Invited Paper)

**Abstract**—High-brightness laser diode technology is progressing rapidly in response to competitive and evolving markets. The large volume resonators required for high-power, high-brightness operation makes their beam parameters and brightness sensitive to thermal- and carrier-induced lensing and also to multimode operation. Power and beam quality are no longer the only concerns for the design of high-brightness lasers. The increased demand for these technologies is accompanied by new performance requirements, including a wider range of wavelengths, direct electrical modulation, spectral purity and stability, and phase-locking techniques for coherent beam combining. This paper explores some of the next-generation technologies being pursued, while illustrating the growing importance of simulation and design tools. The paper begins by investigating the brightness limitations of broad-area laser diodes, including the use of asymmetric feedback to improve the modal discrimination. Next, tapered lasers are considered, with an emphasis on emerging device technologies for applications requiring electrical modulation and high spectral brightness. These include two-contact lasers, self-organizing cavity lasers, and a phase-locked laser array using an external Talbot cavity.

Manuscript received November 8, 2008; revised December 2, 2008; accepted December 9, 2008. First published; current version published. This work was supported in part by the European Commission under Project IST-035266, Project IST-511722 ([www.brighter.eu](http://www.brighter.eu)), Project ULTRABRIGHT (IST-1999-10356), and Project POWERPACK (IST-2000-29447). The work of R. MacKenzie and P. J. Bream was supported by the Engineering and Physical Sciences Research Council, U.K. The work of D. Paboeuf was supported by the French Ministry of Defense (Délégation Générale de l'Armement).

J. J. Lim, S. Sujecki, L. Lang, Z. Zhang, R. MacKenzie, P. Bream, S. Bull and E. C. Larkins are with the Department of Electrical and Electronic Engineering, University of Nottingham, Nottingham NG7 2RD, U.K. (e-mail: [jun.lim@nottingham.ac.uk](mailto:jun.lim@nottingham.ac.uk); [slawomir.sujecki@nottingham.ac.uk](mailto:slawomir.sujecki@nottingham.ac.uk); [eexl12@nottingham.ac.uk](mailto:eexl12@nottingham.ac.uk); [eezz2@nottingham.ac.uk](mailto:eezz2@nottingham.ac.uk); [r.c.i.mackenzie@googlemail.com](mailto:r.c.i.mackenzie@googlemail.com); [phil.bream@gmail.com](mailto:phil.bream@gmail.com); [steve.bull@nottingham.ac.uk](mailto:steve.bull@nottingham.ac.uk); [eric.larkins@nottingham.ac.uk](mailto:eric.larkins@nottingham.ac.uk)).

D. Paboeuf, G. Pauliat, G. Lucas-Leclin, and P. Georges are with the Laboratoire Charles Fabry de l'Institut d'Optique, Centre National de la Recherche Scientifique (CNRS), University Paris Sud, 91127 Palaiseau, France (e-mail: [david.paboeuf@institutoptique.fr](mailto:david.paboeuf@institutoptique.fr); [gilles.pauliat@iota.u-psud.fr](mailto:gilles.pauliat@iota.u-psud.fr); [gaelle.lucas-leclin@institutoptique.fr](mailto:gaelle.lucas-leclin@institutoptique.fr); [patrick.georges@iota.u-psud.fr](mailto:patrick.georges@iota.u-psud.fr)).

K.-H. Hasler, B. Sumpf, H. Wenzel, and G. Erbert are with the Ferdinand-Braun-Institut für Höchstfrequenztechnik, 12489 Berlin, Germany (e-mail: [karl-heinz.hasler@fbh-berlin.de](mailto:karl-heinz.hasler@fbh-berlin.de); [bernd.sumpf@fbh-berlin.de](mailto:bernd.sumpf@fbh-berlin.de); [hans.wenzel@fbh-berlin.de](mailto:hans.wenzel@fbh-berlin.de); [goetz.erbert@fbh-berlin.de](mailto:goetz.erbert@fbh-berlin.de)).

B. Thestrup and P. M. Petersen are with the DTU Fotonik, Technical University of Denmark, 4000 Roskilde, Denmark (e-mail: [birgitte.thestrup@risoe.dk](mailto:birgitte.thestrup@risoe.dk); [paul.michael.petersen@risoe.dk](mailto:paul.michael.petersen@risoe.dk)).

N. Michel and M. Krakowski are with Alcatel-Thales III-V Lab, 91767 Palaiseau, France (e-mail: [nicolas.michel@3-5lab.fr](mailto:nicolas.michel@3-5lab.fr); [michel.krakowski@3-5lab.fr](mailto:michel.krakowski@3-5lab.fr)).

Color versions of one or more of the figures in this paper are available online at <http://ieeexplore.ieee.org>.

Digital Object Identifier 10.1109/JSTQE.2008.2011286

**Index Terms**—External cavity laser diodes, high-brightness lasers, high-power lasers, laser simulation, modal discrimination, phase-coupled laser diode arrays, self-organizing laser.

## I. INTRODUCTION

THERE is a growing demand for high-power diode lasers in a variety of fields today. Traditionally, the largest application for high-power diode lasers has been as pump sources for solid-state lasers, fiber amplifiers in telecommunications, and more recently, fiber lasers [1]. Diode lasers are used because they have a high electrical to optical conversion efficiency and can be designed to fit the absorption band of these applications. They have advantages in terms of reliability, compactness, and cost. In recent years, high-brightness laser technology has been strongly driven by an increasing number and variety of applications, including medicine (e.g., photodynamic therapy, fluorescence spectroscopy, and surgery), display technology (laser displays and mobile projectors), free-space optical wireless communication, and direct-diode materials processing.

As the range of applications increases, the performance demands on high-brightness laser diodes are also becoming more stringent. Performance requirements for next-generation high-brightness laser diodes include good modulation performance, narrow spectral linewidth, and nearly diffraction-limited powers of 20–100 W. At the same time, laser simulation tools are becoming essential for achieving the desired performance. These tools provide an understanding of the physics and operation of the device and permit the exploration of novel designs and concepts needed to provide more than an incremental improvement in the device performance.

In this paper, we provide an overview of recent trends in the design and simulation of next-generation high-power, high-brightness laser diodes. Section II begins with a cursory discussion of the applications, performance requirements, and current state of the art of high-brightness diode lasers and systems, followed by an overview of approaches for achieving high power and brightness, and a discussion of the increased role and demands on simulation and design tools. Section III briefly describes the high-brightness laser diode simulation tools used in this paper and how the simulation parameters are calibrated and validated. Section IV considers a few specific examples to provide insight into the approaches and design considerations

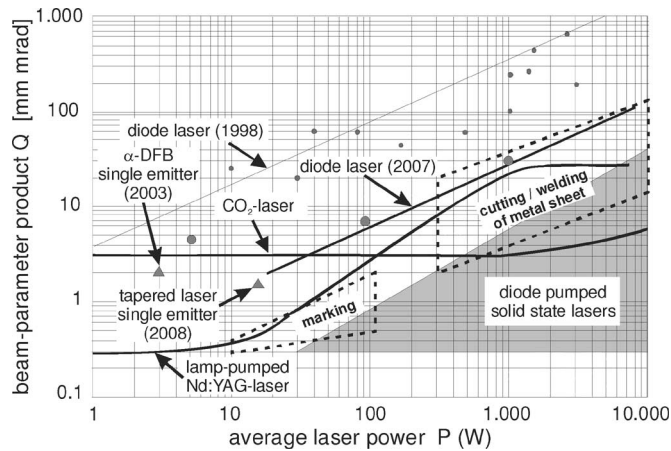


Fig. 1. Typical beam parameters for different laser systems and for applications in materials processing. (Courtesy P. Loosen, Fraunhofer Institute for Laser Technology.)

68 currently being pursued. These examples include an asymmetric  
69 feedback external cavity laser, a multiple section tapered laser,  
70 a self-organizing cavity laser, and a laser array in an external  
71 Talbot cavity.

## 72 II. BACKGROUND

### 73 A. Applications and Performance Requirements

74 The most important performance target for high-power laser  
75 diodes continues to be the combination of power and beam  
76 quality, known as brightness. The brightness of a laser beam  
77 is defined as the optical power density  $P$  per emission area  $A$  and  
78 per unit of solid angle  $\Omega$  in the output beam. The brightness  $B$   
79 describes how well the optical power can be collimated into a  
80 narrow beam, and can be described as

$$B = \frac{P}{A\Omega} \propto \frac{P}{Q^2} = \frac{P}{(\omega_0\theta_f)^2} \propto \frac{P}{(M^2)^2}. \quad (1)$$

81 The brightness is also related to  $M^2$  and the *beam parameter*  
82 *product*  $Q$  (product of the minimum beam diameter  $\omega_0$  and its  
83 divergence  $\theta_f$ ). The current state of the art for power and bright-  
84 ness of diode lasers and systems is shown in Fig. 1. The compar-  
85 ison with other high-power lasers (e.g. CO<sub>2</sub> and diode/lamp  
86 pumped solid-state lasers) in Fig. 1 shows that diode lasers are  
87 approaching the level of power and brightness achievable by the  
88 other laser systems.

89 As the variety of applications for high-brightness laser diodes  
90 increases, so does the range of performance specifications,  
91 which generally depend upon the intended application. For  
92 example, most high-brightness diode lasers operate at 808 or  
93 980 nm, but other wavelengths are emerging for applica-  
94 tions such as medicine, displays, printing, and mark-  
95 ing/cutting/welding of plastics. Display and optical wireless  
96 applications also require that the laser has a controlled emission  
97 spectrum and beam quality during high-frequency modulation  
98 (0.1–1 GHz) and a large modulation efficiency (power/current  
99 ratio). Applications requiring frequency doubling (e.g., blue and  
100 green lasers for displays, blue/near-UV lasers for fluorescence

spectroscopy) are driving the pursuit of ultimate brightness com- 101  
bined with spectral purity/stability. The efficiency of frequency 102  
doubling depends on the square of the optical electric field and 103  
requires a nearly diffraction-limited beam to achieve a high 104  
optical field intensity and good beam coherence. As indicated 105  
in Fig. 1, applications involving the direct processing of materi- 106  
als are driving the development of laser systems with high 107  
output power and brightness. These include marking ( $P = 10$ – 108  
100 W,  $Q = 0.3$ –2 mm·mrad), cutting, and welding of sheet 109  
metal ( $P = 0.3$ –10 kW,  $Q = 2$ –100 mm·mrad). Currently, the 110  
best power and brightness results for single emitters are from 111  
tapered lasers ( $P = 12$  W,  $Q = 1.5$  mm·mrad [2]). Generally, 112  
power levels greater than 10–20 W must be achieved by combin- 113  
ing the beams from multiple emitters. For the most demanding 114  
high-power applications, the beams must be combined coher- 115  
ently through stable phase-locking of an array of emitters to 116  
achieve power densities  $>10^5$  W/mm<sup>2</sup>. 117

### 118 B. Approaches for High Power and Brightness

119 The simplest laser diode to fabricate is the broad-area laser 120  
diode (BA-LD), which is still widely used to provide high 121  
power with high efficiency. However, they are known to have 122  
a large slow-axis far-field divergence and poor beam quality— 123  
primarily due to beam filamentation. This process has been 124  
studied intensively both experimentally and theoretically, e.g., 125  
in [3] and references therein. Spatial filamentation leads to a 126  
complicated multilobed near-field pattern, which negatively af- 127  
fects the brightness. Furthermore, filamentation is sometimes 128  
accompanied by unwanted periodic or chaotic variations in the 129  
laser power. Hence, BA-LDs are fundamentally unsuitable for 130  
high-brightness applications without some form of filtering to 131  
provide a mechanism for modal discrimination.

132 To overcome the deficiencies of the BA-LD, numerous des- 133  
igns have been proposed to increase the brightness of high- 134  
power laser diodes. One technique adopted from traditional non- 135  
diode lasers is the unstable resonator concept, such as lasers with 136  
a curved mirror resonator [4], [5]. Lasers with multiple sections 137  
have also been explored to increase the brightness, including 138  
master oscillator power amplifier (MOPA) lasers [6], tapered 139  
lasers [7], and bow-tie lasers [8]. The  $\alpha$ -DFB laser showed early 140  
promise [9], but has only achieved an output power of 3 W with 141  
 $M^2 = 3.2$  ( $Q = 2$  mm·mrad) from a single emitter [10], [11]. 142  
The far-field divergence of a BA-LD can also be reduced using 143  
asymmetric feedback from an external cavity to a specific lateral 144  
mode [12], [13].

145 The easiest way to scale the power from laser diodes is to 146  
employ an array of emitters. To achieve high brightness, how- 147  
ever, phase locking is needed to coherently combine their out- 148  
put beams. Common approaches include positive guiding [14] 149  
(evanescent-wave coupling) and antiguiding (leaky-wave cou- 150  
pling) arrays [15], with the latter showing stronger in-phase 151  
coupling. Phase locking can also be achieved through diffrac- 152  
tive coupling using the Talbot effect. This can be done mono- 153  
lithically [16] or using an external cavity [17]. Another phase 154  
locking method using diffractive coupling employs a multimode 155  
interference (MMI) coupling section [18].

### 156 C. Role of Simulation and Design Tools

157 Numerous laser models have been reported in the literature.  
 158 These models vary in complexity and have typically been de-  
 159 veloped to target specific applications. Early models ignored  
 160 current spreading in the cladding layers of the device and typi-  
 161 cally solved the 1-D unipolar diffusion equation in the lateral  
 162 direction. These tools were used to explain spatial hole burn-  
 163 ing and carrier lensing effects and were also applied to explain  
 164 the filamentary nature of broad-area lasers [19]. Later, full 2-D  
 165 cross-sectional models were introduced, which were borrowed  
 166 from modeling techniques developed for silicon device simula-  
 167 tors [20]–[22]. These 2-D cross-sectional laser models solved  
 168 the electrical, thermal, and optical problems self-consistently,  
 169 making them more accurate—especially for ridge waveguide  
 170 (RW) lasers. However, since they only considered a single cross  
 171 section, they were unsuitable for longitudinally nonuniform  
 172 structures and high-power operation, where longitudinal spa-  
 173 tial hole burning and carrier/thermal lensing effects are signifi-  
 174 cant. Early models based on beam propagation methods (BPMs)  
 175 were developed to handle nonuniform structures, but typically  
 176 only solved the 1-D electrical problem in the lateral direction  
 177 [23]–[25]. Sophisticated models were also introduced that  
 178 solved the spatiotemporal dynamics of the lasers, but these  
 179 models also used a 1-D electrical model in the lateral direc-  
 180 tion [26], [27]. Quasi-3-D models were introduced in [28]  
 181 and [29], with the optical model separated into 1-D in the lon-  
 182 gitudinal direction and 2-D in the transverse cross section. The  
 183 combination of the 2-D cross-section electrothermal model with  
 184 the BPM was then introduced [30], [31]. By including the lon-  
 185 gitudinal direction and accounting for current and heat spreading  
 186 effects, these models have become predictive and useful design  
 187 tools for high-brightness lasers. By including the spectral and/or  
 188 the dynamic properties of the laser, design tools are reaching  
 189 new levels of accuracy and reliability.

### 190 III. LASER DIODE MODEL AND ITS CALIBRATION

191 Ideally, to capture the complete physical behavior of the de-  
 192 vice, laser models should include all three spatial dimensions  
 193 of the device, as well as their spectral and/or dynamic behav-  
 194 ior. Short design cycles are often needed to respond to market  
 195 demands, so compromises must be made between accuracy and  
 196 efficiency. Models with reduced dimensionality and/or complex-  
 197 ity are often useful early in the design cycle, where the emphasis  
 198 is on designing first-generation devices. In the design optimiza-  
 199 tion stage, it becomes more important to model the device more  
 200 accurately.

201 For advanced simulations and design optimization, the char-  
 202 acteristics to be modeled (apart from the light-current charac-  
 203 teristic) include the near- and far-field patterns, the  $M^2$  beam  
 204 quality factor, and the astigmatism—all as a function of cur-  
 205 rent. In addition to these external device characteristics, internal  
 206 properties such as the temperature and carrier and photon den-  
 207 sity distributions are needed for a physical understanding of  
 208 the operation of the device. At very high power densities, even  
 209 nonequilibrium phenomena like carrier heating and spectral hole  
 210 burning can be significant. This requires careful calibration of

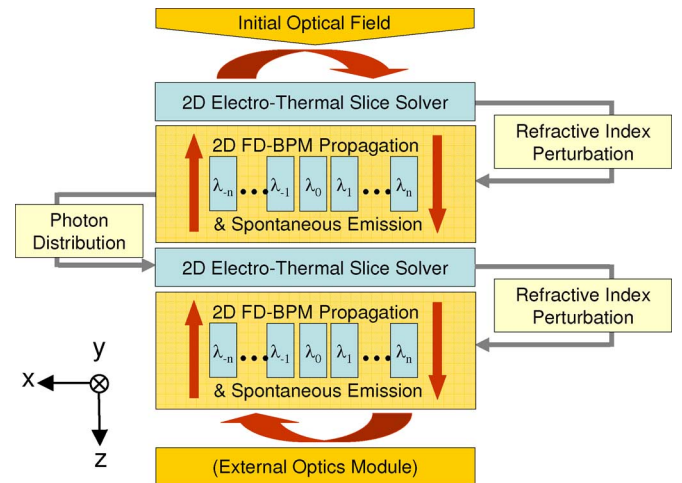


Fig. 2. Flow diagram of the 2.5-D spectral laser model.

the materials parameters and extensive validation of the device  
 models against measured results.

This section begins by describing our simulation tools for  
 high-brightness laser diodes. This is followed by a description  
 of initial calibration procedures and ends with a discussion of  
 advanced validation for more comprehensive simulations.

#### A. Description

Our principal model for high-brightness lasers consists of a  
 2.5-D spectral laser model [32]. This model has been derived  
 from a monochromatic 2.5-D laser model [33]. The term 2.5-D  
 is used to indicate that the model is quasi-3-D, consisting of  
 2-D optical ( $x$ - $z$ ) and electrothermal ( $x$ - $y$ ) solvers (the flow  
 diagram and definition of axes are given in Fig. 2). The flow  
 of carriers and heat in the longitudinal direction is neglected.  
 Comparison with a full 3-D electrothermal model [30], [31]  
 has shown that this approximation is valid for structures that  
 are slowly varying in the longitudinal direction (as investigated  
 in this paper). The electrothermal model is coupled to the opti-  
 cal model through stimulated emission/absorption and spon-  
 taneous emission coupling and also through the carrier- and  
 temperature-induced changes in the complex refractive index.  
 The optical model propagates multiple wavelengths between  
 electrothermal slices using the 2-D wide-angle finite-difference  
 BPM (WA-FD-BPM) [34], the effective index approximation,  
 and PML boundary conditions. The BPM projects the lateral  
 modes onto the same field. Through mode competition, the  
 multiwavelength model responds to both spectral and spatial  
 variations in the gain distribution. The electrothermal and opti-  
 cal models are solved self-consistently, following an accelerated  
 Fox–Li iterative approach [23].

The electrical model calculates the bipolar carrier density pro-  
 files for 2-D transverse slices along the laser cavity and includes  
 drift-diffusion transport and the capture/escape processes be-  
 tween the bound and unbound states of the quantum well(s)  
 (QWs). The thermal model, based upon the solution of the  
 Boltzmann transport equation for heterostructures, solves the  
 lattice heat flux equation (including thermal boundary

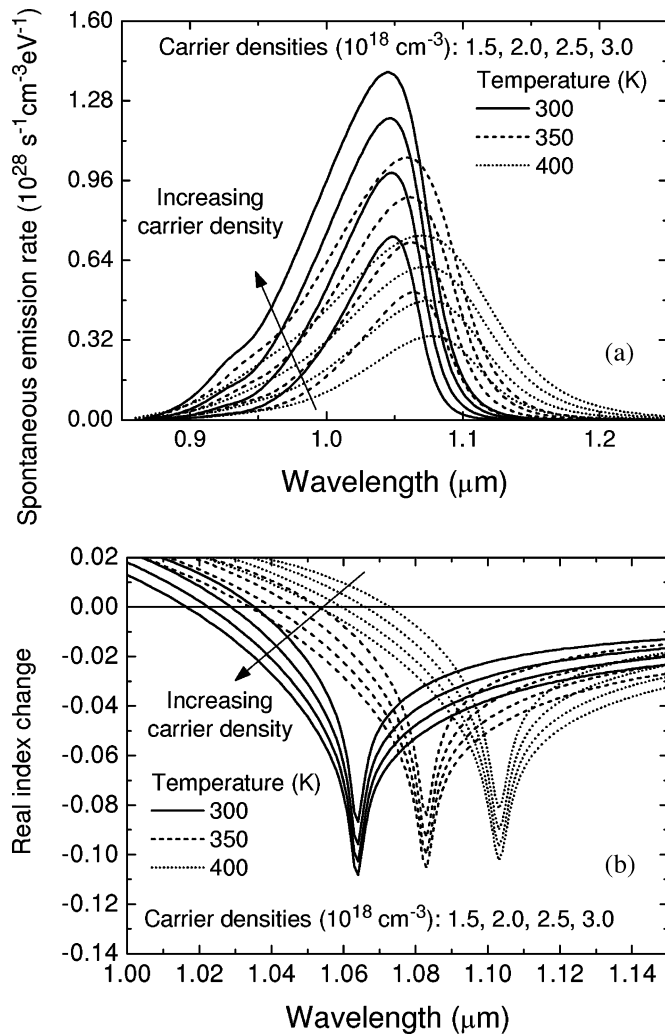


Fig. 3. (a) Spontaneous emission and (b) real index change spectra for a range of carrier densities and temperature.

resistances) and all relevant heat sources [35]. In addition to the classical heat model, our thermal solver also provides the option of including nonequilibrium effects by solving for the electron, hole, and local oscillator (LO) phonon temperatures in the QW active region(s) [36]. Surface recombination, Fermi level pinning, and surface depletion are included self-consistently [37], [38]. The photon density distribution at each wavelength is provided as an input to the electrical solver. The gain, spontaneous emission, and change in refractive index spectra, which are dependent on the electron and hole densities, temperature, and photon density, are parameterized in a table and used by the optical model to propagate the fields to the next electrothermal slice.

An accurate spectral simulation requires a reliable model for the gain, spontaneous emission, and carrier-induced refractive index change. Our model uses the parabolic approximation for the conduction band and a  $4 \times 4$   $\mathbf{k} \cdot \mathbf{p}$  band mixing model for the valence band in order to calculate the QW band structure. Examples of the spontaneous emission and carrier-induced index change spectra for a 1060-nm QW are shown in Fig. 3. The band parameters were taken from the standard literature [39] and a

band offset ratio of  $\Delta E_c/\Delta E_g = 0.65$  was used. The spontaneous emission spectra were calculated and convolved with a sech linewidth broadening function, as shown in Fig. 3(a). The intraband relaxation lifetime was taken to vary as a function of carrier density and temperature [40]. Next, the gain spectra were obtained by transforming the spontaneous emission spectra using Einstein's relation. The spectral change in the real index of the QW [Fig. 3(b)] was calculated with the Kramers–Kronig relation from the change in the calculated gain spectra, but does not include smaller changes due to intraband absorption. The effective index change is obtained by multiplying the QW index change by the confinement factor, but more accurate treatments should also account for index changes in the waveguide and cladding layers.

The 2.5-D spectral laser model can also be coupled to an external optics module to simulate external cavity lasers. This is particularly relevant for high-power lasers, where external cavities can be used to improve the beam quality of the laser. As the output facet reflectivity of a high-brightness laser diode is often  $< 1\%$ , this scheme can also be used to evaluate the impact of back reflections from the external optics.

Various simplifications of the 2.5-D spectral laser model exist to increase the efficiency of the simulation, depending on the application. These include isothermal, unipolar, monochromatic, and reduced dimensionality models, which are useful for obtaining qualitative results or when the size of the problem becomes computationally intractable. For example, the 1.5-D model is used in Section III to simulate large structures such as laser arrays and (in some cases) when the spectral characteristics of the device are required. The 1.5-D model is quasi-2-D in the sense that the optical problem is solved in the  $x$ - $z$  plane and the electrical problem is reduced to 1-D in the lateral ( $x$ ) direction. The 1-D electrical model solves the unipolar carrier-diffusion equation given as

$$D_a \frac{d^2}{dx^2} n(x) = -\frac{J(x)}{qd} + R_{\text{nr}}(x) + R_{\text{sp}}(x) + v_g g(x) S(x) \quad (2)$$

where  $D_a$ ,  $J$ ,  $d$ ,  $n$ ,  $R_{\text{nr}}$ ,  $R_{\text{sp}}$ ,  $g$ , and  $S$  are the ambipolar diffusion coefficient, injection current density, active region thickness, carrier density, nonradiative recombination, spontaneous emission rate, optical gain, and photon density, respectively. The spontaneous emission rate and optical gain data are the same as those used in the 2-D bipolar electrical model for consistency and accuracy. In the 1-D electrical model,  $J(x)$  is constant inside the stripe and zero outside the stripe.

The laser model used in this paper improves upon previous beam-propagation-based laser models [30], [31], [33] by solving the emission spectra of the laser and including the spectral dependence of the gain, spontaneous emission, and carrier-induced refractive index change. It also has additional flexibility by including the option to couple to external optics modules to allow the simulation of a variety of external cavity lasers.

## B. Calibration Procedure

Proper calibration is essential for a predictive laser model. A carefully calibrated simple model can be even more predictive

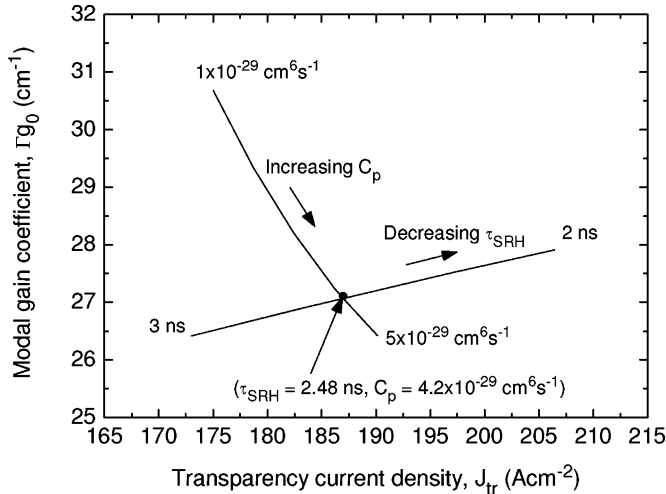


Fig. 4.  $\Gamma_{g_0}$  and  $J_{tr}$  dependence with  $\tau_{SRH}$  and  $C_p$ .

321 than a poorly calibrated sophisticated model. In this section, an  
 322 example of the calibration of the laser model is presented for a  
 323 device emitting at 1060 nm [41].

324 The first step is to calibrate the simulated gain and spon-  
 325 taneous emission spectra with gain spectra measured using the  
 326 Hakki–Paoli [42], Cassidy [43], or segmented contact [44] meth-  
 327 ods. This usually involves slight adjustments to the QW energy  
 328 levels and linewidth broadening.

329 Next, the internal loss is determined. The internal loss can be  
 330 obtained from length-dependent measurements of the external  
 331 differential efficiency of BA-LDs. For this structure, the internal  
 332 loss  $\alpha_i$  was  $0.9 \text{ cm}^{-1}$ . At long wavelengths, the internal loss  
 333 is dominated by intervalence band absorption. Therefore, the  
 334 absorption cross section for holes in the QW was used as a  
 335 fitting parameter and a value of  $3 \times 10^{-17} \text{ cm}^2$  gave an internal  
 336 loss that agreed with experiment.

337 The nonradiative recombination parameters are determined  
 338 next—in particular, the Shockley–Read–Hall (SRH) carrier life-  
 339 time and the Auger recombination coefficient. These param-  
 340 eters can be obtained from length-dependent measurements of  
 341 the threshold current of BA-LDs. From these measurements,  
 342 the transparency current density  $J_{tr}$  and the modal gain coef-  
 343 ficient  $\Gamma_{g_0}$  are extracted. Using the calculated gain and spon-  
 344 taneous recombination spectra, the SRH carrier lifetime and  
 345 Auger recombination parameter were adjusted to obtain agree-  
 346 ment with the experimental values of  $\Gamma_{g_0}$  and  $J_{tr}$ . The SRH  
 347 carrier lifetime for electrons and holes was set equal to each  
 348 other ( $\tau_n = \tau_p = \tau_{SRH}$ ). Only the Auger coefficient for holes  
 349  $C_p$  was adjusted, as it is generally dominant at long wavelengths.  
 350 By keeping  $\tau_{SRH}$  fixed and increasing  $C_p$ , we find that  $\Gamma_{g_0}$  de-  
 351 creases and  $J_{tr}$  increases according to the direction indicated by  
 352 the line “increasing  $C_p$ ” in Fig. 4. Instead, if we keep  $C_p$  fixed  
 353 and decrease  $\tau_{SRH}$ ,  $\Gamma_{g_0}$  and  $J_{tr}$  both increase in the direction  
 354 of the line labeled “decreasing  $\tau_{SRH}$ ” in Fig. 4. If we search the  
 355 entire parameter space of  $\tau_{SRH}$  and  $C_p$ , the set of recombination  
 356 parameters  $\tau_{SRH} = 2.48 \text{ ns}$  and  $C_p = 4.2 \times 10^{-29} \text{ cm}^6\text{s}^{-1}$  can  
 357 be uniquely linked to the set of measured device parameters  
 358  $\Gamma_{g_0} = 27.1 \text{ cm}^{-1}$  and  $J_{tr} = 187 \text{ A/cm}^2$ .

### C. Advanced Validation for Accurate Device Simulation

359

360 In this section, we discuss the general approach we follow for  
 361 the experimental validation and calibration of more advanced  
 362 simulation parameters. (Please note that the examples presented  
 363 in Section IV represent very recent work, for which this valida-  
 364 tion is still being performed.)

365 The electrical and optical properties of laser diodes both de-  
 366 pend upon temperature. Thus, their behavior is sensitive to self-  
 367 heating, and it is important to validate the parameters used in the  
 368 thermal model. As the rise in internal temperature usually causes  
 369 a red-shift in emission wavelength above threshold [45]–[47],  
 370 this can often be used to determine the thermal resistivity of the  
 371 laser diode package. (Frequency-stabilized lasers are an  
 372 exception.)

373 Next, carrier- and temperature-induced lensing effects are  
 374 investigated by comparing the simulated and measured near-  
 375 and far-field profiles. Fig. 3(b) shows that the refractive index  
 376 change near the ground state transition energy of the QW is  
 377 highly sensitive to temperature. Thus, an *a priori* calculation  
 378 of the refractive index change requires precise knowledge of the  
 379 thermal environment (e.g., heat sink performance). Good  
 380 agreement can usually be achieved by adjusting the propor-  
 381 tionality constants relating the index change and changes in carrier  
 382 density and temperature [30], [31], so that the model is able  
 383 to predict the evolution of the far field with bias current with  
 384 reasonable reliability.

385 Direct validation of the carrier distribution inside the cavity  
 386 can be obtained from intracavity spontaneous emission measure-  
 387 ments, which provide spectral and spatial information about the  
 388 spontaneous emission distribution in the cavity. The intensity  
 389 profiles reveal spatial hole burning and electrical overpumping  
 390 effects. The spontaneous emission spectra provide information  
 391 about the local lattice temperature, carrier heating, and spectral  
 392 hole burning effects.

393 Fig. 5(a) shows the spontaneous emission distribution ob-  
 394 tained through a windowed contact in a 975-nm tapered laser  
 395 [48]. Fig. 5(b) compares the simulated and experimental spon-  
 396 taneous emission distributions for a lateral slice near the output  
 397 facet. In this example, the spatial hole in the center of the cav-  
 398 ity observed in the experimental measurement is also seen in  
 399 the simulation. Good quantitative agreement was also obtained.  
 400 The difference in the integrated intensity was  $\sim 12.4\%$ , which  
 401 translates to  $\sim 6\%$  error in the carrier density.

402 Figs. 6 and 7 show experimental and simulated intracavity  
 403 spontaneous emission spectra from the same device for differ-  
 404 ent bias levels [32]. The measured spectra were taken from a  
 405  $5 \mu\text{m} \times 5 \mu\text{m}$  point through a window in the back contact.  
 406 The spikes in the experimental spectra taken above threshold  
 407 are scattered stimulated emission. The simulated spectra have a  
 408 steeper edge on the low energy side than the measured spectra.  
 409 This is because inhomogeneous broadening due to alloy and  
 410 QW width fluctuations has not been accounted for, nor have  
 411 the line shape broadening parameters in the simulation been  
 412 adjusted to obtain agreement with the measured spectra. Nev-  
 413 ertheless, similar trends are observed in the experiment and the  
 414 simulation. First, the spontaneous emission intensity increases

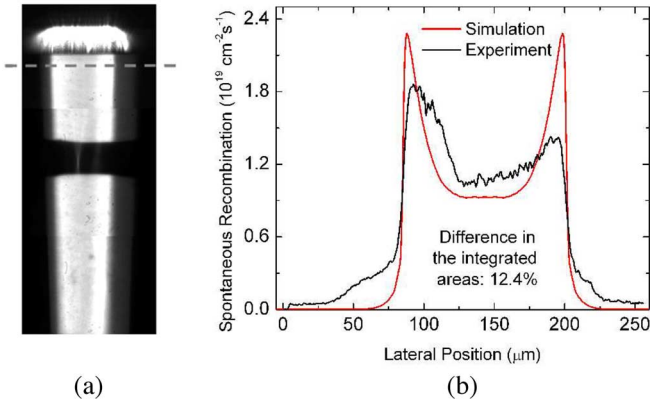


Fig. 5. (a) Image of the spontaneous emission distribution taken through two windows in the contact near the output facet. (b) Experimental and simulated spontaneous emission profiles at the output facet of a tapered laser [48].

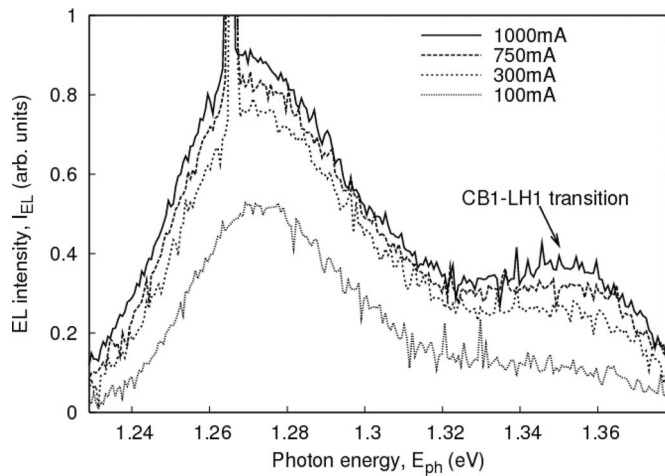


Fig. 6. Experimentally measured spontaneous emission spectra for varying bias taken at the center of the device near the front facet [32].

415 with bias, due to spectral hole burning. The gain, and hence, car- 432  
 416 rier density are pinned at the lasing energy (i.e., bottom of the 433  
 417 spectral hole). As the bias increases, so does the carrier density 434  
 418 around the spectral hole. Second, the CB1-LH1 transition also 435  
 419 increases with bias, which can be attributed to carrier heating. 436  
 420 This conclusion can be obtained from the simulated spectra, 437  
 421 where a larger increase in the CB1-LH1 transition is observed 438  
 422 when a nonequilibrium gain model is used, which includes the 439  
 423 carrier heating effect. 440

#### 424 IV. APPLICATION EXAMPLES

425 In this section, application examples are used to demonstrate 441  
 426 the role of modeling for the design, simulation, and evaluation 442  
 427 of next-generation high-brightness laser diode technologies. 443

##### 428 A. Broad-Area Laser Diodes

429 Conceptually, the simplest and most obvious way to increase 444  
 430 the brightness of a BA-LD is to increase its width, since the far- 445  
 431 field and near-field widths are inversely related. The problem 446

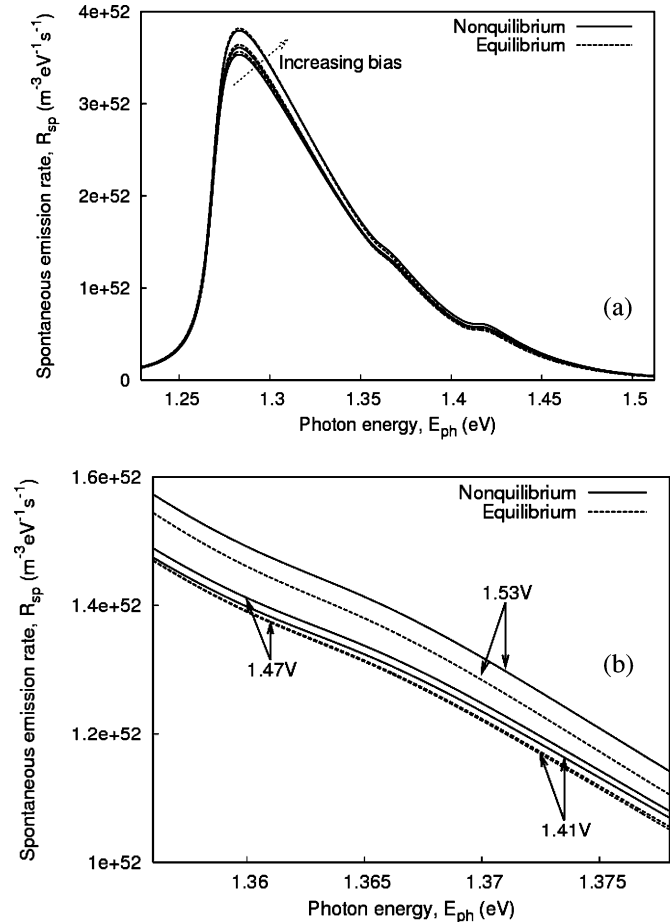


Fig. 7. (a) Simulated spontaneous emission showing nonequilibrium spectral hole burning and carrier heating. (b) Closeup of CB1-LH1 transition [32].

432 with this approach is that filaments start to form in the laser. 433  
 433 This leads to reduced beam quality, since the narrow filaments 434  
 434 cause a large far-field divergence. Furthermore, the number and 435  
 435 position of the filaments change both with time and from device 436  
 436 to device. 437

437 In this study, we investigate the brightness limitations of 438  
 438 broad-area lasers by investigating the effect of the resonator 439  
 439 geometry on the single-mode operation of a BA-LD. The BA- 440  
 440 LD investigated in this paper is a gain-guided laser with a cur- 441  
 441 rent stripe defined by deep ion implantation to eliminate current 442  
 442 spreading in the cladding layers. 443

443 To investigate the operating regime of the BA-LD dominated 444  
 444 by the fundamental mode, we employed the Prony method to 445  
 445 extract the lateral modes of the BA-LD [49]. The eigenvalues 446  
 446 extracted with the Prony method are the round-trip gain/loss of 447  
 447 the individual eigenmodes. Thus, if the BA-LD is to operate 448  
 448 in a single mode, the fundamental mode should have an eigen- 449  
 449 value equal to unity ( $\lambda_0 = 1$ ), while the first-order mode should 450  
 450 have an eigenvalue less than unity ( $\lambda_1 < 1$ ). If we define the 451  
 451 modal discrimination as  $MD = |\lambda_0|/|\lambda_1|$ , the BA-LD operates 452  
 452 in the single fundamental lateral mode when MD is greater than 453  
 453 unity. Thus, to obtain strong single-mode operation, the modal 454  
 454 discrimination should be as large as possible. 455

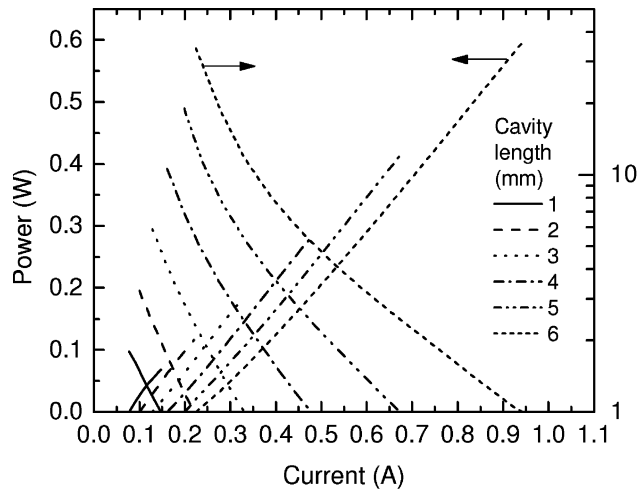


Fig. 8.  $L$ - $I$  characteristic and modal discrimination as a function of current bias for cavity lengths  $L = 1$  to  $6$  mm. The emitter width is  $W = 30 \mu\text{m}$  [33].

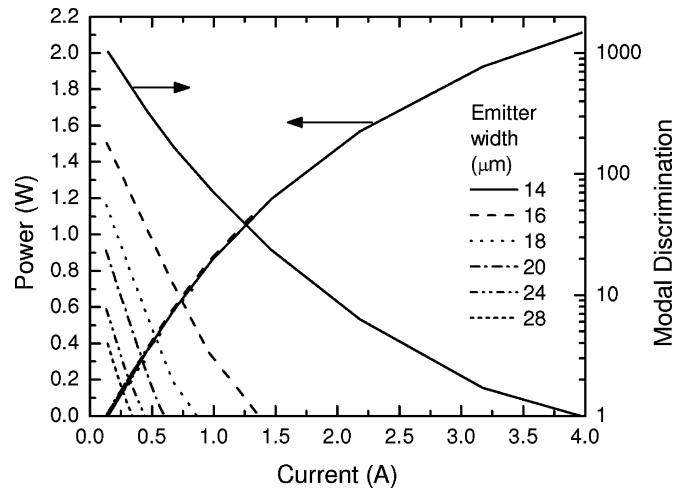


Fig. 9.  $L$ - $I$  characteristic and modal discrimination as a function of current for emitter widths  $W = 14$  to  $28 \mu\text{m}$ . The cavity length is fixed at  $L = 2$  mm [33].

455 Before investigating the effect of the other geometrical parameters, the thickness of the vertical waveguide  $W_g$  needs to be  
 456 determined. It was shown in [33] that increasing the waveguide  
 457 thickness allows for higher modal discrimination by reducing  
 458 the confinement factor, and subsequently, the carrier lensing effect.  
 459 The carrier lens excites higher order modes in the cavity  
 460 and promotes the formation of optical filaments. Only a symmetrical  
 461 vertical structure was considered here with a total vertical  
 462 waveguide thickness of  $2 \mu\text{m}$ . To reduce the confinement factor  
 463 further, it is also possible to employ asymmetric structures,  
 464 where the QW is positioned closer toward the p-cladding [50].  
 465 Having determined the vertical waveguide thickness, the effect  
 466 of the cavity length on the modal discrimination is investigated.  
 467 Fig. 8 shows the variation of modal discrimination and single-mode  
 468 output power versus bias current. The emitter width is fixed at  
 469  $30 \mu\text{m}$  and the cavity length is varied from 1 to 6 mm.  
 470 The longer the cavity length, the higher the modal discrimination  
 471 is at threshold. Also, as the bias current is increased, the  
 472 modal discrimination decreases less rapidly for the longer cavity  
 473 BA-LDs. This can be understood in terms of the round-trip loss  
 474 of a particular mode  $n$  given by  $r_f r_b \exp(-\alpha_n L)$ , where  $r_f$  and  
 475  $r_b$  are the facet reflectances,  $\alpha_n$  is the net modal loss, and  $L$  is  
 476 the cavity length. The round-trip loss of the fundamental mode  
 477 is unity (fixed by the lasing condition), so the modal discrimination  
 478 increases with cavity length as the loss of the first-order mode  
 479 increases.  
 480

481 Next, the effect of emitter width is investigated. The cavity  
 482 length is fixed at 2 mm and the emitter width is varied from  
 483 14 to 28  $\mu\text{m}$  (Fig. 9). For narrower emitter widths, the modal  
 484 discrimination is higher at threshold and decreases less rapidly  
 485 as a function of bias current. For an emitter width of 14  $\mu\text{m}$ ,  
 486 the modal discrimination is greater than unity for powers up  
 487 to  $\sim 2$  W. This maximum single-mode output power is equivalent  
 488 to a facet load of  $\sim 15 \text{ MW}/\text{cm}^2$ , which is close to the reported  
 489 catastrophic optical mirror damage (COMD) values of 18–19  
 490  $\text{MW}/\text{cm}^2$  [51]. In addition, since thermal effects and  
 491 spontaneous emission coupling were not included in these sim-

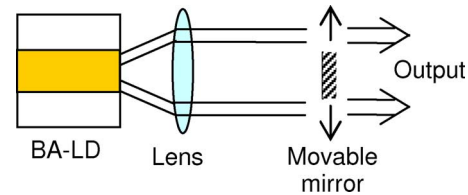


Fig. 10. Schematic diagram of an asymmetric feedback external cavity laser.

492 ulations, this represents an upper limit on the maximum bright-  
 493 ness that can be achieved by a BA-LD. By comparison, tapered  
 494 lasers (discussed in Section III-C and III-D) have achieved  
 495 nearly diffraction-limited operation for powers up to 12 W [2].  
 496 Thus, although single-emitter broad-area lasers can produce  
 497 high output powers, their ultimate brightness is limited by the  
 498 lack of strong modal discrimination for wide emitters and is  
 499 restricted by COMD for narrow emitters.

### B. Asymmetric Feedback External Cavity Laser

500 In this section, an external cavity laser with asymmetric feed-  
 501 back is investigated to improve the modal discrimination and  
 502 beam quality of a BA-LD. The external cavity laser configura-  
 503 tion is shown in Fig. 10. The BA-LD has an emitter width of  
 504  $100 \mu\text{m}$ , a cavity length of 1.5 mm, and an emission wave-  
 505 length of 975 nm. Details of the epitaxial structure are given  
 506 in [52]. The front and back facets are antireflection (AR) and  
 507 high reflection (HR) coated, respectively. A lens with a focal  
 508 length of 75 mm is placed at the focal plane to collimate the  
 509 laser beam along the slow axis. A 0.9-mm-wide mirror is placed  
 510 in a far-field plane located 75 mm from the lens for selective  
 511 spatial feedback. The 1.5-D isothermal unipolar laser model is  
 512 used to simulate the BA-LD and is coupled to an external optics  
 513 module, which models the free-space propagation of the optical  
 514 beam by solving the Fresnel diffraction equations.  
 515

516 A stable operating condition is found when the mirror stripe  
 517 is positioned 5.85 mm from the center. The near-field pattern  
 518 in Fig. 11(a) has an asymmetric shape, in agreement with

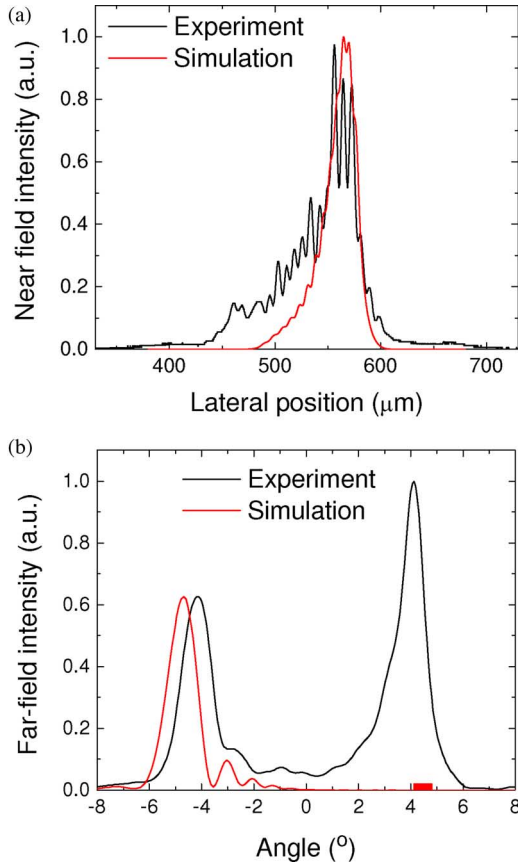


Fig. 11. Converged (a) near-field and (b) far-field patterns of an asymmetric feedback external cavity laser. The mirror width and position used in the simulation are indicated by the stripe in (b).

519 experiment. The far-field pattern in Fig. 11(b) consists of a nar-  
 520 row main lobe with a full-width at half-maximum (FWHM)  
 521 of  $1.26^\circ$ , which is offset from the center by  $\sim 4.69^\circ$ . The ex-  
 522 perimental far-field profile shows a double lobed feature with  
 523 both a significant output lobe (left) and feedback lobe (right).  
 524 Such a behavior is uncommon for this asymmetric feedback  
 525 technique. Usually, a strong and narrow output lobe is observed  
 526 in the far field [53], in agreement with the simulation, and the  
 527 feedback lobe is strongly suppressed. The peculiar behavior of  
 528 this particular laser is due to degradation observed on the front  
 529 facet AR coating. Nevertheless, the position and width of the  
 530 experimental lobe coincide well with the simulated profile.

531 Fig. 12 shows the carrier density (at the front facet) and far-  
 532 field intensity distributions for different output powers. With  
 533 increasing power, larger spatial hole burning occurs at the out-  
 534 put facet on the opposite side of the feedback mirror. A slight  
 535 movement of the peak position of the far-field lobe away from  
 536 the optical axis is seen with increasing power. This is due to spa-  
 537 tial hole burning and carrier lensing, which result in a slightly  
 538 modified waveguiding behavior in the BA-LD.

539 The simulated  $M^2$  value using the second moment definition  
 540 (ISO Standard 11146) is only 2.62, which is small compared  
 541 to that of a typical BA-LD ( $M^2 \approx 30$ ) [9]. This dramatic im-  
 542 provement is attributed to the increased modal discrimination  
 543 provided by the mirror stripe, which provides selective feedback

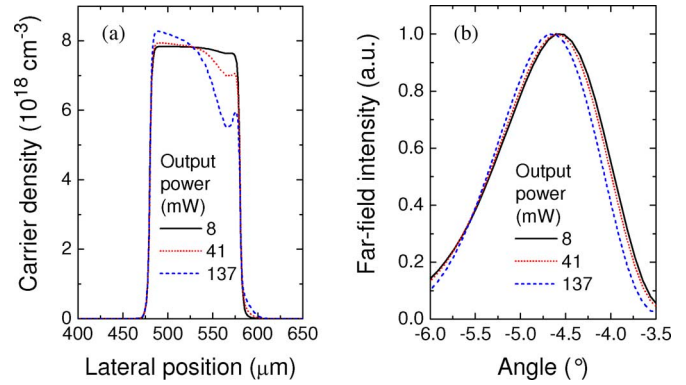


Fig. 12. (a) Carrier density distribution at the output facet. (b) Far-field patterns for different output powers.

544 to a specific lateral mode. The value of  $M^2 \sim 2.6$  is outstanding  
 545 for a BA-LD, but many applications (e.g., frequency doubling  
 546 for display applications) require even better beam quality. This  
 547 can be achieved with tapered lasers, which use a spatial filter to  
 548 improve the modal discrimination.

### 549 C. Tapered Laser

550 Tapered lasers are currently the most popular high-brightness  
 551 laser diodes. Their superior performance is due to several factors  
 552 inherent in their design. First, the straight RW section serves as  
 553 a modal filter, which discriminates against higher order modes.  
 554 Next, a single lateral mode is allowed to expand adiabatically  
 555 in the tapered section, minimizing spatial hole burning and fila-  
 556 mentation. Finally, the complexity of a tapered laser is relatively  
 557 low compared to other high-brightness lasers, making it suitable  
 558 for low-cost manufacturing with a high process yield and reli-  
 559 able operation.

560 Tapered lasers demonstrate clear performance advantages, but  
 561 filamentation can still be an issue if they are not designed prop-  
 562 erly. For instance, the RW section geometry must be designed  
 563 to support a single lateral mode. Figs. 13 and 14 show the 2.5-D  
 564 spectral simulation of a  $5\text{-}\mu\text{m}$ -wide RW laser, which just sup-  
 565 ports two lateral modes. Although the central mode prefers the  
 566 fundamental lateral mode, the modes at the edges of the emis-  
 567 sion spectrum clearly show mode beating between the first and  
 568 second lateral modes. (From the gain profile, it is clear that this  
 569 is mode beating and not gain or index guiding.) The laser is  
 570 able to efficiently use the spatial gain distribution in this way,  
 571 but the result is not good for the modal filtering properties of  
 572 the RW—particularly as the backward wave from the taper will  
 573 excite both modes. In this case, a narrower RW is needed to  
 574 suppress the higher order transverse mode, or the loss of the  
 575 higher order transverse mode must be increased to improve the  
 576 modal discrimination. Furthermore, to achieve good modal fil-  
 577 tering, the taper angle should match the free diffraction angle  
 578 of the mode launched into the tapered section, and the epitaxial  
 579 structure should have a low modal gain to reduce carrier lensing  
 580 effects.

581 Along with the RW design, the front facet reflectivity and  
 582 beam spoiler also affect the modal filtering performance of

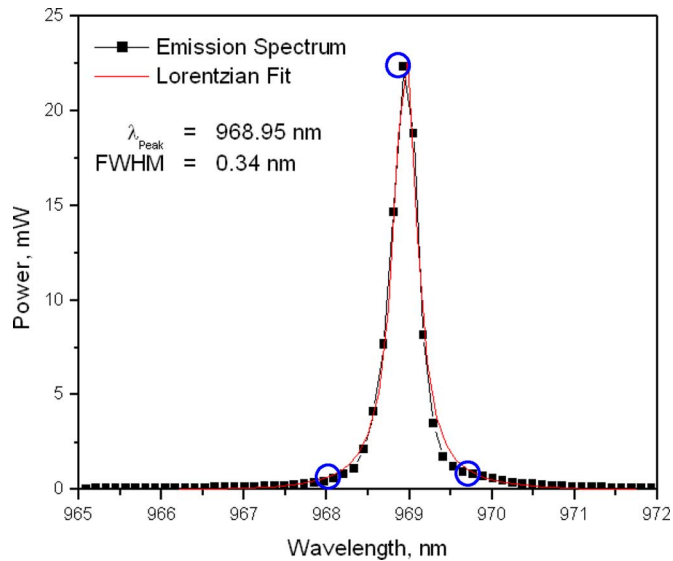


Fig. 13. Simulated emission spectrum of a 5- $\mu\text{m}$ -wide index-guided RW laser. The circled points correspond to the fields shown in Fig. 14.

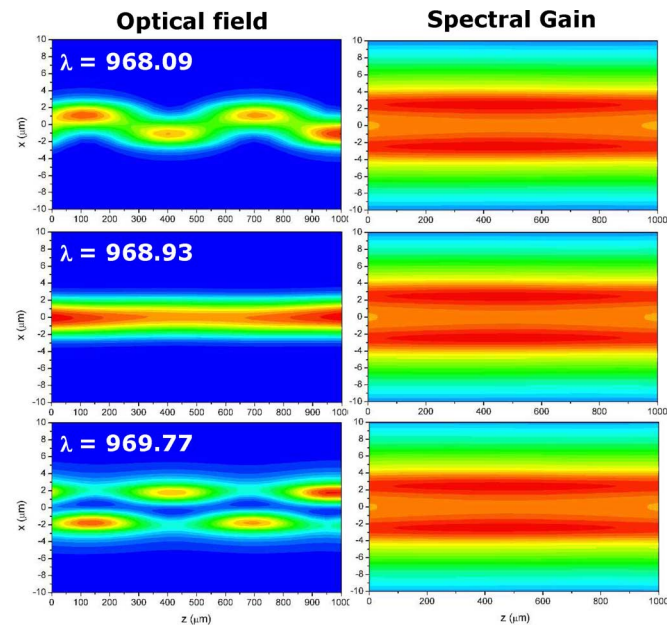


Fig. 14. Spectral field (left) and gain (right) distributions of a 5- $\mu\text{m}$ -wide index-guided 970-nm RW laser at wavelengths of 968.09 (top), 968.93 (middle), and 969.77 nm (bottom).

583 the tapered laser. From earlier investigations on a 2-mm-long  
 584 4° gain-guided tapered laser (using a different monochromatic  
 585 2.5-D laser model [30]), it was shown that a front facet reflectivity  
 586  $R_f = 1\%$  produced filamentation in the near-field profile.  
 587 This filamentation is caused by optical pumping of the regions  
 588 adjacent to the RW, which become transparent and reduce the  
 589 modal filtering efficiency of the RW section. This resulted in  
 590 small side lobes in the forward propagating wave in the RW  
 591 section, which seed the filamentation process and create a mul-  
 592 tilobed near-field pattern. When  $R_f$  is reduced to 0.1%, the  
 593 optical bleaching of the RW section is avoided. This improves  
 594 the modal filtering in the RW and eliminates the filamentation

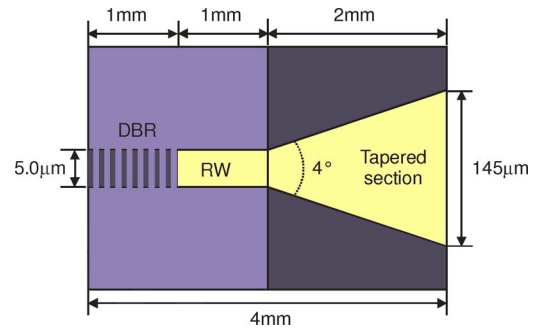


Fig. 15. Schematic diagram of the DBR tapered laser.

595 in the taper. Beam spoilers were also shown to prevent the opti-  
 596 cal bleaching of the regions adjacent to the RW. Even with the  
 597 original front facet reflectivity of 1%, a 6- $\mu\text{m}$  aperture placed  
 598 100  $\mu\text{m}$  from the rear facet filtered the high-order modes out of  
 599 the relatively intense backward wave and prevented filamenta-  
 600 tion and beam quality degradation.

#### D. Multisection Tapered Laser 601

602 There is growing interest in using tapered lasers in display and  
 603 optical wireless applications due to their good beam quality and  
 604 high output power. These applications require a high modulation  
 605 efficiency ( $dP/dI$ ) to minimize the cost and complexity of the  
 606 laser driver. This can be achieved through the use of separate  
 607 contacts for the RW and tapered amplifier sections. By using a  
 608 small modulation bias on the RW and keeping the tapered  
 609 section bias fixed, higher modulation bandwidths and efficiency  
 610 can be achieved. To satisfy the targeted applications, these lasers  
 611 should have a stable beam quality and astigmatism for all bias  
 612 conditions. This is necessary, since the lenses that collimate and  
 613 focus the output beam of the laser are designed for fixed beam  
 614 parameters.

615 Here, we investigate the performance of a 1060-nm DBR  
 616 tapered laser intended for generating 530 nm light by second  
 617 harmonic generation (SHG) for laser displays [41]. At the end of  
 618 the RW, the DBR tapered laser includes a passive DBR section  
 619 to fix the emission wavelength, as shown in Fig. 15. High  
 620 spectral brightness and stability (i.e., a narrow and stable spec-  
 621 tral linewidth) is required by the nonlinear crystal for SHG.  
 622 Since the DBR section locks the emission wavelength, we have  
 623 only simulated a single wavelength fixed at 1060 nm. The las-  
 624 ing wavelength was measured to be stable with RW current  
 625 within 130 pm [41]. The good wavelength stability with re-  
 626 spect to current is due to efficient thermal management and the  
 627 small temperature and index change in the passive DBR section.  
 628 The index-guided RW has an index step of  $\sim 1.5 \times 10^{-3}$ , while  
 629 the taper is gain guided with a shallow implant for electrical  
 630 isolation.

631 The DBR section is passive (unpumped), so it has been repre-  
 632 sented by a fixed reflectivity at the end of the RW. The reflectivity  
 633 of the sixth-order DBR grating of DBR RW lasers was found  
 634 to be around 31% [41]. We used a top-hat profile (in the lateral  
 635 direction) for the reflectivity with a value of 31% for the region  
 636 within the RW and a value of 0.01% outside the RW. The low

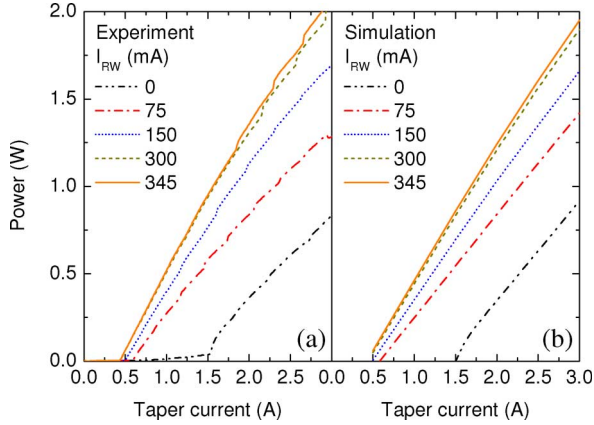


Fig. 16. (a) Experimental and (b) simulated light-current characteristics.

637 reflectivity of the region outside the RW was used, since any  
 638 backward traveling light is strongly absorbed in the unpumped  
 639 region in the DBR section and very little light is reflected back  
 640 from the AR-coated back facet ( $<0.1\%$ ). The front facet was  
 641 AR-coated to 1%.

642 The DBR tapered laser is simulated using the 2.5-D  
 643 monochromatic laser model, employing the material param-  
 644 eters determined in Section II-B. Fig. 16 compares (a) the ex-  
 645 perimental and (b) simulated output power versus taper current  
 646 characteristics of a split-contact 1060-nm DBR tapered laser.  
 647 Good agreement is obtained over the range of RW and taper  
 648 currents investigated. The saturation of the output power with  
 649 increasing RW current is reproduced in the simulations and is  
 650 due to the depletion of carriers in the tapered amplifier with  
 651 increasing optical injection from the RW.

652 The photon density distributions for the combined forward  
 653 and backward waves are plotted in Fig. 17 for RW currents of  
 654 (a) 0 mA and (b) 345 mA at a fixed taper current of 1.6 A. The  
 655 output powers are 100 and 938 mW, respectively. For these con-  
 656 ditions, the simulated modulation efficiency is 2.43 W/A, which  
 657 is slightly smaller than experiment (2.6 W/A). The simulated  
 658 extinction ratio is 9.4, which is bigger than the experimental  
 659 value of 7.7. (The extinction ratio is expected to be squared for  
 660 the frequency-doubled green output.) No filamentation is ob-  
 661 served for either RW current, due to the good modal filtering  
 662 by the passive DBR and low AR coating on the back facet. The  
 663 lack of filamentation is also partly due to the use of a taper an-  
 664 gles that matches the free diffraction angle of the beam from the  
 665 RW. A larger increase in photon density toward the front facet  
 666 in the tapered section is observed for  $I_{RW} = 0$  mA compared  
 667 to  $I_{RW} = 345$  mA, which demonstrates the saturation of the  
 668 tapered amplifier as the RW current is increased.

669 The experimental and simulated far-field patterns are shown  
 670 in Fig. 18. There are discrepancies between the simulated and  
 671 measured far-field patterns, especially at the larger RW currents.  
 672 The lack of perfect agreement is probably because the simula-  
 673 tions were performed with calculated carrier-induced changes in  
 674 the refractive index spectra, which do not include index changes  
 675 in the waveguide core or cladding. Furthermore, index changes  
 676 near the emission wavelength are very sensitive to temperature

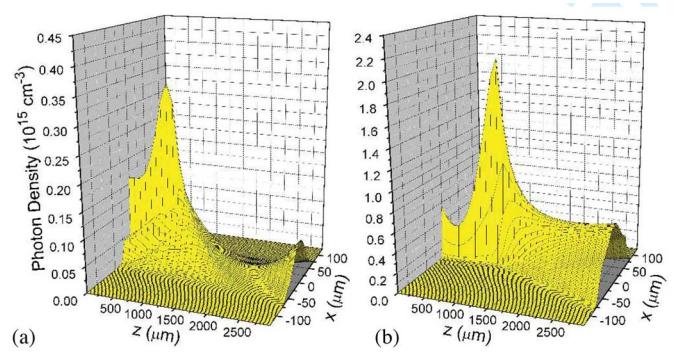


Fig. 17. Simulated photon density distributions (forward and backward waves) at a fixed taper current of 1.6 A and RW currents of (a) 0 mA and (b) 345 mA.

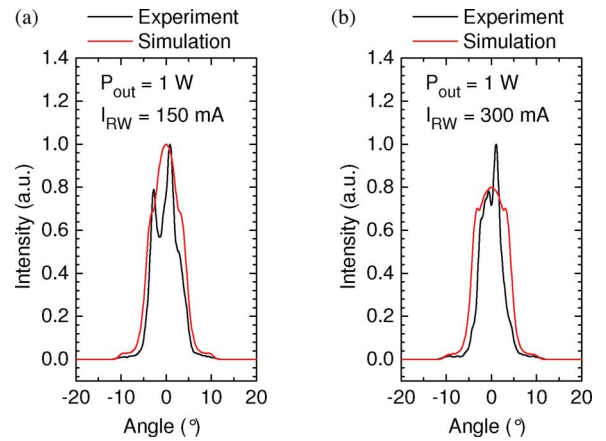


Fig. 18. Measured and simulated far-field profiles for a fixed output power of 1 W and RW currents of (a) 150 mA and (b) 300 mA.

677 changes. The thermal conductivity of the package was not inde-  
 678 pendently measured, since this is usually extracted from changes  
 679 in the emission wavelength above threshold. (As the emission  
 680 wavelength is determined by the DBR, this procedure does not  
 681 work here.)

682 Fig. 19 shows a plot of the beam quality factor and the astig-  
 683 matism versus  $I_{RW}$  at a fixed output power of 1 W. The  $M^2$   
 684 factor (determined using the  $1/e^2$  level) is in reasonable agree-  
 685 ment with experiment and stays at a fairly constant value of  
 686  $\sim 1.2$ . Fig. 19 shows that the simulated astigmatism of the beam  
 687 stays fairly stable versus  $I_{RW}$ , while the experimental data in-  
 688 crease slightly with  $I_{RW}$ . The agreement with experiment seems  
 689 reasonable, but is expected to improve once the spectral index  
 690 change is experimentally validated and calibrated.

691 The stability of the  $M^2$  factor and the astigmatism with re-  
 692 spect to  $I_{RW}$  is due to the use of a thick vertical waveguide  
 693 ( $4.8 \mu\text{m}$ ), since the carrier-induced index depression is reduced  
 694 by the small confinement factor. The exceptional beam quality  
 695 and modulation efficiency are, in part, due to the use of an AR  
 696 coating instead of an HR coating on the rear facet and the pres-  
 697 ence of the passive DBR section. This improves the filtering  
 698 of the higher order modes in the RW section—an approach not  
 699 previously considered.

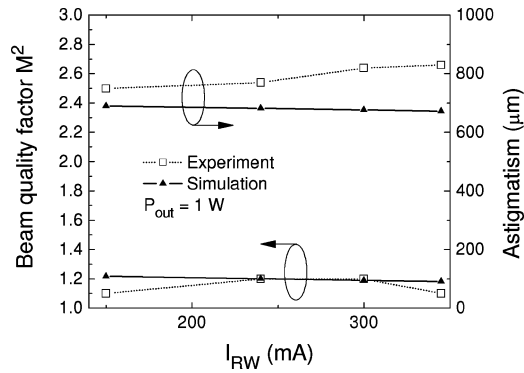


Fig. 19. Beam quality factor and astigmatism versus RW current. The output power is fixed at 1 W.

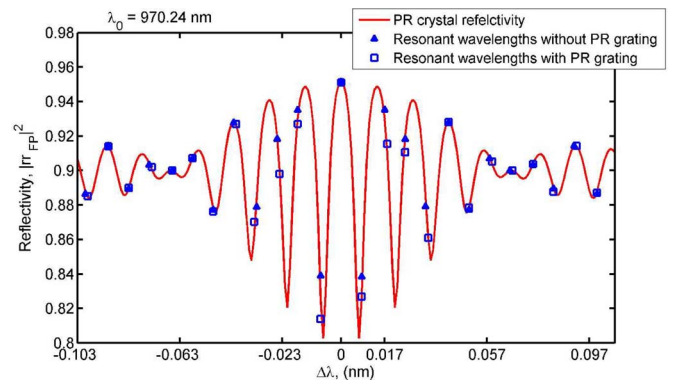


Fig. 21. Dependence of the Fabry-Perot filter reflectivity on wavelength [55].

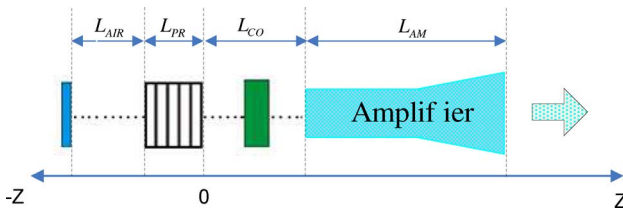


Fig. 20. Schematic diagram of the self-organizing external cavity laser.  $L_{AIR}$ : length of air gap;  $L_{PR}$ : length of the PR crystal;  $L_{CO}$ : length of the collimating optics section;  $L_{AM}$ : length of the tapered amplifier.

### 700 E. Self-Organizing External Cavity Laser

701 In laser technology, photorefractive (PR) crystals are typically  
 702 used in two situations: 1) in tunable external cavity semiconduc-  
 703 tor lasers, where the PR crystal relaxes the alignment tolerances  
 704 and 2) in self-organizing external cavity lasers, where it is used  
 705 to make an adaptive Fabry-Perot mirror to enhance the side  
 706 mode suppression ratio.

707 The schematic diagram of a self-organizing external cavity  
 708 laser is shown in Fig. 20, where a PR crystal is placed between  
 709 a high reflectivity mirror and the rear facet of the high-power tapered  
 710 amplifier. The purpose of assembling a laser cavity in this  
 711 particular configuration is to deliver a beam with high spectral  
 712 and spatial brightness. By using a PR crystal instead of a fixed  
 713 DBR, the laser cavity self-adapts to its operating conditions and  
 714 ensures maximum efficiency.

715 The model of this self-organizing external cavity laser con-  
 716 sists of a PR crystal model, which relies on a phenomenological  
 717 plane wave approach [54], and the 1.5-D spectral laser model.  
 718 (A 1-D unipolar, isothermal electrical model is used for numerical  
 719 efficiency.) In the simulation, the PR crystal and the rear  
 720 mirror are treated as a single adaptive Fabry-Perot filter, which  
 721 provides wavelength-dependent feedback to the tapered ampli-  
 722 fier. The reflectivity of this filter was calculated by solving a set  
 723 of coupled wave equations [54]. The main approximation used  
 724 by the model is that the mode with the largest power writes the  
 725 grating. The other longitudinal modes are scattered from this  
 726 grating.

727 The simulation of the self-organizing high-power external  
 728 cavity laser is performed in three stages. Initially, the resonant

wavelength of the main longitudinal mode is determined by 729  
 the spectral simulation of the free running laser, i.e., while ne- 730  
 glecting the formation of the grating in the PR crystal. This 731  
 simplification is justified because there is no phase shift (and 732  
 hence also no resonant wavelength shift) introduced by the PR 733  
 grating for the main mode. A 1-D simulation cannot be used for 734  
 this purpose, since the energy of the gain maximum depends on 735  
 the carrier density distribution in the tapered amplifier, which 736  
 depends strongly on position. 737

738 Once the wavelength of the main longitudinal mode is deter-  
 739 mined, the reflectivity of the PR crystal grating is obtained,  
 740 along with the values of the resonant wavelengths of all the side  
 741 modes. The calculated values of the resonant wavelength for the  
 742 cavity modes are shown in Fig. 21. The resonant wavelengths  
 743 were calculated with and without the phase shift introduced by  
 744 the PR crystal grating. These results confirm that the recorded  
 745 PR crystal grating has a significant impact on the position and  
 746 the reflectivity of the cavity modes. Without the induced grating  
 747 in the PR crystal, the reflectivity of all the modes would be equal  
 748 to that of the mirror.

749 After the wavelengths of all the cavity modes and the cor-  
 750 responding reflectivities are known, the full spectral simulation  
 751 of the laser is performed. Fig. 22 compares the output power  
 752 spectra, calculated by the spectral model for a bias current of  
 753 0.32 A, for an external cavity laser with and without PR  
 754 crystal. The simulations show that the PR crystal produces  
 755 single longitudinal mode operation. The spectral linewidth  
 756 is less than 18 pm, since the longitudinal mode spacing is  
 757 only 9 pm. Single-mode operation was also found experi-  
 758 mentally, where the instantaneous linewidth was measured to  
 759 be  $\sim 80$  MHz ( $< 0.3$  pm) and is stable up to  $< 2$  pm. The  
 760 simulated side mode suppression ratio is high ( $> 50$  dB),  
 761 as seen experimentally ( $> 30$  dB limited by the spectrum  
 762 analyzer).

763 Previously, self-organized cavity laser diodes have only been  
 764 modeled with 0-D rate equations. The results reported here  
 765 demonstrate the 1.5-D spectral simulation of the spectral bright-  
 766 ness of these devices. The next challenge is to make the wave-  
 767 length selection automatically respond to changes in the oper-  
 768 ating conditions. This requires a more advanced model for the  
 769 PR crystal.

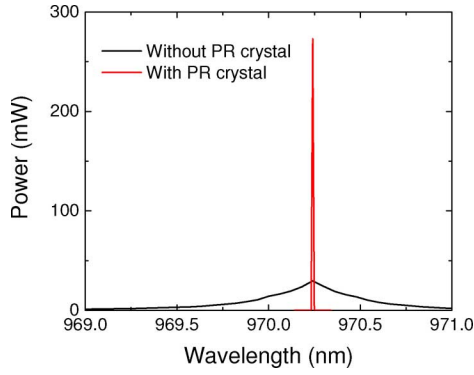


Fig. 22. Calculated output power spectrum for external cavity laser with and without the PR crystal.

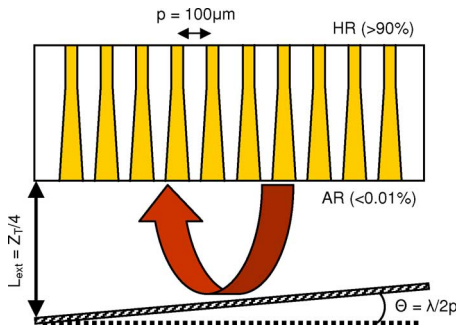


Fig. 23. Schematic diagram of the external Talbot cavity laser.

#### 770 F. External Talbot Cavity Laser

771 Phase-locking of an array of emitters has received great at-  
 772 tention for achieving highly coherent emission with high out-  
 773 put power. Phase-locking can be induced using the Talbot ef-  
 774 fect [17], where the out-of-phase mode is self-imaged and the  
 775 in-phase mode is imaged with a lateral shift of  $p/2$  (where  $p$   
 776 is the emitter pitch) after traveling half the Talbot distance  
 777 ( $Z_T = 2p^2/\lambda$ ). By placing a mirror in an external cavity at a  
 778 distance  $Z_T/4$  with a tilt of  $\lambda/2p$  (Fig. 23), the in-phase mode is  
 779 self-imaged while the out-of-phase mode is laterally displaced  
 780 by  $p/2$ . This increases the modal discrimination between the  
 781 in-phase and out-of-phase modes, thus phase-locking the emit-  
 782 ters in the in-phase mode.

783 The array studied here consists of ten narrow index-guided  
 784 tapered lasers emitting at 975 nm. Further details of the tapered  
 785 laser and epitaxial structure can be found in [52] and [56].

786 For the simulations, the 1.5-D isothermal unipolar laser model  
 787 was coupled to a free-space propagation model (based on the  
 788 Fresnel diffraction equations) for the external cavity [57]. The  
 789 reflectivity of the tilted output mirror was 40%. The operation  
 790 of the Talbot cavity was confirmed by investigating the effect  
 791 of the tilt of the mirror. With an untilted mirror, the laser oscil-  
 792 lates in the out-of-phase mode, but with a tilt angle of  $\lambda/2p$ , the laser  
 793 operates in the in-phase mode. This confirms the strong modal  
 794 discrimination of the Talbot cavity.

795 The front facet near-field distribution (intensity and phase)  
 796 for the in-phase and out-of-phase modes are shown in Fig. 24.  
 797 Comprehensive modeling of the beam propagation in the whole

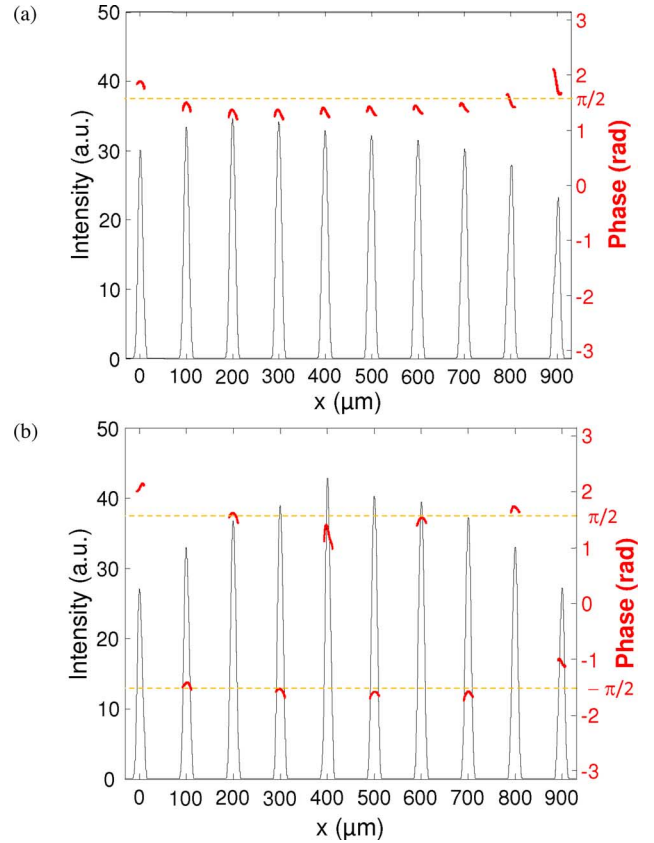


Fig. 24. Field intensity and phase at the front facet for the (a) in-phase and (b) out-of-phase mode operation at an operating current of 3.88 A.

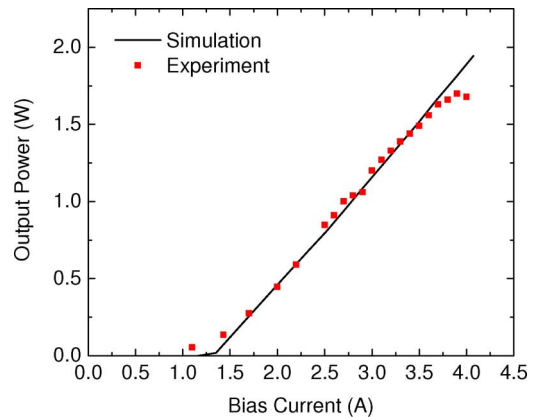


Fig. 25. Experimental versus simulated  $L-I$  characteristic.

cavity predicts some interesting features of the spatial modes 798  
 under external cavity operation and leads to better understanding 799  
 of the laser array behavior. The asymmetry of the intensity 800  
 profile of the in-phase mode is a consequence of the tilt of the 801  
 mirror. In both cases, the phase distributions show the expected 802  
 in-phase and out-of-phase behavior. 803

804 Fig. 25 shows that the simulated  $L-I$  characteristics for the  
 805 in-phase supermode operation of the laser bar agree well with  
 806 experiment. The slight discrepancies are probably due to current  
 807 spreading and self-heating effects in the experiments.

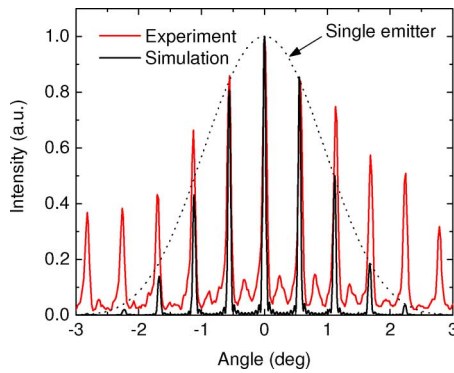


Fig. 26. Far-field profile for the in-phase mode operation at a current of 3 A.

In Fig. 26, the simulated far-field profile for lasing of the in-phase mode shows interference peaks, which agree with experiment. The simulated and measured interference peaks have a width of  $0.07^\circ$ . The envelope of the simulated profile has a Gaussian shape, corresponding to the output of a single emitter. The experimental far-field envelope is wider due to the presence of multimode emission from the tapered emitters.

These results demonstrate the model's ability to reproduce the experimental characteristics and provide insight into the field distribution in the array. Further work will include the detailed investigations of the modal discrimination behavior of the laser and the use of the 2.5-D model to accurately investigate the impact of carrier and thermal lensing effects.

## V. CONCLUSION

To satisfy increasing application demands and enter new markets, next-generation high-brightness laser diodes require not only good beam quality but also high spectral brightness and added functionality (e.g., direct modulation). Several next-generation high-brightness laser diodes were considered, including the asymmetric feedback broad-area laser, the multi-section tapered laser, the self-organizing cavity laser, and the external Talbot cavity laser.

Using the Prony method, it was shown that the modal discrimination of BA-LD improves as the cavity width decreases and the cavity length and waveguide thickness increase. To achieve high power levels, however, the devices must be quite long (up to 6 mm) and the width of the cavity must be narrow. This results in a high facet load of  $>100 \text{ mW}/\mu\text{m}$ . Using asymmetric feedback to increase the modal discrimination dramatically improves the beam quality and reduces  $M^2$  from  $\sim 30$  to  $\sim 2.6$ , without strong limitations on cavity length or width. Nevertheless, their performance falls short of that of recent tapered lasers. Still, asymmetric feedback may play a role in external cavity approaches for the phase coupling of high-power BA-LD arrays.

Methods to improve the brightness of tapered lasers were demonstrated, including optimizing the RW design to improve the modal discrimination, reducing the front facet AR coating, and using a beam spoiler. Through proper calibration, the laser simulator is able to reproduce the experimental operating char-

acteristic of the multisection 1060-nm DBR tapered laser with good accuracy. The DBR tapered laser has stable spectrum,  $M^2$ , and astigmatism versus RW current, which are important for efficient frequency doubling through a nonlinear crystal. The rear reflector, comprised of a passive DBR with an AR-coated back facet, improved the modulation efficiency of the device.

The spatial and spectral brightness of a tapered self-organizing cavity laser was simulated for the first time. This approach provides a mechanism for improving the spectral brightness of lasers without incurring strict alignment constraints. Finally, we demonstrated the simulation of phase-locking in an array of independent tapered lasers through the use of an external Talbot cavity. The in-phase and out-of-phase modes can be selected by changing the tilt of the external mirror

In summary, the complexity of the devices and increasing range of exacting performance specifications make the use of accurate simulation tools essential for the design and optimization of next-generation high-brightness laser diodes and systems. The examples presented demonstrate the need for laser models that include beam propagation and spectral effects. The beam propagation model is needed to reproduce the evolution with temperature and current of the near- and far-field distributions,  $M^2$ , and the astigmatism. It is also needed for diffraction effects, which are important for the phase coupling of emitters. Spectral laser models are needed to evaluate the spectral brightness of a laser and the dependence of the lasing wavelength on temperature and current. Finally, laser models that are able to handle more general structures are needed to simulate a wider range of devices such as multicontact lasers, external cavity lasers, and phase-coupled arrays to address new and emerging applications.

## ACKNOWLEDGMENT

The authors gratefully acknowledge L. Borruel and I. Esquivias for their contribution to the work on tapered lasers in Section III-C and T. M. Benson for useful discussions about optical modeling.

## REFERENCES

- [1] R. Diehl, Ed., *High-Power Diode Lasers: Fundamentals, Technology, Applications*. Berlin, Germany: Springer-Verlag, 2000.
- [2] B. Sumpf, Ferdinand-Braun-Institut für Höchstfrequenztechnik, Berlin, private communication, Oct. 2008.
- [3] J. R. Marcianite and G. P. Agrawal, "Spatio-temporal characteristics of filamentation in broad-area semiconductor lasers: Experimental results," *IEEE Photon. Technol. Lett.*, vol. 10, no. 1, pp. 54–56, Jan. 1998.
- [4] Z. Bao, R. K. DeFreez, P. D. Carleson, C. Largent, C. Moeller, and G. C. Dente, "Spatio-spectral characteristics of a high power, high brightness CW InGaAs/AlGaAs unstable resonator semiconductor laser," *Electron. Lett.*, vol. 29, no. 18, pp. 1597–1599, 1993.
- [5] L. M. Tilton, G. C. Dente, A. H. Paxton, J. Cser, R. K. DeFreez, C. E. Moeller, and D. Depatie, "High power, nearly diffraction-limited output from a semiconductor laser with an unstable resonator," *IEEE J. Quantum Electron.*, vol. 27, no. 9, pp. 2098–2108, Sep. 1991.
- [6] R. Parke, D. F. Welch, A. Hardy, R. Lang, D. Mehuys, S. O'Brien, K. Dzurko, and D. Scifres, "2.0 W CW, diffraction-limited operation of a monolithically integrated master oscillator power-amplifier," *IEEE Photon. Technol. Lett.*, vol. 5, no. 3, pp. 297–300, May 1993.
- [7] E. S. Kintzer, J. N. Walpole, S. R. Chinn, C. A. Wang, and L. J. Missaggia, "High power, strained-layer amplifiers and lasers with tapered gain regions," *IEEE Photon. Technol. Lett.*, vol. 5, no. 6, pp. 605–608, Jun. 1993.

- [8] D. Masanotti and F. Causa, "Optical guiding properties of high-brightness parabolic bow-tie laser arrays," *IEEE J. Quantum Electron.*, vol. 41, no. 7, pp. 909–916, Jul. 2005.
- [9] R. J. Lang, K. M. Dzurko, A. Hardy, S. Demars, A. Schoenfelder, and D. F. Welch, "Theory of grating-confined broad-area lasers," *IEEE J. Quantum Electron.*, vol. 34, no. 11, pp. 2197–2210, Nov. 1998.
- [10] K. Paschke, R. Güther, J. Fricke, F. Bugge, G. Erbert, and G. Tränkle, "High power and high spectral brightness in 1060 nm  $\alpha$ -DFB lasers with long resonators," *Electron. Lett.*, vol. 39, no. 4, pp. 369–370, 2003.
- [11] K. Paschke, A. Bogatov, A. E. Drakin, R. Güther, A. A. Strattonnikov, H. Wenzel, G. Erbert, and G. Tränkle, "Modelling and measurements of the radiative characteristics of high-power  $\alpha$ -DFB lasers," *IEEE J. Sel. Topics Quantum Electron.*, vol. 9, no. 3, pp. 835–43, May/Jun. 2003.
- [12] B. Thestrup, M. Chi, B. Sass, and P. M. Petersen, "High brightness laser source based on polarization coupling of two diode lasers with asymmetric feedback," *Appl. Phys. Lett.*, vol. 82, no. 5, pp. 680–682, 2003.
- [13] S. Wolff, A. Rodionov, V. E. Sherstobitov, and H. Fouckhardt, "Fourier-optical transverse mode selection in external-cavity broad-area lasers: Experimental and numerical results," *IEEE J. Quantum Electron.*, vol. 39, no. 3, pp. 448–458, Mar. 2003.
- [14] D. E. Ackley, "Single longitudinal mode operation of high power multiple-stripe injection lasers," *Appl. Phys. Lett.*, vol. 42, no. 2, pp. 152–154, 1983.
- [15] H. Yang, L. J. Mawst, M. Nesnidal, J. Lopez, A. Bhattacharya, and D. Botez, "10 W near-diffraction-limited peak pulsed power from Al-free, 0.98  $\mu\text{m}$ -emitting phase-locked antiguidded arrays," *Electron. Lett.*, vol. 33, no. 2, pp. 136–137, 1997.
- [16] L. J. Mawst, D. Botez, T. J. Roth, W. W. Simmons, G. Peterson, M. Jansen, J. Z. Wilcox, and J. J. Yang, "Phase-locked array of antiguided lasers with monolithic spatial filter," *Electron. Lett.*, vol. 25, no. 5, pp. 365–366, 1989.
- [17] J. R. Leger, "Lateral mode control of an AlGaAs laser in a Talbot cavity," *Appl. Phys. Lett.*, vol. 55, no. 4, pp. 334–336, 1989.
- [18] F. Camacho, C. J. Hamilton, K. McIlvaney, A. C. Bryce, and J. H. Marsh, "Laser structure for generating high optical power in a single mode waveguide," *Electron. Lett.*, vol. 34, pp. 460–461, Mar. 1998.
- [19] R. J. Lang, A. G. Larsson, and J. G. Cody, "Lateral modes of broad area semiconductor lasers: Theory and experiment," *IEEE J. Quantum Electron.*, vol. 27, no. 3, pp. 312–320, Mar. 1991.
- [20] Z.-M. Li, K. M. Dzurko, A. Delage, and S. P. McAlister, "A self-consistent two dimensional model of quantum well semiconductor lasers: Optimization of a GRIN-SCH SQW laser structure," *IEEE J. Quantum Electron.*, vol. 28, no. 4, pp. 792–803, Apr. 1992.
- [21] M. Grupen and K. Hess, "Simulation of carrier transport and nonlinearities in quantum well laser diodes," *IEEE J. Quantum Electron.*, vol. 34, no. 1, pp. 120–139, Jan. 1998.
- [22] M. A. Alam, M. S. Hybertsen, R. K. Smith, and G. A. Baraff, "Simulation of semiconductor quantum well lasers," *IEEE Trans. Electron Devices*, vol. 47, no. 10, pp. 1917–1925, Oct. 2000.
- [23] G. P. Agrawal, "Fast-Fourier-transform based beam-propagation model for stripe-geometry semiconductor-lasers-inclusion of axial effects," *J. Appl. Phys.*, vol. 56, pp. 3100–3109, 1984.
- [24] M. Mikulla, P. Chazan, A. Schmitt, S. Morgott, A. Wetzel, M. Walther, R. Kiefer, W. Pletschen, J. Braunstein, and G. Weimann, "High-brightness tapered semiconductor laser oscillators and amplifiers with low-modal gain epilayer structures," *IEEE Photon. Technol. Lett.*, vol. 10, no. 5, pp. 654–656, May 1998.
- [25] K. A. Williams, R. W. Penty, I. H. White, D. J. Robbins, F. J. Wilson, J. J. Lewandowski, and B. K. Nayar, "Design of high-brightness tapered laser arrays," *IEEE J. Sel. Topics Quantum Electron.*, vol. 5, no. 3, pp. 822–831, May/Jun. 1999.
- [26] O. Hess, S. W. Koch, and J. V. Moloney, "Filamentation and beam propagation in broad-area semiconductor lasers," *IEEE J. Quantum Electron.*, vol. 31, no. 1, pp. 35–43, Jan. 1995.
- [27] J. V. Moloney, R. A. Indik, and C. Z. Nong, "Full space time simulation for high brightness semiconductor lasers," *IEEE Photon. Technol. Lett.*, vol. 9, no. 6, pp. 731–733, Jun. 1997.
- [28] B. Witzigmann, A. Witzig, and W. Fichtner, "A multidimensional laser simulator for edge-emitters including quantum carrier capture," *IEEE Trans. Electron Devices*, vol. 47, no. 10, pp. 1926–2000, Oct. 2000.
- [29] U. Bandelow, R. Hünlich, and T. Koprucki, "Simulation of static and dynamic properties of edge-emitting multiple-quantum-well lasers," *IEEE J. Sel. Topics Quantum Electron.*, vol. 9, no. 3, pp. 798–806, May/Jun. 2003.
- [30] S. Sujecki, L. Borruel, J. Wykes, P. Moreno, B. Sumpf, P. Sewell, H. Wenzel, T. M. Benson, G. Erbert, I. Esquivias, and E. C. Larkins, "Nonlinear properties of tapered laser cavities," *IEEE J. Sel. Topics Quantum Electron.*, vol. 9, no. 3, pp. 823–834, May/Jun. 2003.
- [31] L. Borruel, S. Sujecki, P. Moreno, J. Wykes, M. Krakowski, B. Sumpf, P. Sewell, S.-C. Auzanneau, H. Wenzel, D. Rodríguez, T. M. Benson, E. C. Larkins, and I. Esquivias, "Quasi-3-D simulation of high-brightness tapered lasers," *IEEE J. Quantum Electron.*, vol. 50, no. 5, pp. 463–472, May 2004.
- [32] P. J. Bream, J. J. Lim, S. Bull, A. V. Andrianov, S. Sujecki, and E. C. Larkins, "The impact of nonequilibrium gain in a spectral laser diode model," *Opt. Quantum Electron.*, vol. 38, pp. 1019–1027, Sep. 2006.
- [33] J. J. Lim, T. M. Benson, and E. C. Larkins, "Design of wide-emitter single-mode laser diodes," *IEEE J. Quantum Electron.*, vol. 41, no. 4, pp. 506–516, Apr. 2005.
- [34] G. R. Hadley, "Multistep method for wide-angle beam propagation," *Opt. Lett.*, vol. 17, pp. 1743–1745, 1992.
- [35] R. Mackenzie, J. J. Lim, S. Bull, S. Sujecki, and E. C. Larkins, "Inclusion of thermal boundary resistance in the simulation of high-power 980 nm ridge waveguide lasers," *Opt. Quantum Electron.*, vol. 40, no. 5/6, pp. 373–377, Apr. 2008.
- [36] R. Mackenzie, J. J. Lim, S. Bull, S. Sujecki, A. J. Kent, and E. C. Larkins, "The impact of hot-phonons on the performance of dilute nitride edge-emitting quantum well lasers," *J. Phys. Conf. Ser.*, vol. 92, no. 012068, pp. 1–4, 2007.
- [37] J. J. Lim, S. Sujecki, and E. C. Larkins, "The influence of surface effects on the simulation of 1.3  $\mu\text{m}$  InGaAsN edge-emitting lasers," presented at the NUSOD, Singapore, Sep. 11–14, 2006, Paper ThPD1.
- [38] R. B. Darling, "Defect-state occupation, Fermi-level pinning, and illumination effects on free semiconductor surfaces," *Phys. Rev. B*, vol. 43, no. 5, pp. 4071–83, 1991.
- [39] I. Vurgaftman, J. R. Meyer, and L. R. Ram-Mohan, "Band parameters for III–V compound semiconductors and their alloys," *J. Appl. Phys.*, vol. 89, no. 11, pp. 5815–5875, 2001.
- [40] J. J. Lim, R. MacKenzie, S. Sujecki, E. C. Larkins, M. Sadeghi, S. M. Wang, Y. Q. Wei, J. S. Gustavsson, A. Larsson, P. Melanen, P. Sipilä, P. Uusimaa, A. A. George, and P. M. Smowton, "Simulation of DQW GaInNAs laser diodes," *IET Optoelectron.*, vol. 1, no. 6, pp. 259–265, 2007.
- [41] K.-H. Hasler, B. Sumpf, P. Adamiec, F. Bugge, J. Fricke, P. Ressel, H. Wenzel, G. Erbert, and G. Tränkle, "5-W DBR tapered lasers emitting at 1060 nm with a narrow spectral linewidth and a nearly diffraction-limited beam quality," *IEEE Photon. Technol. Lett.*, vol. 20, no. 19, pp. 1648–1650, Oct. 2008.
- [42] B. W. Hakki and L. Paoli, "Gain spectra in GaAs double-heterostructure injection lasers," *J. Appl. Phys.*, vol. 46, no. 3, pp. 1299–1306, 1975.
- [43] D. T. Cassidy, "Technique for measurement of the gain spectra of semiconductor diode lasers," *J. Appl. Phys.*, vol. 56, no. 11, pp. 3096–3099, 1984.
- [44] P. Blood, G. M. Lewis, P. M. Smowton, H. Summers, J. Thomson, and J. Lutti, "Characterization of semiconductor laser gain media by the segmented contact method," *IEEE J. Sel. Topics Quantum Electron.*, vol. 9, no. 5, pp. 1275–1282, Sep/Oct. 2003.
- [45] M. Fukuda, *Reliability and Degradation of Semiconductor Lasers and LEDs*. Boston, MA: Artech House, 1991.
- [46] N. C. Gerhardt, M. R. Hofmann, J. Hader, J. V. Moloney, S. W. Koch, and H. Riechert, "Linewidth enhancement factor and optical gain in (GaIn)(NAs)/GaAs lasers," *Appl. Phys. Lett.*, vol. 84, no. 1, pp. 1–3, 2004.
- [47] R. MacKenzie, J. J. Lim, S. Bull, S. Chao, S. Sujecki, M. Sadeghi, S. M. Wang, A. Larsson, P. Melanen, P. Sipilä, P. Uusimaa, and E. C. Larkins, "Measurement of optical gain, effective group index and linewidth enhancement factor in 1.3  $\mu\text{m}$  dilute nitride double-quantum-well lasers," *IET Optoelectron.*, vol. 1, no. 6, pp. 284–288, 2007.
- [48] S. Bull, A. V. Andrianov, J. G. Wykes, J. J. Lim, S. Sujecki, S. C. Auzanneau, M. Calligaro, M. Lecomte, O. Parillaud, M. Krakowski, and E. C. Larkins, "Quantitative imaging of intracavity spontaneous emission distributions using tapered lasers fabricated with windowed n-contacts," *Proc. Inst. Electr. Eng. Optoelectron.*, vol. 153, no. 1, pp. 2–7, Feb. 2006.
- [49] A. E. Siegman and H. Y. Miller, "Unstable optical resonator loss calculations using the Prony method," *Appl. Opt.*, vol. 9, no. 12, pp. 2729–2736, 1970.
- [50] J. M. G. Tijero, H. Odriozola, L. Borruel, I. Esquivias, S. Sujecki, and E. C. Larkins, "Enhanced brightness of tapered laser diodes based on

an asymmetric epitaxial design," *IEEE Photon. Technol. Lett.*, vol. 19, no. 20, pp. 1640–1642, Oct. 2007.

[51] A. Al-Muhanna, L. J. Mawst, D. Botez, D. Z. Garbuzov, R. U. Martinelli, and J. C. Connolly, "High-power (>10 W) continuous-wave operation from 100  $\mu\text{m}$  aperture 0.97  $\mu\text{m}$  emitting Al-free diode lasers," *Appl. Phys. Lett.*, vol. 73, no. 9, pp. 1182–1184, 1998.

[52] M. Krakowski, S. C. Auzanneau, F. Berlie, M. Calligaro, Y. Robert, O. Parillaud, and M. Lecomte, "1W high brightness index guided tapered laser at 980 nm using Al-free active region materials," *Electron. Lett.*, vol. 39, no. 15, pp. 1122–1123, 2003.

[53] B. Thestrup, M. Chi, and P. M. Petersen, "Lateral mode selection in a broad area laser diode by self-injection locking with a mirror stripe," *Proc. SPIE*, vol. 5336, pp. 38–44, 2004.

[54] G. Pauliat, N. Dubreuil, and G. Roosen, "Self-organizing laser cavities," in *Photorefractive Materials and Their Applications 3: Applications* (Springer Series in Optical Science), P. Günter and J.-P. Huignard, Eds. New York: Springer-Verlag, 2007, pp. 253–275.

[55] Z. Zhang, G. Pauliat, J. J. Lim, P. J. Bream, N. Dubreuil, A. J. Kent, E. C. Larkins, and S. Sujecki, "Numerical modeling of high-power self-organizing external cavity lasers," *Opt. Quantum Electron.*, to be published.

[56] G. L. Bourdet, I. Hassiaoui, R. McBride, J. F. Monjardin, H. Baker, N. Michel, and M. Krakowski, "High-power, low-divergence, linear array of quasi-diffraction-limited beams supplied by tapered diodes," *Appl. Opt.*, vol. 46, no. 25, pp. 6297–6301, 2007.

[57] D. Paboeuf, G. Lucas-Leclin, P. Georges, N. Michel, M. Krakowski, J. J. Lim, S. Sujecki, and E. C. Larkins, "Narrow-line coherently-combined tapered laser diodes in a Talbot external cavity with a volume Bragg grating," *Appl. Phys. Lett.*, vol. 93, pp. 211102-1–211102-3, 2008.



1087

1088

1089

1090

1091

1092

1093

1094

1095

1096

1097

1098

1099

1100

1101

1102

1103

1104

1105

1106

1107

1108

1109

1110

1111

1112

1113

1114

1115

1116

1117

1118

1119

1120

1121

1122

1123

**Jun Jun Lim** (S'01–M'04) was born in Batu Pahat, Malaysia, in 1978. He received the B.Eng. degree (with first-class honors) in electronic engineering and the Ph.D. degree from the University of Nottingham, Nottingham, U.K., in 1999 and 2003, respectively.

Since 2004, he has been a Research Fellow at the University of Nottingham, where he was involved in several projects on the modeling of high-speed and high-brightness laser diodes. His current research interests include the simulation, analysis, and design of optoelectronic devices.

**Slawomir Sujecki** was born in Grojec, Poland, in 1969. He received the M.Sc. and Ph.D. degrees in electronic engineering from Warsaw University of Technology, Warsaw, Poland, in 1993 and 1997, respectively.

During 1994–1995, he was a Deutscher Akademischer Austauschdienst Fellow with the Technische Universität Berlin. During 1996–1998, he was a British Council Fellow and then a Royal Society/Wolfson Foundation Fellow at the University of Nottingham, Nottingham, U.K., where he joined the Department of Electrical and Electronic Engineering in April 2001. He started lecturing at Kielce University of Technology, Poland, in 1998. He joined the National Institute of Telecommunications, Poland, in 1999.

**Lei Lang** (S'07) was born in Shijiazhuang, China, in 1981. He received the B.Eng. degree in electronic information engineering from Hebei University of Technology, Tianjin, China, in 2004, and the M.Sc. degree in electronic communications and computer engineering in 2005 from the University of Nottingham, Nottingham, U.K., where he is currently working toward the Ph.D. degree in electrical and electronic engineering.



**Zhichao Zhang** (S'01–M'05) received the B.Eng. and M.Sc. degrees in electrical and electronic engineering from Shandong University, Jinan, China, in 1987 and 1990, respectively. He is currently working toward the Ph.D. degree in electrical and electronic engineering at the University of Nottingham, Nottingham, U.K.

1124  
1125  
1126  
1127  
1128  
1129  
1130  
1131

**David Paboeuf** was born in Nantes, France, in 1984. He received the Engineering degree from the Ecole Supérieure d'Optique, Orsay, France, and the Master's degree in optics and photonics from the University Paris Sud, Orsay, France, in 2006. He is currently working toward the Ph.D. at the Laboratoire Charles Fabry de l'Institut d'Optique, Palaiseau, France, on the development of external cavities for brightness improvement of laser diodes.

1132  
1133  
1134  
1135  
1136  
1137  
1138



**Gilles Pauliat** received the Ph.D. degree from the University Paris Sud, Orsay, France, in 1986.

He was a Postdoctoral Researcher in the Quantum Electronic Laboratory, Federal Polytechnic School, Zurich, for one year. He joined the Centre National de la Recherche Scientifique, Palaiseau, France, where he is currently the Head of the Matériaux non Linéaires et Applications Research Group, Laboratoire Charles Fabry de l'Institut d'Optique. His current research interests include high-density data storage with holographic memories and self-organizing

1139  
1140  
1141  
1142  
1143  
1144  
1145  
1146  
1147  
1148  
1149

laser cavities.

Dr. Pauliat is a member of the Board of Directors of the European Optical Society.

1150  
1151  
1152  
1153



1109

1110

1111

1112

1113

1114

1115

1116

1117

1118

1119

1120

1121

1122

1123

1124

1125

1126

1127

1128

1129

1130

1131

1132

1133

1134

1135

1136

1137

1138

1139

**Gaëlle Lucas-Leclin** was born in Guérande, France. She received the M.Sc. degree in optics from the Ecole Supérieure d'Optique, Orsay, France, in 1994, and the Ph.D. degree from the University Paris XI, Orsay, in 1998.

Since 1998, she has been an Assistant Professor at the Institut d'Optique Graduate School, Centre National de la Recherche Scientifique (CNRS), University Paris Sud, Palaiseau, France, where she is with the Laboratoire Charles Fabry de l'Institut d'Optique, and is in charge of the semiconductor physics and semiconductor sources lectures. Her current research interests include extended cavity laser diodes and vertical external cavity semiconductor lasers.

1154  
1155  
1156  
1157  
1158  
1159  
1160  
1161  
1162  
1163

Q8



**Patrick Georges** was born in Metz, France, in 1962. He received the Engineering degree from the Ecole Supérieure d'Optique, Orsay, France, in 1985, and the Ph.D. degree in 1989 on colliding pulses mode locked dye lasers at different wavelengths and pulse compression.

He is currently a Senior Scientist at the Centre National de la Recherche Scientifique (CNRS), Palaiseau, France, where he is with the Institut d'Optique, and leads the Lasers and Biophotonics Group, Laboratoire Charles Fabry de l'Institut

1164  
1165  
1166  
1167  
1168  
1169  
1170  
1171  
1172  
1173  
1174

Q9

1175 d'Optique. His current research interests include diode-pumped solid-state  
1176 lasers, new laser materials, picosecond and femtosecond lasers, high-brightness  
1177 laser diodes, fiber amplifier systems, and applications of picosecond or fem-  
1178 tosecond lasers in biophotonics (time-resolved fluorescence spectroscopy, two-  
1179 photon microscopy).

1180 Dr. Georges is a Fellow of the Optical Society of America.  
1181

1182 **Roderick C. I. MacKenzie** received the M.Eng. and Ph.D. degrees in electronic  
1183 engineering from the University of Nottingham, Nottingham, U.K., in 2004 and  
1184 2008, respectively.

1185 He was engaged in the measurement and simulation of 1.3- $\mu\text{m}$  dilute ni-  
1186 tride laser diodes, focusing specifically on self-heating and its impact on de-  
1187 vice performance. He is currently with the University of Nottingham. His cur-  
1188 rent research interests include measurement of device gain and thermographic  
1189 imagery.  
1190

1191 **Philip Bream** received the M.Eng. degree (with first-class honors) in electronic  
1192 engineering and the Ph.D. degree from the University of Nottingham, Notting-  
1193 ham, U.K., in 2002 and 2006, respectively.

1194 He was engaged in research on nonequilibrium carrier dynamics and gain  
1195 in semiconductor quantum wells (QWs). He is currently with the University of  
1196 Nottingham.  
1197

1198  
1199  
1200  
1201  
1202  
1203  
1204  
1205  
1206  
1207  
1208  
1209  
1210



**Stephen Bull** (S'01–M'04) received the M.Eng. de-  
gree (with first-class honors) in electronic engineer-  
ing with German and the Ph.D. degree from the Uni-  
versity of Nottingham, Nottingham, U.K., in 2001  
and 2004, respectively.

He is currently a Postdoctoral Research Fellow at  
the University of Nottingham. His current research  
interests include spectroscopic imaging techniques  
for the characterization of laser diodes, including ex-  
ternal cavity lasers, the validation of simulation tools  
using these techniques, and the degradation dynam-

ics of high-power laser bars.

1211  
1212  
1213  
1214  
1215  
1216  
1217  
1218  
1219  
1220  
1221  
1222  
1223  
1224



**Karl-Heinz Hasler** was born in Ludwigslust, Ger-  
many, in 1952. He received the Dipl.-Phys. degree  
from Humboldt University, Berlin, Germany, in 1978.

From 1978 to 1991, he was with the semicon-  
ductor industry, where he was involved in the de-  
velopment of LEDs, near-infrared response (NIR)  
detectors, and laser diodes. From 1992 to 2000, he  
was with the Astrophysikalisches Institut Potsdam  
(AIP), where he was involved in the field of magne-  
tohydrodynamics and helioseismology. Since 2000,  
he has been with the Ferdinand-Braun-Institut für  
Höchstfrequenztechnik, Berlin, where he is engaged in the development of  
high-power, high-brightness semiconductor lasers.



**Bernd Sumpf** was born in Berlin, Germany, in 1958. He received the Diploma in physics and the Ph.D. degree from Humboldt-Universität Berlin, Berlin, in 1981 and 1987, respectively.

He was engaged in research on lead salt diode lasers for spectroscopic applications. From 1993 till 1997, he was with the Technische Universität Berlin, where he was engaged in research on high-resolution spectroscopy and difference-frequency generation. In 1997, he received the postdoctoral lecture qualification. Since 2000, he has been with the Ferdinand-Braun-Institut für Höchstfrequenztechnik, Berlin, where he is involved in the field of high-power and high-brightness diode lasers.

**Hans Wenzel** received the Diploma and Doctoral degrees in physics from Humboldt University, Berlin, Germany, in 1986 and 1991, respectively.

He was engaged in research on electrooptical modeling of semiconductor lasers. From 1991 to 1994, he was involved in a research project on the 3-D simulation of DFB lasers. In 1994, he joined the Ferdinand-Braun-Institut für Höchstfrequenztechnik, Berlin, where he is engaged in the development of high-brightness semiconductor lasers. His current research interests include the analysis, modeling, and simulation of optoelectronic devices.



**Götz Erbert** (M'95) received the Diploma in physics from Humboldt University, Berlin, Germany, in 1973, and the Doctoral degree in physics from the Academy of Sciences of the German Democratic Republic (GDR), in 1990.

From 1973 to 1991, he was with the Academy of Sciences, where he was first engaged in the field of integrated optics and dynamic holographic gratings in semiconductors, and later in semiconductor lasers. In 1992, he joined the Ferdinand-Braun-Institut für Höchstfrequenztechnik, Berlin, where he has been engaged in the optoelectronic activities since 1996. He is also involved in research on high-power semiconductor lasers based on GaAs using strained-layer quantum-well active regions in the wavelength range from 650 to 1200 nm.

**Birgitte Thestrup** received the Ph.D. degree in physics from the University of Copenhagen, Copenhagen, Denmark, in 1999.

She is currently a Senior Scientist in the Department of Photonics Engineering, Technical University of Denmark, Roskilde, Denmark. From 2001 to 2007, she was with the Diode Laser Group, Optics and Plasma Research Department, Risoe National Laboratory, Denmark, where she also worked on laser-induced plasmas. She is the author or coauthor of more than 30 papers and one book. She holds two patents. Her current research interests include external cavity diode laser systems for industrial and medical applications, and high-quality and energy-efficient solid-state lighting systems for specific applications.

**Paul Michael Petersen** received the M.Sc. degree in engineering and the Ph.D. degree in physics from the Technical University of Denmark (DTU), Roskilde, Denmark, in 1983 and 1986, respectively.

He has 15 years of research experience in laser physics, nonlinear optics, and optical measurement techniques, and has headed several collaborative research projects within laser physics. He is currently the Head of light sources and industrial sensors in the Department of Photonics Engineering, DTU. He is also an Adjunct Professor of optics at Niels Bohr Institute, Copenhagen University, Copenhagen, Denmark. He is the Head of the Center for Biomedical Optics and New Laser Systems. He has authored or coauthored more than 100 scientific publications and nine patents. He has 20 years of teaching experience in optics, quantum optics, laser technique, and nonlinear optics.

Q1

Q1

1287 **Nicolas Michel**, photograph and biography not available at the time of  
1288 publication.  
1289

1290 **Michel Krakowski**, photograph and biography not available at the time of  
1291 publication.  
1292



**Eric C. Larkins** received the B.S.E.E. degree from 1293  
Cornell University, Ithaca, NY, in 1980, and the 1294  
M.S.E.E. degree and the Ph.D. degree in electrical 1295  
engineering from Stanford University, Stanford, CA, 1296  
in 1985 and 1991, respectively. 1297

In 1994, joined the Department of Electrical and 1298  
Electronic Engineering, University of Nottingham, 1299  
Nottingham, U.K., where he became a Professor of 1300  
optoelectronics in 2002. From 1991 to 1994, he was a 1301  
Visiting Scientist at the Fraunhofer Institut für Ange- 1302  
wandte Festkörperphysik, Freiburg, Germany. His 1303

current research interests include laser diodes, and functional and nanopho- 1304  
tonic devices. 1305  
1306

## QUERIES

- 1308 Q1: Author: Please provide the IEEE membership details (membership grades and years in which these were obtained), if any,  
1309 for all the authors except J. J. Lim, L. Lang, Z. Zhang, S. Bull, and G. Erbert.
- 1310 Q2: Author: Please check the funding information in the first footnote. Is it Ok as edited?
- 1311 Q3: Author: A table has been referred to in this sentence, whereas the same is not provided. Please check.
- 1312 Q4: Author: Is the edit OK?
- 1313 Q5: Author: Please check Ref. [54] if it is OK as typeset.
- 1314 Q6: Author: Please update Ref. [55] if possible.
- 1315 Q7: Author: Please check the IEEE membership details of Z. Zhang for correctness.
- 1316 Q8: Author: Please check the affiliations of G. Lucas-Leclin and P. Georges in their biographies. Are they OK as typeset?
- 1317 Q9: Author: Please provide the university name from where P. Georges received the Ph.D. degree.
- 1318 Q10: Author: Please specify what does “with German” indicate in the biography of S. Bull.
- 1319 Q11: Author: Please specify if the postdoctoral lecture qualification refers to an academic degree received by B. Sumpf.
- 1320 Q12: Author: Please provide the location (city and country names) of the Academy of Sciences of the German Democratic  
1321 Republic (GDR).
- 1322 Q13: Author: Please specify if the Center for Biomedical Optics and New Laser Systems is a subdivision of Copenhagen  
1323 University.

# Design and Simulation of Next-Generation High-Power, High-Brightness Laser Diodes

Jun Jun Lim, *Member, IEEE*, Slawomir Sujecki, Lei Lang, *Student Member, IEEE*, Zhichao Zhang, *Member, IEEE*, David Paboeuf, Gilles Pauliat, Gaëlle Lucas-Leclin, Patrick Georges, Roderick C. I. MacKenzie, Philip Bream, Stephen Bull, *Member, IEEE*, Karl-Heinz Hasler, Bernd Sumpf, Hans Wenzel, Götz Erbert, *Member, IEEE*, Birgitte Thestrup, Paul Michael Petersen, Nicolas Michel, Michel Krakowski, and Eric C. Larkins

(Invited Paper)

**Abstract**—High-brightness laser diode technology is progressing rapidly in response to competitive and evolving markets. The large volume resonators required for high-power, high-brightness operation makes their beam parameters and brightness sensitive to thermal- and carrier-induced lensing and also to multimode operation. Power and beam quality are no longer the only concerns for the design of high-brightness lasers. The increased demand for these technologies is accompanied by new performance requirements, including a wider range of wavelengths, direct electrical modulation, spectral purity and stability, and phase-locking techniques for coherent beam combining. This paper explores some of the next-generation technologies being pursued, while illustrating the growing importance of simulation and design tools. The paper begins by investigating the brightness limitations of broad-area laser diodes, including the use of asymmetric feedback to improve the modal discrimination. Next, tapered lasers are considered, with an emphasis on emerging device technologies for applications requiring electrical modulation and high spectral brightness. These include two-contact lasers, self-organizing cavity lasers, and a phase-locked laser array using an external Talbot cavity.

Manuscript received November 8, 2008; revised December 2, 2008; accepted December 9, 2008. First published; current version published. This work was supported in part by the European Commission under Project IST-035266, Project IST-511722 ([www.brighter.eu](http://www.brighter.eu)), Project ULTRABRIGHT (IST-1999-10356), and Project POWERPACK (IST-2000-29447). The work of R. MacKenzie and P. J. Bream was supported by the Engineering and Physical Sciences Research Council, U.K. The work of D. Paboeuf was supported by the French Ministry of Defense (Délégation Générale de l'Armement).

J. J. Lim, S. Sujecki, L. Lang, Z. Zhang, R. MacKenzie, P. Bream, S. Bull and E. C. Larkins are with the Department of Electrical and Electronic Engineering, University of Nottingham, Nottingham NG7 2RD, U.K. (e-mail: [jun.lim@nottingham.ac.uk](mailto:jun.lim@nottingham.ac.uk); [slawomir.sujecki@nottingham.ac.uk](mailto:slawomir.sujecki@nottingham.ac.uk); [eexl12@nottingham.ac.uk](mailto:eexl12@nottingham.ac.uk); [eezz2@nottingham.ac.uk](mailto:eezz2@nottingham.ac.uk); [r.c.i.mackenzie@googlemail.com](mailto:r.c.i.mackenzie@googlemail.com); [phil.bream@gmail.com](mailto:phil.bream@gmail.com); [steve.bull@nottingham.ac.uk](mailto:steve.bull@nottingham.ac.uk); [eric.larkins@nottingham.ac.uk](mailto:eric.larkins@nottingham.ac.uk)).

D. Paboeuf, G. Pauliat, G. Lucas-Leclin, and P. Georges are with the Laboratoire Charles Fabry de l'Institut d'Optique, Centre National de la Recherche Scientifique (CNRS), University Paris Sud, 91127 Palaiseau, France (e-mail: [david.paboeuf@institutoptique.fr](mailto:david.paboeuf@institutoptique.fr); [gilles.pauliat@iota.u-psud.fr](mailto:gilles.pauliat@iota.u-psud.fr); [gaelle.lucas-leclin@institutoptique.fr](mailto:gaelle.lucas-leclin@institutoptique.fr); [patrick.georges@iota.u-psud.fr](mailto:patrick.georges@iota.u-psud.fr)).

K.-H. Hasler, B. Sumpf, H. Wenzel, and G. Erbert are with the Ferdinand-Braun-Institut für Höchstfrequenztechnik, 12489 Berlin, Germany (e-mail: [karl-heinz.hasler@fbh-berlin.de](mailto:karl-heinz.hasler@fbh-berlin.de); [bernd.sumpf@fbh-berlin.de](mailto:bernd.sumpf@fbh-berlin.de); [hans.wenzel@fbh-berlin.de](mailto:hans.wenzel@fbh-berlin.de); [goetz.erbert@fbh-berlin.de](mailto:goetz.erbert@fbh-berlin.de)).

B. Thestrup and P. M. Petersen are with the DTU Fotonik, Technical University of Denmark, 4000 Roskilde, Denmark (e-mail: [birgitte.thestrup@risoe.dk](mailto:birgitte.thestrup@risoe.dk); [paul.michael.petersen@risoe.dk](mailto:paul.michael.petersen@risoe.dk)).

N. Michel and M. Krakowski are with Alcatel-Thales III-V Lab, 91767 Palaiseau, France (e-mail: [nicolas.michel@3-5lab.fr](mailto:nicolas.michel@3-5lab.fr); [michel.krakowski@3-5lab.fr](mailto:michel.krakowski@3-5lab.fr)).

Color versions of one or more of the figures in this paper are available online at <http://ieeexplore.ieee.org>.

Digital Object Identifier 10.1109/JSTQE.2008.2011286

**Index Terms**—External cavity laser diodes, high-brightness lasers, high-power lasers, laser simulation, modal discrimination, phase-coupled laser diode arrays, self-organizing laser.

## I. INTRODUCTION

THERE is a growing demand for high-power diode lasers in a variety of fields today. Traditionally, the largest application for high-power diode lasers has been as pump sources for solid-state lasers, fiber amplifiers in telecommunications, and more recently, fiber lasers [1]. Diode lasers are used because they have a high electrical to optical conversion efficiency and can be designed to fit the absorption band of these applications. They have advantages in terms of reliability, compactness, and cost. In recent years, high-brightness laser technology has been strongly driven by an increasing number and variety of applications, including medicine (e.g., photodynamic therapy, fluorescence spectroscopy, and surgery), display technology (laser displays and mobile projectors), free-space optical wireless communication, and direct-diode materials processing.

As the range of applications increases, the performance demands on high-brightness laser diodes are also becoming more stringent. Performance requirements for next-generation high-brightness laser diodes include good modulation performance, narrow spectral linewidth, and nearly diffraction-limited powers of 20–100 W. At the same time, laser simulation tools are becoming essential for achieving the desired performance. These tools provide an understanding of the physics and operation of the device and permit the exploration of novel designs and concepts needed to provide more than an incremental improvement in the device performance.

In this paper, we provide an overview of recent trends in the design and simulation of next-generation high-power, high-brightness laser diodes. Section II begins with a cursory discussion of the applications, performance requirements, and current state of the art of high-brightness diode lasers and systems, followed by an overview of approaches for achieving high power and brightness, and a discussion of the increased role and demands on simulation and design tools. Section III briefly describes the high-brightness laser diode simulation tools used in this paper and how the simulation parameters are calibrated and validated. Section IV considers a few specific examples to provide insight into the approaches and design considerations

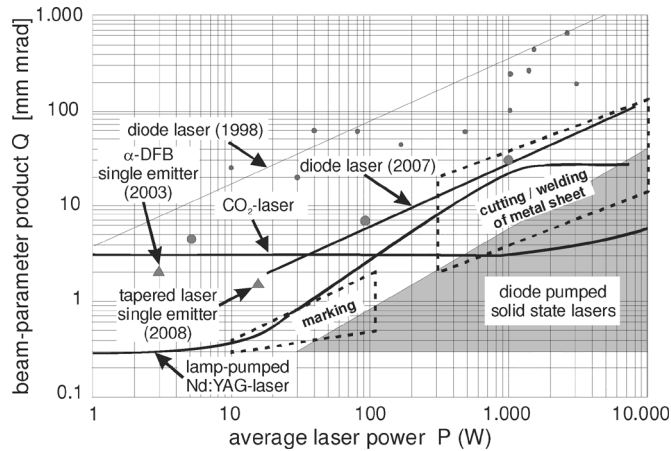


Fig. 1. Typical beam parameters for different laser systems and for applications in materials processing. (Courtesy P. Loosen, Fraunhofer Institute for Laser Technology.)

68 currently being pursued. These examples include an asymmetric  
69 feedback external cavity laser, a multiple section tapered laser,  
70 a self-organizing cavity laser, and a laser array in an external  
71 Talbot cavity.

## 72 II. BACKGROUND

### 73 A. Applications and Performance Requirements

74 The most important performance target for high-power laser diodes  
75 continues to be the combination of power and beam  
76 quality, known as brightness. The brightness of a laser beam  
77 is defined as the optical power density  $P$  per emission area  $A$  and  
78 per unit of solid angle  $\Omega$  in the output beam. The brightness  $B$   
79 describes how well the optical power can be collimated into a  
80 narrow beam, and can be described as

$$B = \frac{P}{A\Omega} \propto \frac{P}{Q^2} = \frac{P}{(\omega_0\theta_f)^2} \propto \frac{P}{(M^2)^2}. \quad (1)$$

81 The brightness is also related to  $M^2$  and the *beam parameter*  
82 *product*  $Q$  (product of the minimum beam diameter  $\omega_0$  and its  
83 divergence  $\theta_f$ ). The current state of the art for power and bright-  
84 ness of diode lasers and systems is shown in Fig. 1. The compar-  
85 ison with other high-power lasers (e.g. CO<sub>2</sub> and diode/lamp  
86 pumped solid-state lasers) in Fig. 1 shows that diode lasers are  
87 approaching the level of power and brightness achievable by the  
88 other laser systems.

89 As the variety of applications for high-brightness laser diodes  
90 increases, so does the range of performance specifications,  
91 which generally depend upon the intended application. For  
92 example, most high-brightness diode lasers operate at 808 or  
93 980 nm, but other wavelengths are emerging for applica-  
94 tions such as medicine, displays, printing, and mark-  
95 ing/cutting/welding of plastics. Display and optical wireless  
96 applications also require that the laser has a controlled emission  
97 spectrum and beam quality during high-frequency modulation  
98 (0.1–1 GHz) and a large modulation efficiency (power/current  
99 ratio). Applications requiring frequency doubling (e.g., blue and  
100 green lasers for displays, blue/near-UV lasers for fluorescence

spectroscopy) are driving the pursuit of ultimate brightness com- 101  
bined with spectral purity/stability. The efficiency of frequency 102  
doubling depends on the square of the optical electric field and 103  
requires a nearly diffraction-limited beam to achieve a high 104  
optical field intensity and good beam coherence. As indicated 105  
in Fig. 1, applications involving the direct processing of materi- 106  
als are driving the development of laser systems with high 107  
output power and brightness. These include marking ( $P = 10$ – 108  
100 W,  $Q = 0.3$ –2 mm-mrad), cutting, and welding of sheet 109  
metal ( $P = 0.3$ –10 kW,  $Q = 2$ –100 mm-mrad). Currently, the 110  
best power and brightness results for single emitters are from 111  
tapered lasers ( $P = 12$  W,  $Q = 1.5$  mm-mrad [2]). Generally, 112  
power levels greater than 10–20 W must be achieved by combin- 113  
ing the beams from multiple emitters. For the most demanding 114  
high-power applications, the beams must be combined coher- 115  
ently through stable phase-locking of an array of emitters to 116  
achieve power densities  $>10^5$  W/mm<sup>2</sup>. 117

### 118 B. Approaches for High Power and Brightness

119 The simplest laser diode to fabricate is the broad-area laser 120  
diode (BA-LD), which is still widely used to provide high 121  
power with high efficiency. However, they are known to have 122  
a large slow-axis far-field divergence and poor beam quality— 123  
primarily due to beam filamentation. This process has been 124  
studied intensively both experimentally and theoretically, e.g., 125  
in [3] and references therein. Spatial filamentation leads to a 126  
complicated multilobed near-field pattern, which negatively af- 127  
fects the brightness. Furthermore, filamentation is sometimes 128  
accompanied by unwanted periodic or chaotic variations in the 129  
laser power. Hence, BA-LDs are fundamentally unsuitable for 130  
high-brightness applications without some form of filtering to 131  
provide a mechanism for modal discrimination.

132 To overcome the deficiencies of the BA-LD, numerous de- 133  
signs have been proposed to increase the brightness of high- 134  
power laser diodes. One technique adopted from traditional non- 135  
diode lasers is the unstable resonator concept, such as lasers with 136  
a curved mirror resonator [4], [5]. Lasers with multiple sections 137  
have also been explored to increase the brightness, including 138  
master oscillator power amplifier (MOPA) lasers [6], tapered 139  
lasers [7], and bow-tie lasers [8]. The  $\alpha$ -DFB laser showed early 140  
promise [9], but has only achieved an output power of 3 W with 141  
 $M^2 = 3.2$  ( $Q = 2$  mm-mrad) from a single emitter [10], [11]. 142  
The far-field divergence of a BA-LD can also be reduced using 143  
asymmetric feedback from an external cavity to a specific lateral 144  
mode [12], [13].

145 The easiest way to scale the power from laser diodes is to 146  
employ an array of emitters. To achieve high brightness, how- 147  
ever, phase locking is needed to coherently combine their out- 148  
put beams. Common approaches include positive guiding [14] 149  
(evanescent-wave coupling) and antiguiding (leaky-wave cou- 150  
pling) arrays [15], with the latter showing stronger in-phase 151  
coupling. Phase locking can also be achieved through diffrac- 152  
tive coupling using the Talbot effect. This can be done mono- 153  
lithically [16] or using an external cavity [17]. Another phase 154  
locking method using diffractive coupling employs a multimode 155  
interference (MMI) coupling section [18].

### 156 C. Role of Simulation and Design Tools

157 Numerous laser models have been reported in the literature.  
 158 These models vary in complexity and have typically been de-  
 159 veloped to target specific applications. Early models ignored  
 160 current spreading in the cladding layers of the device and typi-  
 161 cally solved the 1-D unipolar diffusion equation in the lateral  
 162 direction. These tools were used to explain spatial hole burn-  
 163 ing and carrier lensing effects and were also applied to explain  
 164 the filamentary nature of broad-area lasers [19]. Later, full 2-D  
 165 cross-sectional models were introduced, which were borrowed  
 166 from modeling techniques developed for silicon device simula-  
 167 tors [20]–[22]. These 2-D cross-sectional laser models solved  
 168 the electrical, thermal, and optical problems self-consistently,  
 169 making them more accurate—especially for ridge waveguide  
 170 (RW) lasers. However, since they only considered a single cross  
 171 section, they were unsuitable for longitudinally nonuniform  
 172 structures and high-power operation, where longitudinal spa-  
 173 tial hole burning and carrier/thermal lensing effects are signifi-  
 174 cant. Early models based on beam propagation methods (BPMs)  
 175 were developed to handle nonuniform structures, but typically  
 176 only solved the 1-D electrical problem in the lateral direction  
 177 [23]–[25]. Sophisticated models were also introduced that  
 178 solved the spatiotemporal dynamics of the lasers, but these  
 179 models also used a 1-D electrical model in the lateral direc-  
 180 tion [26], [27]. Quasi-3-D models were introduced in [28]  
 181 and [29], with the optical model separated into 1-D in the lon-  
 182 gitudinal direction and 2-D in the transverse cross section. The  
 183 combination of the 2-D cross-section electrothermal model with  
 184 the BPM was then introduced [30], [31]. By including the longi-  
 185 tudinal direction and accounting for current and heat spreading  
 186 effects, these models have become predictive and useful design  
 187 tools for high-brightness lasers. By including the spectral and/or  
 188 the dynamic properties of the laser, design tools are reaching  
 189 new levels of accuracy and reliability.

### 190 III. LASER DIODE MODEL AND ITS CALIBRATION

191 Ideally, to capture the complete physical behavior of the de-  
 192 vice, laser models should include all three spatial dimensions  
 193 of the device, as well as their spectral and/or dynamic behav-  
 194 ior. Short design cycles are often needed to respond to market  
 195 demands, so compromises must be made between accuracy and  
 196 efficiency. Models with reduced dimensionality and/or complex-  
 197 ity are often useful early in the design cycle, where the emphasis  
 198 is on designing first-generation devices. In the design optimiza-  
 199 tion stage, it becomes more important to model the device more  
 200 accurately.

201 For advanced simulations and design optimization, the char-  
 202 acteristics to be modeled (apart from the light-current charac-  
 203 teristic) include the near- and far-field patterns, the  $M^2$  beam  
 204 quality factor, and the astigmatism—all as a function of cur-  
 205 rent. In addition to these external device characteristics, internal  
 206 properties such as the temperature and carrier and photon den-  
 207 sity distributions are needed for a physical understanding of  
 208 the operation of the device. At very high power densities, even  
 209 nonequilibrium phenomena like carrier heating and spectral hole  
 210 burning can be significant. This requires careful calibration of

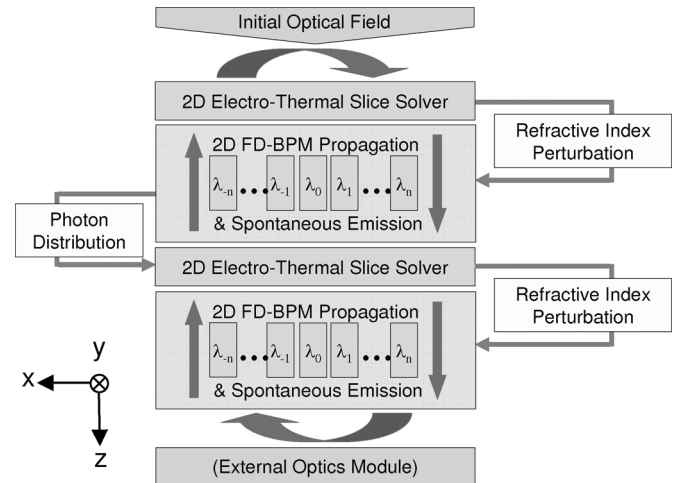


Fig. 2. Flow diagram of the 2.5-D spectral laser model.

the materials parameters and extensive validation of the device 211  
 models against measured results. 212

This section begins by describing our simulation tools for 213  
 high-brightness laser diodes. This is followed by a description 214  
 of initial calibration procedures and ends with a discussion of 215  
 advanced validation for more comprehensive simulations. 216

#### A. Description 217

Our principal model for high-brightness lasers consists of a 218  
 2.5-D spectral laser model [32]. This model has been derived 219  
 from a monochromatic 2.5-D laser model [33]. The term 2.5-D 220  
 is used to indicate that the model is quasi-3-D, consisting of 221  
 2-D optical ( $x$ - $z$ ) and electrothermal ( $x$ - $y$ ) solvers (the flow 222  
 diagram and definition of axes are given in Fig. 2). The flow 223  
 of carriers and heat in the longitudinal direction is neglected. 224  
 Comparison with a full 3-D electrothermal model [30], [31] 225  
 has shown that this approximation is valid for structures that 226  
 are slowly varying in the longitudinal direction (as investigated 227  
 in this paper). The electrothermal model is coupled to the opti- 228  
 cal model through stimulated emission/absorption and spon- 229  
 taneous emission coupling and also through the carrier- and 230  
 temperature-induced changes in the complex refractive index. 231  
 The optical model propagates multiple wavelengths between 232  
 electrothermal slices using the 2-D wide-angle finite-difference 233  
 BPM (WA-FD-BPM) [34], the effective index approximation, 234  
 and PML boundary conditions. The BPM projects the lateral 235  
 modes onto the same field. Through mode competition, the 236  
 multiwavelength model responds to both spectral and spatial 237  
 variations in the gain distribution. The electrothermal and opti- 238  
 cal models are solved self-consistently, following an accelerated 239  
 Fox–Li iterative approach [23]. 240

The electrical model calculates the bipolar carrier density pro- 241  
 files for 2-D transverse slices along the laser cavity and includes 242  
 drift-diffusion transport and the capture/escape processes be- 243  
 tween the bound and unbound states of the quantum well(s) 244  
 (QWs). The thermal model, based upon the solution of the 245  
 Boltzmann transport equation for heterostructures, solves the 246  
 lattice heat flux equation (including thermal boundary 247

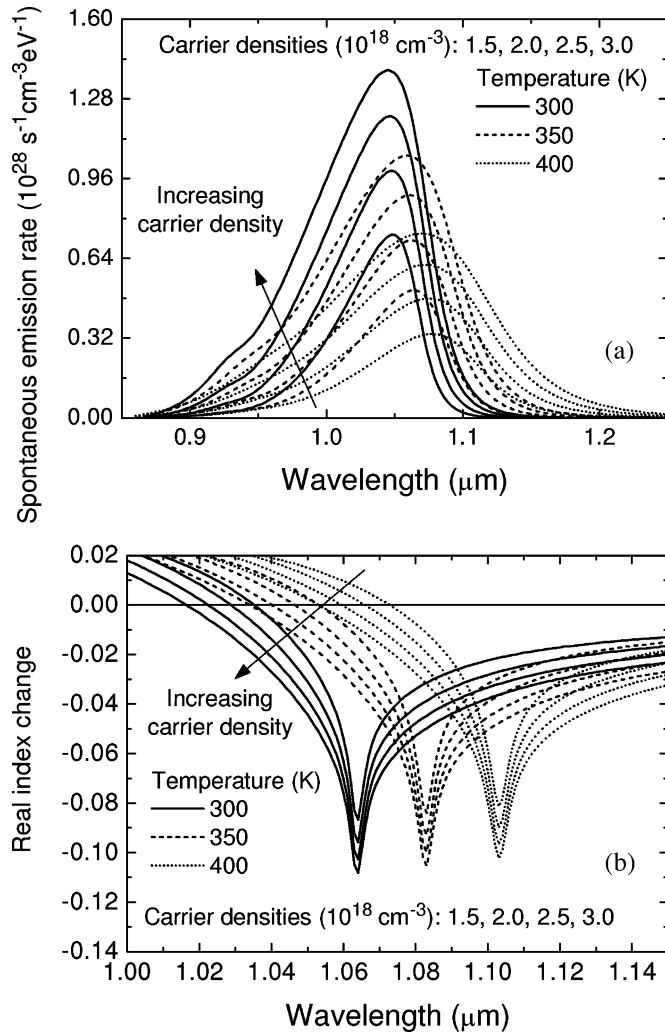


Fig. 3. (a) Spontaneous emission and (b) real index change spectra for a range of carrier densities and temperature.

resistances) and all relevant heat sources [35]. In addition to the classical heat model, our thermal solver also provides the option of including nonequilibrium effects by solving for the electron, hole, and local oscillator (LO) phonon temperatures in the QW active region(s) [36]. Surface recombination, Fermi level pinning, and surface depletion are included self-consistently [37], [38]. The photon density distribution at each wavelength is provided as an input to the electrical solver. The gain, spontaneous emission, and change in refractive index spectra, which are dependent on the electron and hole densities, temperature, and photon density, are parameterized in a table and used by the optical model to propagate the fields to the next electrothermal slice.

An accurate spectral simulation requires a reliable model for the gain, spontaneous emission, and carrier-induced refractive index change. Our model uses the parabolic approximation for the conduction band and a  $4 \times 4$   $\mathbf{k} \cdot \mathbf{p}$  band mixing model for the valence band in order to calculate the QW band structure. Examples of the spontaneous emission and carrier-induced index change spectra for a 1060-nm QW are shown in Fig. 3. The band parameters were taken from the standard literature [39] and a

band offset ratio of  $\Delta E_c / \Delta E_g = 0.65$  was used. The spontaneous emission spectra were calculated and convolved with a sech linewidth broadening function, as shown in Fig. 3(a). The intraband relaxation lifetime was taken to vary as a function of carrier density and temperature [40]. Next, the gain spectra were obtained by transforming the spontaneous emission spectra using Einstein's relation. The spectral change in the real index of the QW [Fig. 3(b)] was calculated with the Kramers–Kronig relation from the change in the calculated gain spectra, but does not include smaller changes due to intraband absorption. The effective index change is obtained by multiplying the QW index change by the confinement factor, but more accurate treatments should also account for index changes in the waveguide and cladding layers.

The 2.5-D spectral laser model can also be coupled to an external optics module to simulate external cavity lasers. This is particularly relevant for high-power lasers, where external cavities can be used to improve the beam quality of the laser. As the output facet reflectivity of a high-brightness laser diode is often  $< 1\%$ , this scheme can also be used to evaluate the impact of back reflections from the external optics.

Various simplifications of the 2.5-D spectral laser model exist to increase the efficiency of the simulation, depending on the application. These include isothermal, unipolar, monochromatic, and reduced dimensionality models, which are useful for obtaining qualitative results or when the size of the problem becomes computationally intractable. For example, the 1.5-D model is used in Section III to simulate large structures such as laser arrays and (in some cases) when the spectral characteristics of the device are required. The 1.5-D model is quasi-2-D in the sense that the optical problem is solved in the  $x$ - $z$  plane and the electrical problem is reduced to 1-D in the lateral ( $x$ ) direction. The 1-D electrical model solves the unipolar carrier-diffusion equation given as

$$D_a \frac{d^2}{dx^2} n(x) = -\frac{J(x)}{qd} + R_{nr}(x) + R_{spn}(x) + v_g g(x) S(x) \quad (2)$$

where  $D_a$ ,  $J$ ,  $d$ ,  $n$ ,  $R_{nr}$ ,  $R_{spn}$ ,  $g$ , and  $S$  are the ambipolar diffusion coefficient, injection current density, active region thickness, carrier density, nonradiative recombination, spontaneous emission rate, optical gain, and photon density, respectively. The spontaneous emission rate and optical gain data are the same as those used in the 2-D bipolar electrical model for consistency and accuracy. In the 1-D electrical model,  $J(x)$  is constant inside the stripe and zero outside the stripe.

The laser model used in this paper improves upon previous beam-propagation-based laser models [30], [31], [33] by solving the emission spectra of the laser and including the spectral dependence of the gain, spontaneous emission, and carrier-induced refractive index change. It also has additional flexibility by including the option to couple to external optics modules to allow the simulation of a variety of external cavity lasers.

## B. Calibration Procedure

Proper calibration is essential for a predictive laser model. A carefully calibrated simple model can be even more predictive

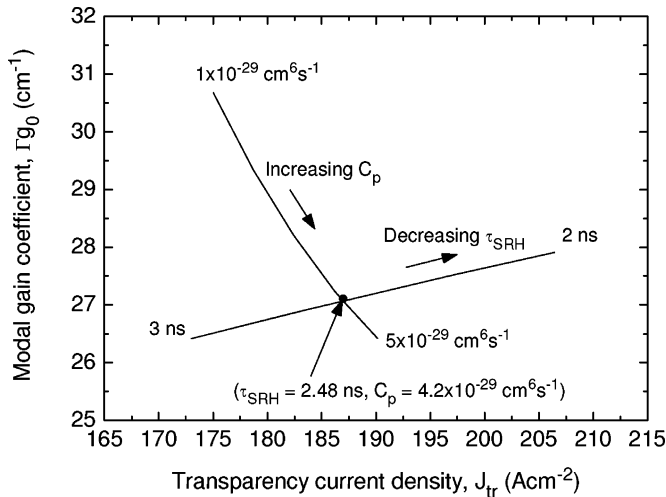


Fig. 4.  $\Gamma_{g0}$  and  $J_{tr}$  dependence with  $\tau_{SRH}$  and  $C_p$ .

321 than a poorly calibrated sophisticated model. In this section, an  
 322 example of the calibration of the laser model is presented for a  
 323 device emitting at 1060 nm [41].

324 The first step is to calibrate the simulated gain and spon-  
 325 taneous emission spectra with gain spectra measured using the  
 326 Hakki–Paoli [42], Cassidy [43], or segmented contact [44] meth-  
 327 ods. This usually involves slight adjustments to the QW energy  
 328 levels and linewidth broadening.

329 Next, the internal loss is determined. The internal loss can be  
 330 obtained from length-dependent measurements of the external  
 331 differential efficiency of BA-LDs. For this structure, the internal  
 332 loss  $\alpha_i$  was  $0.9 \text{ cm}^{-1}$ . At long wavelengths, the internal loss  
 333 is dominated by intervalence band absorption. Therefore, the  
 334 absorption cross section for holes in the QW was used as a  
 335 fitting parameter and a value of  $3 \times 10^{-17} \text{ cm}^2$  gave an internal  
 336 loss that agreed with experiment.

337 The nonradiative recombination parameters are determined  
 338 next—in particular, the Shockley–Read–Hall (SRH) carrier life-  
 339 time and the Auger recombination coefficient. These param-  
 340 eters can be obtained from length-dependent measurements of  
 341 the threshold current of BA-LDs. From these measurements,  
 342 the transparency current density  $J_{tr}$  and the modal gain coef-  
 343 ficient  $\Gamma_{g0}$  are extracted. Using the calculated gain and spon-  
 344 taneous recombination spectra, the SRH carrier lifetime and  
 345 Auger recombination parameter were adjusted to obtain agree-  
 346 ment with the experimental values of  $\Gamma_{g0}$  and  $J_{tr}$ . The SRH  
 347 carrier lifetime for electrons and holes was set equal to each  
 348 other ( $\tau_n = \tau_p = \tau_{SRH}$ ). Only the Auger coefficient for holes  
 349  $C_p$  was adjusted, as it is generally dominant at long wavelengths.  
 350 By keeping  $\tau_{SRH}$  fixed and increasing  $C_p$ , we find that  $\Gamma_{g0}$  de-  
 351 creases and  $J_{tr}$  increases according to the direction indicated by  
 352 the line “increasing  $C_p$ ” in Fig. 4. Instead, if we keep  $C_p$  fixed  
 353 and decrease  $\tau_{SRH}$ ,  $\Gamma_{g0}$  and  $J_{tr}$  both increase in the direction  
 354 of the line labeled “decreasing  $\tau_{SRH}$ ” in Fig. 4. If we search the  
 355 entire parameter space of  $\tau_{SRH}$  and  $C_p$ , the set of recombination  
 356 parameters  $\tau_{SRH} = 2.48 \text{ ns}$  and  $C_p = 4.2 \times 10^{-29} \text{ cm}^6 \text{ s}^{-1}$  can  
 357 be uniquely linked to the set of measured device parameters  
 358  $\Gamma_{g0} = 27.1 \text{ cm}^{-1}$  and  $J_{tr} = 187 \text{ A/cm}^2$ .

### C. Advanced Validation for Accurate Device Simulation

359

360 In this section, we discuss the general approach we follow for  
 361 the experimental validation and calibration of more advanced  
 362 simulation parameters. (Please note that the examples presented  
 363 in Section IV represent very recent work, for which this valida-  
 364 tion is still being performed.)

365 The electrical and optical properties of laser diodes both de-  
 366 pend upon temperature. Thus, their behavior is sensitive to self-  
 367 heating, and it is important to validate the parameters used in the  
 368 thermal model. As the rise in internal temperature usually causes  
 369 a red-shift in emission wavelength above threshold [45]–[47],  
 370 this can often be used to determine the thermal resistivity of the  
 371 laser diode package. (Frequency-stabilized lasers are an  
 372 exception.)

373 Next, carrier- and temperature-induced lensing effects are  
 374 investigated by comparing the simulated and measured near-  
 375 and far-field profiles. Fig. 3(b) shows that the refractive index  
 376 change near the ground state transition energy of the QW is  
 377 highly sensitive to temperature. Thus, an *a priori* calculation  
 378 of the refractive index change requires precise knowledge of the  
 379 thermal environment (e.g., heat sink performance). Good  
 380 agreement can usually be achieved by adjusting the propor-  
 381 tionality constants relating the index change and changes in carrier  
 382 density and temperature [30], [31], so that the model is able  
 383 to predict the evolution of the far field with bias current with  
 384 reasonable reliability.

385 Direct validation of the carrier distribution inside the cavity  
 386 can be obtained from intracavity spontaneous emission measure-  
 387 ments, which provide spectral and spatial information about the  
 388 spontaneous emission distribution in the cavity. The intensity  
 389 profiles reveal spatial hole burning and electrical overpumping  
 390 effects. The spontaneous emission spectra provide information  
 391 about the local lattice temperature, carrier heating, and spectral  
 392 hole burning effects.

393 Fig. 5(a) shows the spontaneous emission distribution ob-  
 394 tained through a windowed contact in a 975-nm tapered laser  
 395 [48]. Fig. 5(b) compares the simulated and experimental spon-  
 396 taneous emission distributions for a lateral slice near the output  
 397 facet. In this example, the spatial hole in the center of the cav-  
 398 ity observed in the experimental measurement is also seen in  
 399 the simulation. Good quantitative agreement was also obtained.  
 400 The difference in the integrated intensity was  $\sim 12.4\%$ , which  
 401 translates to  $\sim 6\%$  error in the carrier density.

402 Figs. 6 and 7 show experimental and simulated intracavity  
 403 spontaneous emission spectra from the same device for differ-  
 404 ent bias levels [32]. The measured spectra were taken from a  
 405  $5 \mu\text{m} \times 5 \mu\text{m}$  point through a window in the back contact.  
 406 The spikes in the experimental spectra taken above threshold  
 407 are scattered stimulated emission. The simulated spectra have a  
 408 steeper edge on the low energy side than the measured spectra.  
 409 This is because inhomogeneous broadening due to alloy and  
 410 QW width fluctuations has not been accounted for, nor have  
 411 the line shape broadening parameters in the simulation been  
 412 adjusted to obtain agreement with the measured spectra. Nev-  
 413 ertheless, similar trends are observed in the experiment and the  
 414 simulation. First, the spontaneous emission intensity increases

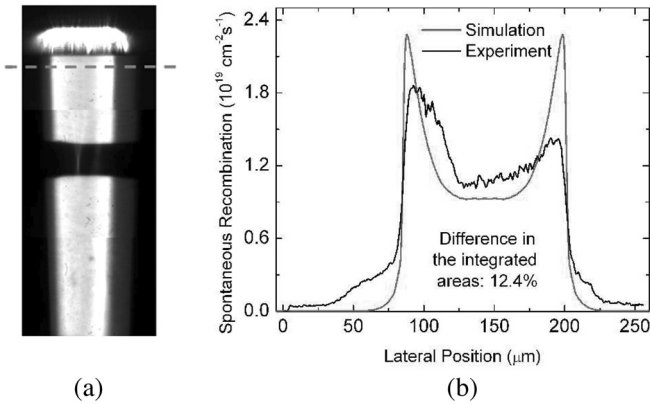


Fig. 5. (a) Image of the spontaneous emission distribution taken through two windows in the contact near the output facet. (b) Experimental and simulated spontaneous emission profiles at the output facet of a tapered laser [48].

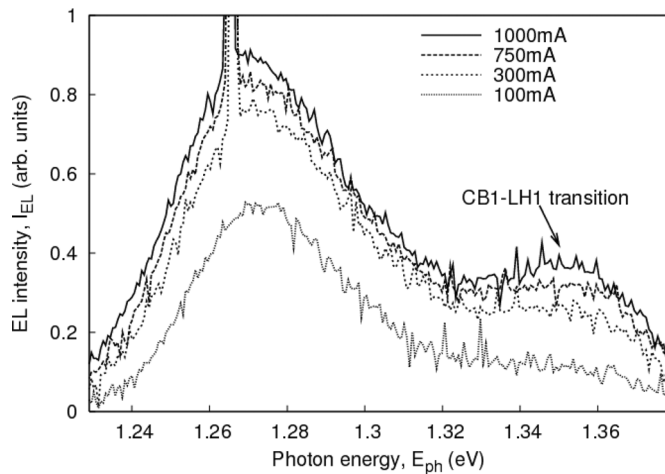


Fig. 6. Experimentally measured spontaneous emission spectra for varying bias taken at the center of the device near the front facet [32].

415 with bias, due to spectral hole burning. The gain, and hence, car- 432  
 416 rier density are pinned at the lasing energy (i.e., bottom of the 433  
 417 spectral hole). As the bias increases, so does the carrier density 434  
 418 around the spectral hole. Second, the CB1-LH1 transition also 435  
 419 increases with bias, which can be attributed to carrier heating. 436  
 420 This conclusion can be obtained from the simulated spectra, 437  
 421 where a larger increase in the CB1-LH1 transition is observed 438  
 422 when a nonequilibrium gain model is used, which includes the 439  
 423 carrier heating effect. 440

#### 424 IV. APPLICATION EXAMPLES

425 In this section, application examples are used to demonstrate 441  
 426 the role of modeling for the design, simulation, and evaluation 442  
 427 of next-generation high-brightness laser diode technologies. 443

##### 428 A. Broad-Area Laser Diodes

429 Conceptually, the simplest and most obvious way to increase 444  
 430 the brightness of a BA-LD is to increase its width, since the far- 445  
 431 field and near-field widths are inversely related. The problem 446

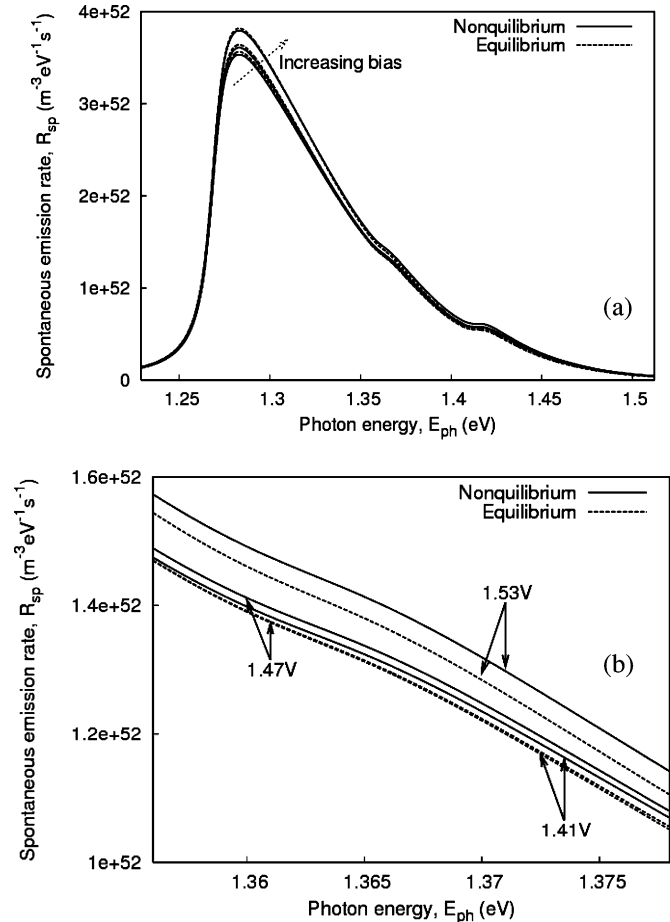


Fig. 7. (a) Simulated spontaneous emission showing nonequilibrium spectral hole burning and carrier heating. (b) Closeup of CB1-LH1 transition [32].

432 with this approach is that filaments start to form in the laser. 433  
 433 This leads to reduced beam quality, since the narrow filaments 434  
 434 cause a large far-field divergence. Furthermore, the number and 435  
 435 position of the filaments change both with time and from device 436  
 436 to device. 437

437 In this study, we investigate the brightness limitations of 438  
 438 broad-area lasers by investigating the effect of the resonator 439  
 439 geometry on the single-mode operation of a BA-LD. The BA- 440  
 440 LD investigated in this paper is a gain-guided laser with a cur- 441  
 441 rent stripe defined by deep ion implantation to eliminate current 442  
 442 spreading in the cladding layers. 443

443 To investigate the operating regime of the BA-LD dominated 444  
 444 by the fundamental mode, we employed the Prony method to 445  
 445 extract the lateral modes of the BA-LD [49]. The eigenvalues 446  
 446 extracted with the Prony method are the round-trip gain/loss of 447  
 447 the individual eigenmodes. Thus, if the BA-LD is to operate 448  
 448 in a single mode, the fundamental mode should have an eigen- 449  
 449 value equal to unity ( $\lambda_0 = 1$ ), while the first-order mode should 450  
 450 have an eigenvalue less than unity ( $\lambda_1 < 1$ ). If we define the 451  
 451 modal discrimination as  $MD = |\lambda_0|/|\lambda_1|$ , the BA-LD operates 452  
 452 in the single fundamental lateral mode when MD is greater than 453  
 453 unity. Thus, to obtain strong single-mode operation, the modal 454  
 454 discrimination should be as large as possible. 455

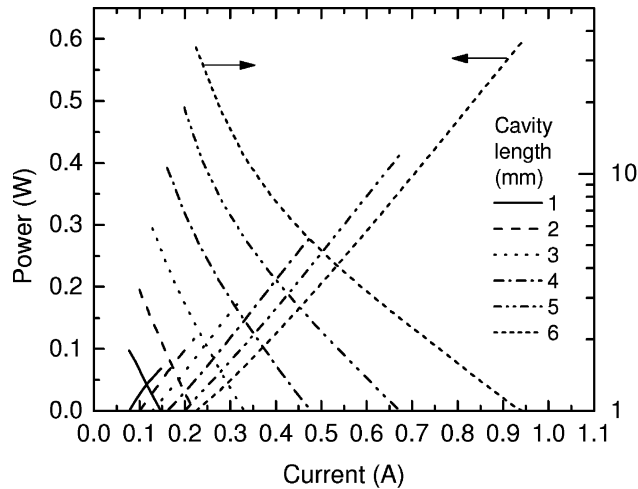


Fig. 8.  $L$ - $I$  characteristic and modal discrimination as a function of current bias for cavity lengths  $L = 1$  to  $6$  mm. The emitter width is  $W = 30 \mu\text{m}$  [33].

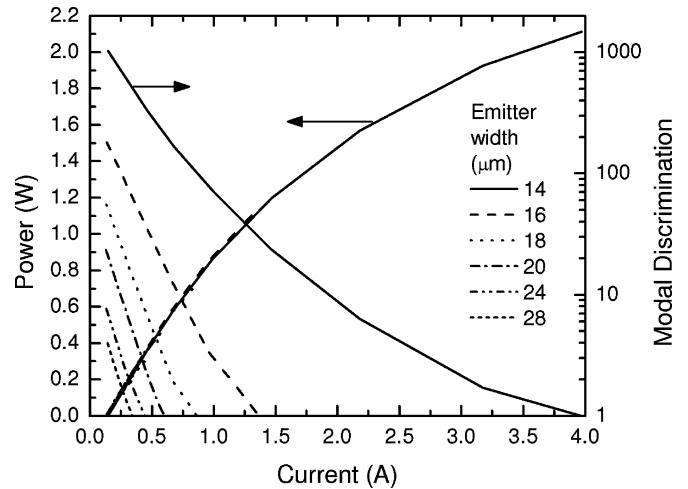


Fig. 9.  $L$ - $I$  characteristic and modal discrimination as a function of current for emitter widths  $W = 14$  to  $28 \mu\text{m}$ . The cavity length is fixed at  $L = 2$  mm [33].

455 Before investigating the effect of the other geometrical parameters, the thickness of the vertical waveguide  $W_g$  needs to be  
 456 determined. It was shown in [33] that increasing the waveguide thickness allows for higher modal discrimination by reducing  
 457 the confinement factor, and subsequently, the carrier lensing effect. The carrier lens excites higher order modes in the cavity  
 458 and promotes the formation of optical filaments. Only a symmetrical vertical structure was considered here with a total vertical  
 459 waveguide thickness of  $2 \mu\text{m}$ . To reduce the confinement factor further, it is also possible to employ asymmetric structures,  
 460 where the QW is positioned closer toward the p-cladding [50].  
 461 Having determined the vertical waveguide thickness, the effect of the cavity length on the modal discrimination is investigated.  
 462 Fig. 8 shows the variation of modal discrimination and single-mode output power versus bias current. The emitter width  
 463 is fixed at  $30 \mu\text{m}$  and the cavity length is varied from 1 to 6 mm. The longer the cavity length, the higher the modal discrimination  
 464 is at threshold. Also, as the bias current is increased, the modal discrimination decreases less rapidly for the longer cavity  
 465 BA-LDs. This can be understood in terms of the round-trip loss of a particular mode  $n$  given by  $r_f r_b \exp(-\alpha_n L)$ , where  $r_f$  and  
 466  $r_b$  are the facet reflectances,  $\alpha_n$  is the net modal loss, and  $L$  is the cavity length. The round-trip loss of the fundamental mode  
 467 is unity (fixed by the lasing condition), so the modal discrimination increases with cavity length as the loss of the first-order  
 468 mode increases.

481 Next, the effect of emitter width is investigated. The cavity length is fixed at 2 mm and the emitter width is varied from  
 482 14 to 28  $\mu\text{m}$  (Fig. 9). For narrower emitter widths, the modal discrimination is higher at threshold and decreases less rapidly  
 483 as a function of bias current. For an emitter width of 14  $\mu\text{m}$ , the modal discrimination is greater than unity for powers up  
 484 to  $\sim 2$  W. This maximum single-mode output power is equivalent to a facet load of  $\sim 15 \text{ MW}/\text{cm}^2$ , which is close to the  
 485 reported catastrophic optical mirror damage (COMD) values of 18–19  $\text{MW}/\text{cm}^2$  [51]. In addition, since thermal effects and  
 486 spontaneous emission coupling were not included in these sim-

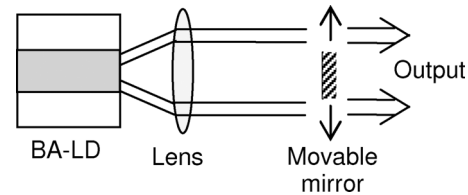


Fig. 10. Schematic diagram of an asymmetric feedback external cavity laser.

492 ulations, this represents an upper limit on the maximum brightness that can be achieved by a BA-LD. By comparison, tapered lasers (discussed in Section III-C and III-D) have achieved  
 493 nearly diffraction-limited operation for powers up to 12 W [2]. Thus, although single-emitter broad-area lasers can produce high output powers, their ultimate brightness is limited by the  
 494 lack of strong modal discrimination for wide emitters and is restricted by COMD for narrow emitters.

### B. Asymmetric Feedback External Cavity Laser

501 In this section, an external cavity laser with asymmetric feedback is investigated to improve the modal discrimination and beam quality of a BA-LD. The external cavity laser configuration  
 502 is shown in Fig. 10. The BA-LD has an emitter width of 100  $\mu\text{m}$ , a cavity length of 1.5 mm, and an emission wavelength of 975 nm. Details of the epitaxial structure are given  
 503 in [52]. The front and back facets are antireflection (AR) and high reflection (HR) coated, respectively. A lens with a focal length of 75 mm is placed at the focal plane to collimate the  
 504 laser beam along the slow axis. A 0.9-mm-wide mirror is placed in a far-field plane located 75 mm from the lens for selective spatial feedback. The 1.5-D isothermal unipolar laser model  
 505 is used to simulate the BA-LD and is coupled to an external optics module, which models the free-space propagation of the optical beam by solving the Fresnel diffraction equations.

517 A stable operating condition is found when the mirror stripe is positioned 5.85 mm from the center. The near-field pattern in Fig. 11(a) has an asymmetric shape, in agreement with

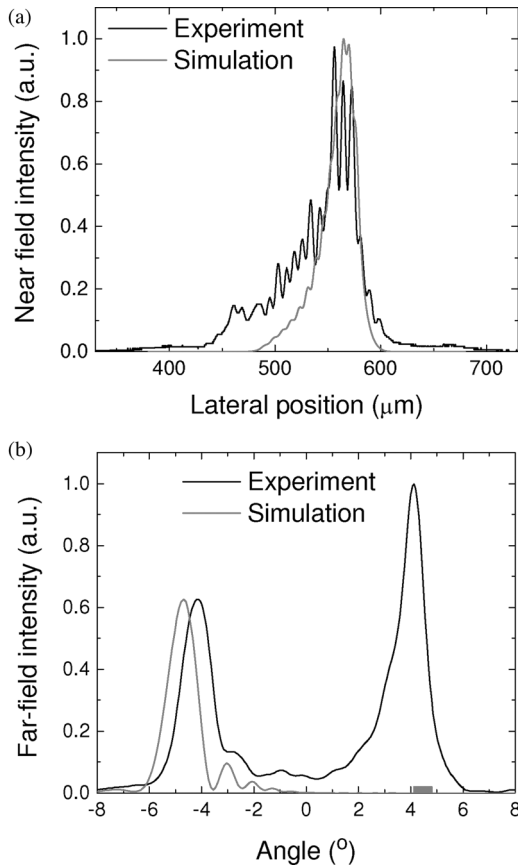


Fig. 11. Converged (a) near-field and (b) far-field patterns of an asymmetric feedback external cavity laser. The mirror width and position used in the simulation are indicated by the stripe in (b).

519 experiment. The far-field pattern in Fig. 11(b) consists of a nar-  
 520 row main lobe with a full-width at half-maximum (FWHM)  
 521 of  $1.26^\circ$ , which is offset from the center by  $\sim 4.69^\circ$ . The ex-  
 522 perimental far-field profile shows a double lobed feature with  
 523 both a significant output lobe (left) and feedback lobe (right).  
 524 Such a behavior is uncommon for this asymmetric feedback  
 525 technique. Usually, a strong and narrow output lobe is observed  
 526 in the far field [53], in agreement with the simulation, and the  
 527 feedback lobe is strongly suppressed. The peculiar behavior of  
 528 this particular laser is due to degradation observed on the front  
 529 facet AR coating. Nevertheless, the position and width of the  
 530 experimental lobe coincide well with the simulated profile.

531 Fig. 12 shows the carrier density (at the front facet) and far-  
 532 field intensity distributions for different output powers. With  
 533 increasing power, larger spatial hole burning occurs at the out-  
 534 put facet on the opposite side of the feedback mirror. A slight  
 535 movement of the peak position of the far-field lobe away from  
 536 the optical axis is seen with increasing power. This is due to spa-  
 537 tial hole burning and carrier lensing, which result in a slightly  
 538 modified waveguiding behavior in the BA-LD.

539 The simulated  $M^2$  value using the second moment definition  
 540 (ISO Standard 11146) is only 2.62, which is small compared  
 541 to that of a typical BA-LD ( $M^2 \approx 30$ ) [9]. This dramatic im-  
 542 provement is attributed to the increased modal discrimination  
 543 provided by the mirror stripe, which provides selective feedback

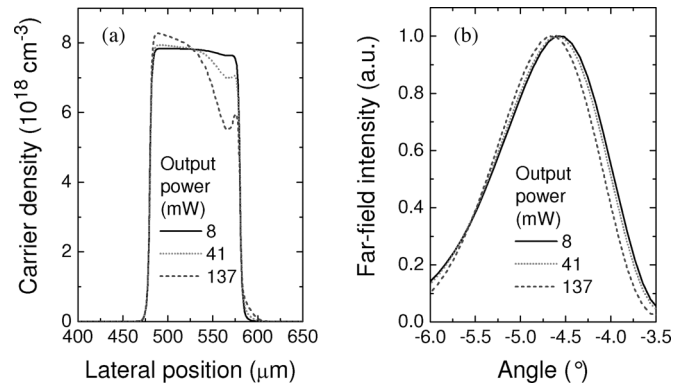


Fig. 12. (a) Carrier density distribution at the output facet. (b) Far-field patterns for different output powers.

to a specific lateral mode. The value of  $M^2 \sim 2.6$  is outstanding  
 for a BA-LD, but many applications (e.g., frequency doubling  
 for display applications) require even better beam quality. This  
 can be achieved with tapered lasers, which use a spatial filter to  
 improve the modal discrimination.

### C. Tapered Laser

Tapered lasers are currently the most popular high-brightness  
 laser diodes. Their superior performance is due to several factors  
 inherent in their design. First, the straight RW section serves as  
 a modal filter, which discriminates against higher order modes.  
 Next, a single lateral mode is allowed to expand adiabatically  
 in the tapered section, minimizing spatial hole burning and fila-  
 mentation. Finally, the complexity of a tapered laser is relatively  
 low compared to other high-brightness lasers, making it suitable  
 for low-cost manufacturing with a high process yield and reli-  
 able operation.

Tapered lasers demonstrate clear performance advantages, but  
 filamentation can still be an issue if they are not designed prop-  
 erly. For instance, the RW section geometry must be designed  
 to support a single lateral mode. Figs. 13 and 14 show the 2.5-D  
 spectral simulation of a  $5\text{-}\mu\text{m}$ -wide RW laser, which just sup-  
 ports two lateral modes. Although the central mode prefers the  
 fundamental lateral mode, the modes at the edges of the emis-  
 sion spectrum clearly show mode beating between the first and  
 second lateral modes. (From the gain profile, it is clear that this  
 is mode beating and not gain or index guiding.) The laser is  
 able to efficiently use the spatial gain distribution in this way,  
 but the result is not good for the modal filtering properties of  
 the RW—particularly as the backward wave from the taper will  
 excite both modes. In this case, a narrower RW is needed to  
 suppress the higher order transverse mode, or the loss of the  
 higher order transverse mode must be increased to improve the  
 modal discrimination. Furthermore, to achieve good modal fil-  
 tering, the taper angle should match the free diffraction angle  
 of the mode launched into the tapered section, and the epitaxial  
 structure should have a low modal gain to reduce carrier lensing  
 effects.

Along with the RW design, the front facet reflectivity and  
 beam spoiler also affect the modal filtering performance of

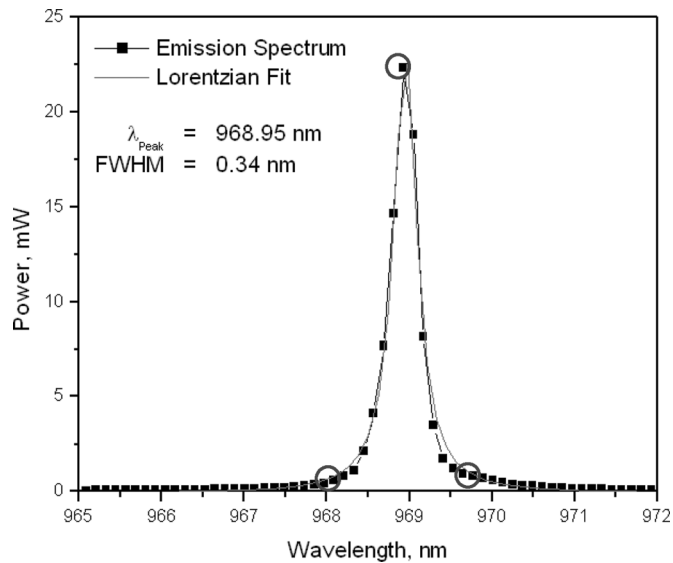


Fig. 13. Simulated emission spectrum of a 5- $\mu\text{m}$ -wide index-guided RW laser. The circled points correspond to the fields shown in Fig. 14.

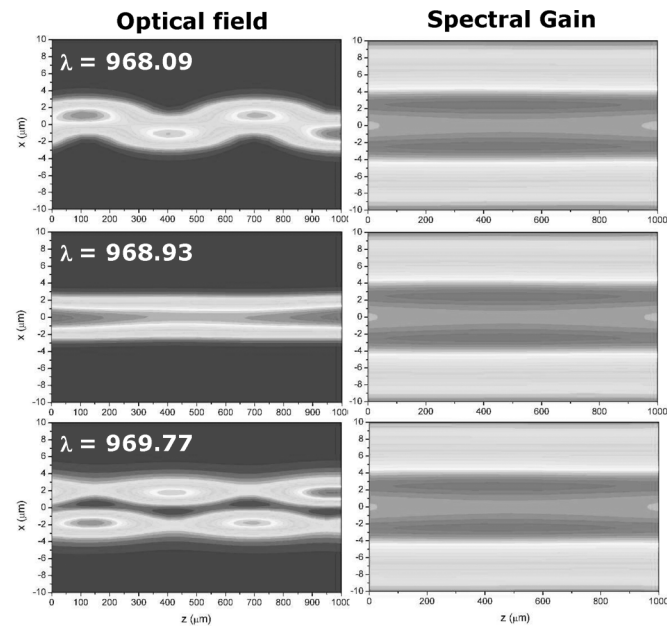


Fig. 14. Spectral field (left) and gain (right) distributions of a 5- $\mu\text{m}$ -wide index-guided 970-nm RW laser at wavelengths of 968.09 (top), 968.93 (middle), and 969.77 nm (bottom).

583 the tapered laser. From earlier investigations on a 2-mm-long  
 584 4° gain-guided tapered laser (using a different monochromatic  
 585 2.5-D laser model [30]), it was shown that a front facet reflectivity  
 586  $R_f = 1\%$  produced filamentation in the near-field profile.  
 587 This filamentation is caused by optical pumping of the regions  
 588 adjacent to the RW, which become transparent and reduce the  
 589 modal filtering efficiency of the RW section. This resulted in  
 590 small side lobes in the forward propagating wave in the RW  
 591 section, which seed the filamentation process and create a mul-  
 592 tilobed near-field pattern. When  $R_f$  is reduced to 0.1%, the  
 593 optical bleaching of the RW section is avoided. This improves  
 594 the modal filtering in the RW and eliminates the filamentation

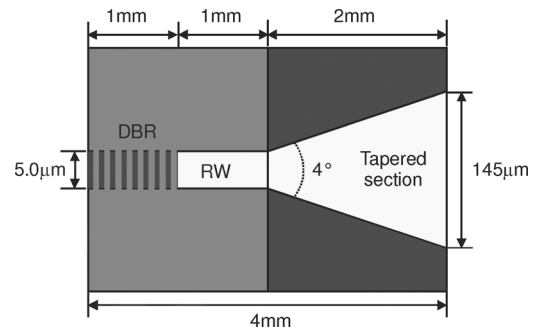


Fig. 15. Schematic diagram of the DBR tapered laser.

in the taper. Beam spoilers were also shown to prevent the opti- 595  
 cal bleaching of the regions adjacent to the RW. Even with the 596  
 original front facet reflectivity of 1%, a 6- $\mu\text{m}$  aperture placed 597  
 100  $\mu\text{m}$  from the rear facet filtered the high-order modes out of 598  
 the relatively intense backward wave and prevented filamenta- 599  
 tion and beam quality degradation. 600

#### D. Multisection Tapered Laser 601

There is growing interest in using tapered lasers in display and 602  
 optical wireless applications due to their good beam quality and 603  
 high output power. These applications require a high modulation 604  
 efficiency ( $dP/dI$ ) to minimize the cost and complexity of the 605  
 laser driver. This can be achieved through the use of separate 606  
 contacts for the RW and tapered amplifier sections. By using 607  
 a small modulation bias on the RW and keeping the tapered 608  
 section bias fixed, higher modulation bandwidths and efficiency 609  
 can be achieved. To satisfy the targeted applications, these lasers 610  
 should have a stable beam quality and astigmatism for all bias 611  
 conditions. This is necessary, since the lenses that collimate and 612  
 focus the output beam of the laser are designed for fixed beam 613  
 parameters. 614

Here, we investigate the performance of a 1060-nm DBR 615  
 tapered laser intended for generating 530 nm light by second 616  
 harmonic generation (SHG) for laser displays [41]. At the end of 617  
 the RW, the DBR tapered laser includes a passive DBR section 618  
 to fix the emission wavelength, as shown in Fig. 15. High 619  
 spectral brightness and stability (i.e., a narrow and stable spec- 620  
 tral linewidth) is required by the nonlinear crystal for SHG. 621  
 Since the DBR section locks the emission wavelength, we have 622  
 only simulated a single wavelength fixed at 1060 nm. The las- 623  
 ing wavelength was measured to be stable with RW current 624  
 within 130 pm [41]. The good wavelength stability with re- 625  
 spect to current is due to efficient thermal management and the 626  
 small temperature and index change in the passive DBR section. 627  
 The index-guided RW has an index step of  $\sim 1.5 \times 10^{-3}$ , while 628  
 the taper is gain guided with a shallow implant for electrical 629  
 isolation. 630

The DBR section is passive (unpumped), so it has been repre- 631  
 sented by a fixed reflectivity at the end of the RW. The reflectivity 632  
 of the sixth-order DBR grating of DBR RW lasers was found 633  
 to be around 31% [41]. We used a top-hat profile (in the lateral 634  
 direction) for the reflectivity with a value of 31% for the region 635  
 within the RW and a value of 0.01% outside the RW. The low 636

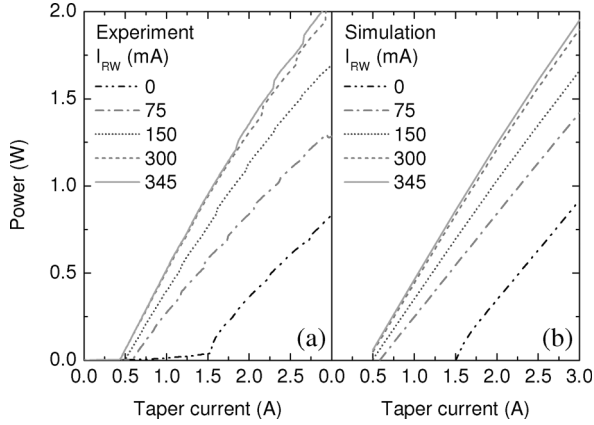


Fig. 16. (a) Experimental and (b) simulated light-current characteristics.

637 reflectivity of the region outside the RW was used, since any  
 638 backward traveling light is strongly absorbed in the unpumped  
 639 region in the DBR section and very little light is reflected back  
 640 from the AR-coated back facet ( $<0.1\%$ ). The front facet was  
 641 AR-coated to 1%.

642 The DBR tapered laser is simulated using the 2.5-D  
 643 monochromatic laser model, employing the material param-  
 644 eters determined in Section II-B. Fig. 16 compares (a) the ex-  
 645 perimental and (b) simulated output power versus taper current  
 646 characteristics of a split-contact 1060-nm DBR tapered laser.  
 647 Good agreement is obtained over the range of RW and taper  
 648 currents investigated. The saturation of the output power with  
 649 increasing RW current is reproduced in the simulations and is  
 650 due to the depletion of carriers in the tapered amplifier with  
 651 increasing optical injection from the RW.

652 The photon density distributions for the combined forward  
 653 and backward waves are plotted in Fig. 17 for RW currents of  
 654 (a) 0 mA and (b) 345 mA at a fixed taper current of 1.6 A. The  
 655 output powers are 100 and 938 mW, respectively. For these con-  
 656 ditions, the simulated modulation efficiency is 2.43 W/A, which  
 657 is slightly smaller than experiment (2.6 W/A). The simulated  
 658 extinction ratio is 9.4, which is bigger than the experimental  
 659 value of 7.7. (The extinction ratio is expected to be squared for  
 660 the frequency-doubled green output.) No filamentation is ob-  
 661 served for either RW current, due to the good modal filtering  
 662 by the passive DBR and low AR coating on the back facet. The  
 663 lack of filamentation is also partly due to the use of a taper an-  
 664 gles that matches the free diffraction angle of the beam from the  
 665 RW. A larger increase in photon density toward the front facet  
 666 in the tapered section is observed for  $I_{RW} = 0$  mA compared  
 667 to  $I_{RW} = 345$  mA, which demonstrates the saturation of the  
 668 tapered amplifier as the RW current is increased.

669 The experimental and simulated far-field patterns are shown  
 670 in Fig. 18. There are discrepancies between the simulated and  
 671 measured far-field patterns, especially at the larger RW currents.  
 672 The lack of perfect agreement is probably because the simula-  
 673 tions were performed with calculated carrier-induced changes in  
 674 the refractive index spectra, which do not include index changes  
 675 in the waveguide core or cladding. Furthermore, index changes  
 676 near the emission wavelength are very sensitive to temperature

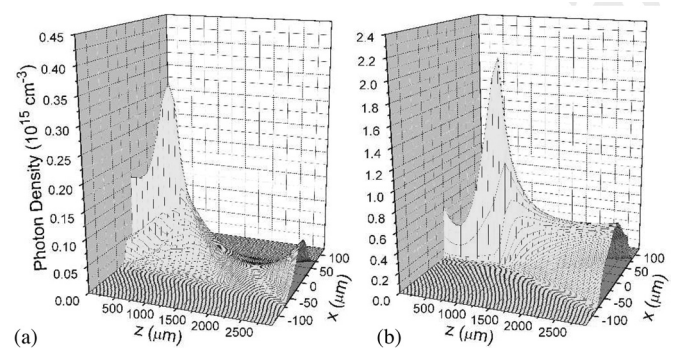


Fig. 17. Simulated photon density distributions (forward and backward waves) at a fixed taper current of 1.6 A and RW currents of (a) 0 mA and (b) 345 mA.

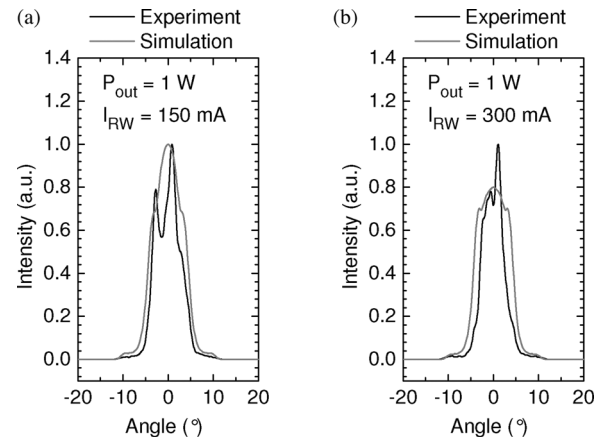


Fig. 18. Measured and simulated far-field profiles for a fixed output power of 1 W and RW currents of (a) 150 mA and (b) 300 mA.

677 changes. The thermal conductivity of the package was not inde-  
 678 pendently measured, since this is usually extracted from changes  
 679 in the emission wavelength above threshold. (As the emission  
 680 wavelength is determined by the DBR, this procedure does not  
 681 work here.)

682 Fig. 19 shows a plot of the beam quality factor and the astig-  
 683 matism versus  $I_{RW}$  at a fixed output power of 1 W. The  $M^2$   
 684 factor (determined using the  $1/e^2$  level) is in reasonable agree-  
 685 ment with experiment and stays at a fairly constant value of  
 686  $\sim 1.2$ . Fig. 19 shows that the simulated astigmatism of the beam  
 687 stays fairly stable versus  $I_{RW}$ , while the experimental data in-  
 688 crease slightly with  $I_{RW}$ . The agreement with experiment seems  
 689 reasonable, but is expected to improve once the spectral index  
 690 change is experimentally validated and calibrated.

691 The stability of the  $M^2$  factor and the astigmatism with re-  
 692 spect to  $I_{RW}$  is due to the use of a thick vertical waveguide  
 693 ( $4.8 \mu\text{m}$ ), since the carrier-induced index depression is reduced  
 694 by the small confinement factor. The exceptional beam quality  
 695 and modulation efficiency are, in part, due to the use of an AR  
 696 coating instead of an HR coating on the rear facet and the pres-  
 697 ence of the passive DBR section. This improves the filtering  
 698 of the higher order modes in the RW section—an approach not  
 699 previously considered.

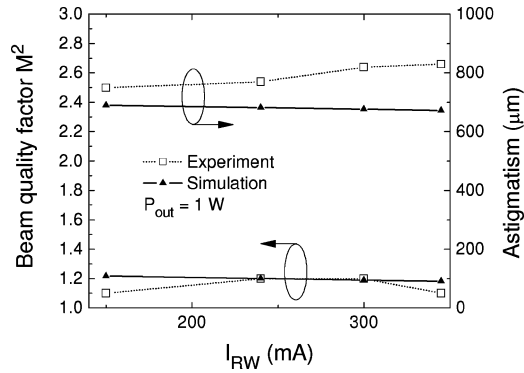


Fig. 19. Beam quality factor and astigmatism versus RW current. The output power is fixed at 1 W.

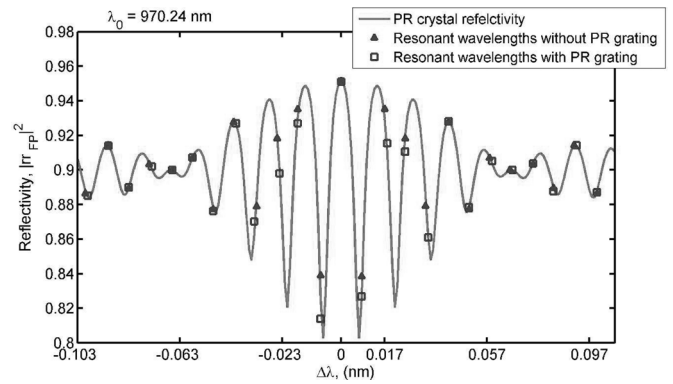


Fig. 21. Dependence of the Fabry-Perot filter reflectivity on wavelength [55].

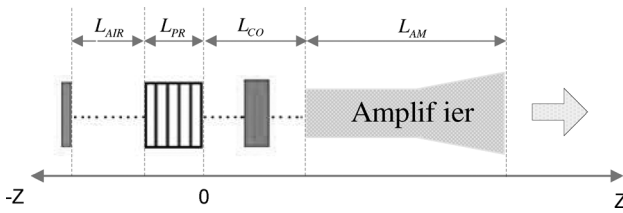


Fig. 20. Schematic diagram of the self-organizing external cavity laser.  $L_{AIR}$ : length of air gap;  $L_{PR}$ : length of the PR crystal;  $L_{CO}$ : length of the collimating optics section;  $L_{AM}$ : length of the tapered amplifier.

### 700 E. Self-Organizing External Cavity Laser

701 In laser technology, photorefractive (PR) crystals are typically  
 702 used in two situations: 1) in tunable external cavity semiconduc-  
 703 tor lasers, where the PR crystal relaxes the alignment tolerances  
 704 and 2) in self-organizing external cavity lasers, where it is used  
 705 to make an adaptive Fabry-Perot mirror to enhance the side  
 706 mode suppression ratio.

707 The schematic diagram of a self-organizing external cavity  
 708 laser is shown in Fig. 20, where a PR crystal is placed between  
 709 a high reflectivity mirror and the rear facet of the high-power tapered  
 710 amplifier. The purpose of assembling a laser cavity in this  
 711 particular configuration is to deliver a beam with high spectral  
 712 and spatial brightness. By using a PR crystal instead of a fixed  
 713 DBR, the laser cavity self-adapts to its operating conditions and  
 714 ensures maximum efficiency.

715 The model of this self-organizing external cavity laser con-  
 716 sists of a PR crystal model, which relies on a phenomenological  
 717 plane wave approach [54], and the 1.5-D spectral laser model.  
 718 (A 1-D unipolar, isothermal electrical model is used for numerical  
 719 efficiency.) In the simulation, the PR crystal and the rear  
 720 mirror are treated as a single adaptive Fabry-Perot filter, which  
 721 provides wavelength-dependent feedback to the tapered ampli-  
 722 fier. The reflectivity of this filter was calculated by solving a set  
 723 of coupled wave equations [54]. The main approximation used  
 724 by the model is that the mode with the largest power writes the  
 725 grating. The other longitudinal modes are scattered from this  
 726 grating.

727 The simulation of the self-organizing high-power external  
 728 cavity laser is performed in three stages. Initially, the resonant

wavelength of the main longitudinal mode is determined by 729  
 the spectral simulation of the free running laser, i.e., while ne- 730  
 glecting the formation of the grating in the PR crystal. This 731  
 simplification is justified because there is no phase shift (and 732  
 hence also no resonant wavelength shift) introduced by the PR 733  
 grating for the main mode. A 1-D simulation cannot be used for 734  
 this purpose, since the energy of the gain maximum depends on 735  
 the carrier density distribution in the tapered amplifier, which 736  
 depends strongly on position. 737

738 Once the wavelength of the main longitudinal mode is deter-  
 739 mined, the reflectivity of the PR crystal grating is obtained,  
 740 along with the values of the resonant wavelengths of all the side  
 741 modes. The calculated values of the resonant wavelength for the  
 742 cavity modes are shown in Fig. 21. The resonant wavelengths  
 743 were calculated with and without the phase shift introduced by  
 744 the PR crystal grating. These results confirm that the recorded  
 745 PR crystal grating has a significant impact on the position and  
 746 the reflectivity of the cavity modes. Without the induced grating  
 747 in the PR crystal, the reflectivity of all the modes would be equal  
 748 to that of the mirror.

749 After the wavelengths of all the cavity modes and the cor-  
 750 responding reflectivities are known, the full spectral simulation  
 751 of the laser is performed. Fig. 22 compares the output power  
 752 spectra, calculated by the spectral model for a bias current of  
 753 0.32 A, for an external cavity laser with and without PR  
 754 crystal. The simulations show that the PR crystal produces  
 755 single longitudinal mode operation. The spectral linewidth  
 756 is less than 18 pm, since the longitudinal mode spacing is  
 757 only 9 pm. Single-mode operation was also found experi-  
 758 mentally, where the instantaneous linewidth was measured to  
 759 be  $\sim 80$  MHz ( $< 0.3$  pm) and is stable up to  $< 2$  pm. The  
 760 simulated side mode suppression ratio is high ( $> 50$  dB),  
 761 as seen experimentally ( $> 30$  dB limited by the spectrum  
 762 analyzer).

763 Previously, self-organized cavity laser diodes have only been  
 764 modeled with 0-D rate equations. The results reported here  
 765 demonstrate the 1.5-D spectral simulation of the spectral bright-  
 766 ness of these devices. The next challenge is to make the wave-  
 767 length selection automatically respond to changes in the oper-  
 768 ating conditions. This requires a more advanced model for the  
 769 PR crystal.

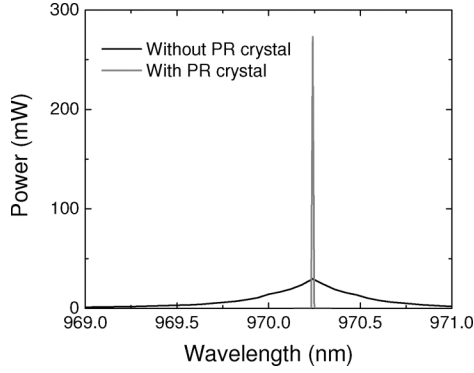


Fig. 22. Calculated output power spectrum for external cavity laser with and without the PR crystal.

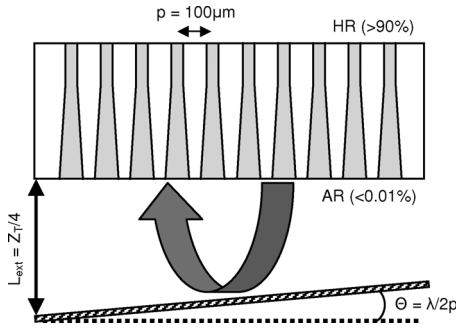


Fig. 23. Schematic diagram of the external Talbot cavity laser.

#### 770 F. External Talbot Cavity Laser

771 Phase-locking of an array of emitters has received great at-  
 772 tention for achieving highly coherent emission with high out-  
 773 put power. Phase-locking can be induced using the Talbot ef-  
 774 fect [17], where the out-of-phase mode is self-imaged and the  
 775 in-phase mode is imaged with a lateral shift of  $p/2$  (where  $p$   
 776 is the emitter pitch) after traveling half the Talbot distance  
 777 ( $Z_T = 2p^2/\lambda$ ). By placing a mirror in an external cavity at a  
 778 distance  $Z_T/4$  with a tilt of  $\lambda/2p$  (Fig. 23), the in-phase mode is  
 779 self-imaged while the out-of-phase mode is laterally displaced  
 780 by  $p/2$ . This increases the modal discrimination between the  
 781 in-phase and out-of-phase modes, thus phase-locking the emit-  
 782 ters in the in-phase mode.

783 The array studied here consists of ten narrow index-guided  
 784 tapered lasers emitting at 975 nm. Further details of the tapered  
 785 laser and epitaxial structure can be found in [52] and [56].

786 For the simulations, the 1.5-D isothermal unipolar laser model  
 787 was coupled to a free-space propagation model (based on the  
 788 Fresnel diffraction equations) for the external cavity [57]. The  
 789 reflectivity of the tilted output mirror was 40%. The operation  
 790 of the Talbot cavity was confirmed by investigating the effect  
 791 of the tilt of the mirror. With an untilted mirror, the laser oscil-  
 792 lates in the out-of-phase mode, but with a tilt angle of  $\lambda/2p$ , the laser  
 793 operates in the in-phase mode. This confirms the strong modal  
 794 discrimination of the Talbot cavity.

795 The front facet near-field distribution (intensity and phase)  
 796 for the in-phase and out-of-phase modes are shown in Fig. 24.  
 797 Comprehensive modeling of the beam propagation in the whole

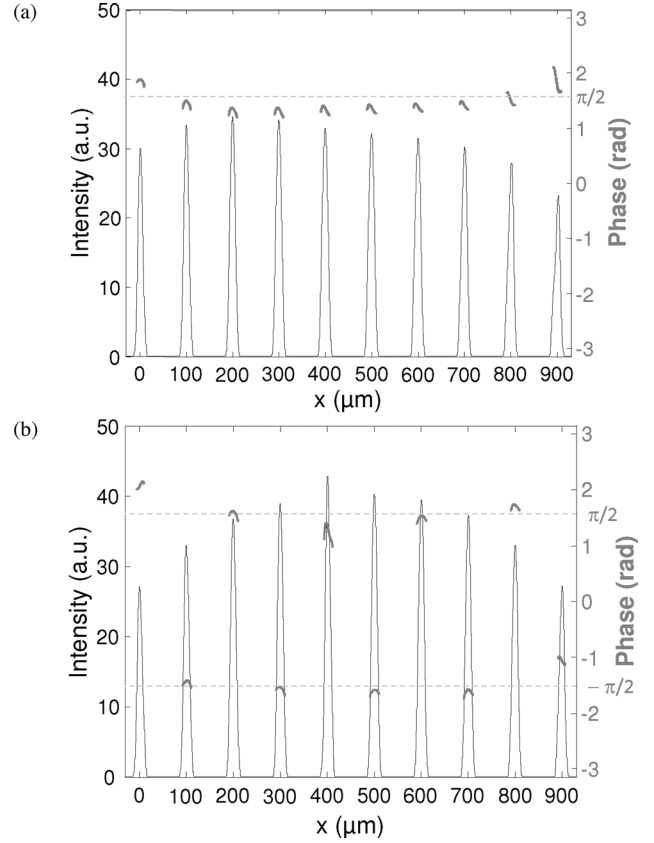


Fig. 24. Field intensity and phase at the front facet for the (a) in-phase and (b) out-of-phase mode operation at an operating current of 3.88 A.

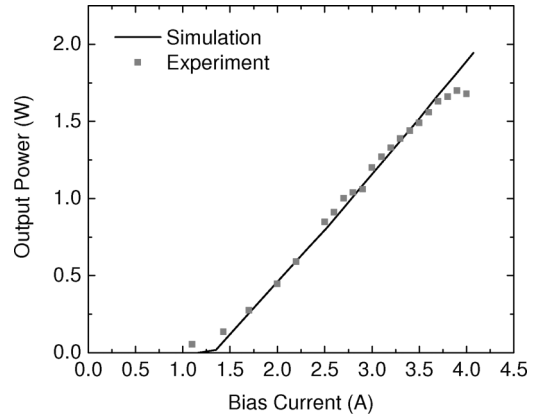


Fig. 25. Experimental versus simulated  $L-I$  characteristic.

cavity predicts some interesting features of the spatial modes 798  
 under external cavity operation and leads to better understanding 799  
 of the laser array behavior. The asymmetry of the intensity 800  
 profile of the in-phase mode is a consequence of the tilt of the 801  
 mirror. In both cases, the phase distributions show the expected 802  
 in-phase and out-of-phase behavior. 803

Fig. 25 shows that the simulated  $L-I$  characteristics for the 804  
 in-phase supermode operation of the laser bar agree well with 805  
 experiment. The slight discrepancies are probably due to current 806  
 spreading and self-heating effects in the experiments. 807

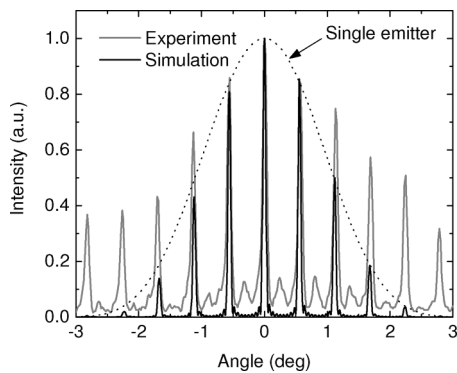


Fig. 26. Far-field profile for the in-phase mode operation at a current of 3 A.

In Fig. 26, the simulated far-field profile for lasing of the in-phase mode shows interference peaks, which agree with experiment. The simulated and measured interference peaks have a width of  $0.07^\circ$ . The envelope of the simulated profile has a Gaussian shape, corresponding to the output of a single emitter. The experimental far-field envelope is wider due to the presence of multimode emission from the tapered emitters.

These results demonstrate the model's ability to reproduce the experimental characteristics and provide insight into the field distribution in the array. Further work will include the detailed investigations of the modal discrimination behavior of the laser and the use of the 2.5-D model to accurately investigate the impact of carrier and thermal lensing effects.

## V. CONCLUSION

To satisfy increasing application demands and enter new markets, next-generation high-brightness laser diodes require not only good beam quality but also high spectral brightness and added functionality (e.g., direct modulation). Several next-generation high-brightness laser diodes were considered, including the asymmetric feedback broad-area laser, the multi-section tapered laser, the self-organizing cavity laser, and the external Talbot cavity laser.

Using the Prony method, it was shown that the modal discrimination of BA-LD improves as the cavity width decreases and the cavity length and waveguide thickness increase. To achieve high power levels, however, the devices must be quite long (up to 6 mm) and the width of the cavity must be narrow. This results in a high facet load of  $>100 \text{ mW}/\mu\text{m}$ . Using asymmetric feedback to increase the modal discrimination dramatically improves the beam quality and reduces  $M^2$  from  $\sim 30$  to  $\sim 2.6$ , without strong limitations on cavity length or width. Nevertheless, their performance falls short of that of recent tapered lasers. Still, asymmetric feedback may play a role in external cavity approaches for the phase coupling of high-power BA-LD arrays.

Methods to improve the brightness of tapered lasers were demonstrated, including optimizing the RW design to improve the modal discrimination, reducing the front facet AR coating, and using a beam spoiler. Through proper calibration, the laser simulator is able to reproduce the experimental operating char-

acteristic of the multisection 1060-nm DBR tapered laser with good accuracy. The DBR tapered laser has stable spectrum,  $M^2$ , and astigmatism versus RW current, which are important for efficient frequency doubling through a nonlinear crystal. The rear reflector, comprised of a passive DBR with an AR-coated back facet, improved the modulation efficiency of the device.

The spatial and spectral brightness of a tapered self-organizing cavity laser was simulated for the first time. This approach provides a mechanism for improving the spectral brightness of lasers without incurring strict alignment constraints. Finally, we demonstrated the simulation of phase-locking in an array of independent tapered lasers through the use of an external Talbot cavity. The in-phase and out-of-phase modes can be selected by changing the tilt of the external mirror

In summary, the complexity of the devices and increasing range of exacting performance specifications make the use of accurate simulation tools essential for the design and optimization of next-generation high-brightness laser diodes and systems. The examples presented demonstrate the need for laser models that include beam propagation and spectral effects. The beam propagation model is needed to reproduce the evolution with temperature and current of the near- and far-field distributions,  $M^2$ , and the astigmatism. It is also needed for diffraction effects, which are important for the phase coupling of emitters. Spectral laser models are needed to evaluate the spectral brightness of a laser and the dependence of the lasing wavelength on temperature and current. Finally, laser models that are able to handle more general structures are needed to simulate a wider range of devices such as multicontact lasers, external cavity lasers, and phase-coupled arrays to address new and emerging applications.

## ACKNOWLEDGMENT

The authors gratefully acknowledge L. Borruel and I. Esquivias for their contribution to the work on tapered lasers in Section III-C and T. M. Benson for useful discussions about optical modeling.

## REFERENCES

- [1] R. Diehl, Ed., *High-Power Diode Lasers: Fundamentals, Technology, Applications*. Berlin, Germany: Springer-Verlag, 2000.
- [2] B. Sumpf, Ferdinand-Braun-Institut für Höchstfrequenztechnik, Berlin, private communication, Oct. 2008.
- [3] J. R. Marcianite and G. P. Agrawal, "Spatio-temporal characteristics of filamentation in broad-area semiconductor lasers: Experimental results," *IEEE Photon. Technol. Lett.*, vol. 10, no. 1, pp. 54–56, Jan. 1998.
- [4] Z. Bao, R. K. DeFreez, P. D. Carleson, C. Largent, C. Moeller, and G. C. Dente, "Spatio-spectral characteristics of a high power, high brightness CW InGaAs/AlGaAs unstable resonator semiconductor laser," *Electron. Lett.*, vol. 29, no. 18, pp. 1597–1599, 1993.
- [5] L. M. Tilton, G. C. Dente, A. H. Paxton, J. Cser, R. K. DeFreez, C. E. Moeller, and D. Depatie, "High power, nearly diffraction-limited output from a semiconductor laser with an unstable resonator," *IEEE J. Quantum Electron.*, vol. 27, no. 9, pp. 2098–2108, Sep. 1991.
- [6] R. Parke, D. F. Welch, A. Hardy, R. Lang, D. Mehuys, S. O'Brien, K. Dzurko, and D. Scifres, "2.0 W CW, diffraction-limited operation of a monolithically integrated master oscillator power-amplifier," *IEEE Photon. Technol. Lett.*, vol. 5, no. 3, pp. 297–300, May 1993.
- [7] E. S. Kintzer, J. N. Walpole, S. R. Chinn, C. A. Wang, and L. J. Missaggia, "High power, strained-layer amplifiers and lasers with tapered gain regions," *IEEE Photon. Technol. Lett.*, vol. 5, no. 6, pp. 605–608, Jun. 1993.

- [8] D. Masanotti and F. Causa, "Optical guiding properties of high-brightness parabolic bow-tie laser arrays," *IEEE J. Quantum Electron.*, vol. 41, no. 7, pp. 909–916, Jul. 2005.
- [9] R. J. Lang, K. M. Dzurko, A. Hardy, S. Demars, A. Schoenfelder, and D. F. Welch, "Theory of grating-confined broad-area lasers," *IEEE J. Quantum Electron.*, vol. 34, no. 11, pp. 2197–2210, Nov. 1998.
- [10] K. Paschke, R. Güther, J. Fricke, F. Bugge, G. Erbert, and G. Tränkle, "High power and high spectral brightness in 1060 nm  $\alpha$ -DFB lasers with long resonators," *Electron. Lett.*, vol. 39, no. 4, pp. 369–370, 2003.
- [11] K. Paschke, A. Bogatov, A. E. Drakin, R. Güther, A. A. Strattonnikov, H. Wenzel, G. Erbert, and G. Tränkle, "Modelling and measurements of the radiative characteristics of high-power  $\alpha$ -DFB lasers," *IEEE J. Sel. Topics Quantum Electron.*, vol. 9, no. 3, pp. 835–843, May/Jun. 2003.
- [12] B. Thestrup, M. Chi, B. Sass, and P. M. Petersen, "High brightness laser source based on polarization coupling of two diode lasers with asymmetric feedback," *Appl. Phys. Lett.*, vol. 82, no. 5, pp. 680–682, 2003.
- [13] S. Wolff, A. Rodionov, V. E. Sherstobitov, and H. Fouckhardt, "Fourier-optical transverse mode selection in external-cavity broad-area lasers: Experimental and numerical results," *IEEE J. Quantum Electron.*, vol. 39, no. 3, pp. 448–458, Mar. 2003.
- [14] D. E. Ackley, "Single longitudinal mode operation of high power multiple-stripe injection lasers," *Appl. Phys. Lett.*, vol. 42, no. 2, pp. 152–154, 1983.
- [15] H. Yang, L. J. Mawst, M. Nesnidal, J. Lopez, A. Bhattacharya, and D. Botez, "10 W near-diffraction-limited peak pulsed power from Al-free, 0.98  $\mu\text{m}$ -emitting phase-locked antiguide arrays," *Electron. Lett.*, vol. 33, no. 2, pp. 136–137, 1997.
- [16] L. J. Mawst, D. Botez, T. J. Roth, W. W. Simmons, G. Peterson, M. Jansen, J. Z. Wilcox, and J. J. Yang, "Phase-locked array of antiguided lasers with monolithic spatial filter," *Electron. Lett.*, vol. 25, no. 5, pp. 365–366, 1989.
- [17] J. R. Leger, "Lateral mode control of an AlGaAs laser in a Talbot cavity," *Appl. Phys. Lett.*, vol. 55, no. 4, pp. 334–336, 1989.
- [18] F. Camacho, C. J. Hamilton, K. McIlvaney, A. C. Bryce, and J. H. Marsh, "Laser structure for generating high optical power in a single mode waveguide," *Electron. Lett.*, vol. 34, pp. 460–461, Mar. 1998.
- [19] R. J. Lang, A. G. Larsson, and J. G. Cody, "Lateral modes of broad area semiconductor lasers: Theory and experiment," *IEEE J. Quantum Electron.*, vol. 27, no. 3, pp. 312–320, Mar. 1991.
- [20] Z.-M. Li, K. M. Dzurko, A. Delage, and S. P. McAlister, "A self-consistent two dimensional model of quantum well semiconductor lasers: Optimization of a GRIN-SCH SQW laser structure," *IEEE J. Quantum Electron.*, vol. 28, no. 4, pp. 792–803, Apr. 1992.
- [21] M. Grupen and K. Hess, "Simulation of carrier transport and nonlinearities in quantum well laser diodes," *IEEE J. Quantum Electron.*, vol. 34, no. 1, pp. 120–139, Jan. 1998.
- [22] M. A. Alam, M. S. Hybertsen, R. K. Smith, and G. A. Baraff, "Simulation of semiconductor quantum well lasers," *IEEE Trans. Electron Devices*, vol. 47, no. 10, pp. 1917–1925, Oct. 2000.
- [23] G. P. Agrawal, "Fast-Fourier-transform based beam-propagation model for stripe-geometry semiconductor-lasers-inclusion of axial effects," *J. Appl. Phys.*, vol. 56, pp. 3100–3109, 1984.
- [24] M. Mikulla, P. Chazan, A. Schmitt, S. Morgott, A. Wetzel, M. Walther, R. Kiefer, W. Pletschen, J. Braunstein, and G. Weimann, "High-brightness tapered semiconductor laser oscillators and amplifiers with low-modal gain epilayer structures," *IEEE Photon. Technol. Lett.*, vol. 10, no. 5, pp. 654–656, May 1998.
- [25] K. A. Williams, R. W. Penty, I. H. White, D. J. Robbins, F. J. Wilson, J. J. Lewandowski, and B. K. Nayar, "Design of high-brightness tapered laser arrays," *IEEE J. Sel. Topics Quantum Electron.*, vol. 5, no. 3, pp. 822–831, May/Jun. 1999.
- [26] O. Hess, S. W. Koch, and J. V. Moloney, "Filamentation and beam propagation in broad-area semiconductor lasers," *IEEE J. Quantum Electron.*, vol. 31, no. 1, pp. 35–43, Jan. 1995.
- [27] J. V. Moloney, R. A. Indik, and C. Z. Nong, "Full space time simulation for high brightness semiconductor lasers," *IEEE Photon. Technol. Lett.*, vol. 9, no. 6, pp. 731–733, Jun. 1997.
- [28] B. Witzigmann, A. Witzig, and W. Fichtner, "A multidimensional laser simulator for edge-emitters including quantum carrier capture," *IEEE Trans. Electron Devices*, vol. 47, no. 10, pp. 1926–2000, Oct. 2000.
- [29] U. Bandelow, R. Hünlich, and T. Koprucki, "Simulation of static and dynamic properties of edge-emitting multiple-quantum-well lasers," *IEEE J. Sel. Topics Quantum Electron.*, vol. 9, no. 3, pp. 798–806, May/Jun. 2003.
- [30] S. Sujecki, L. Borrueal, J. Wykes, P. Moreno, B. Sumpf, P. Sewell, H. Wenzel, T. M. Benson, G. Erbert, I. Esquivias, and E. C. Larkins, "Nonlinear properties of tapered laser cavities," *IEEE J. Sel. Topics Quantum Electron.*, vol. 9, no. 3, pp. 823–834, May/Jun. 2003.
- [31] L. Borrueal, S. Sujecki, P. Moreno, J. Wykes, M. Krakowski, B. Sumpf, P. Sewell, S.-C. Auzanneau, H. Wenzel, D. Rodríguez, T. M. Benson, E. C. Larkins, and I. Esquivias, "Quasi-3-D simulation of high-brightness tapered lasers," *IEEE J. Quantum Electron.*, vol. 50, no. 5, pp. 463–472, May 2004.
- [32] P. J. Bream, J. J. Lim, S. Bull, A. V. Andrianov, S. Sujecki, and E. C. Larkins, "The impact of nonequilibrium gain in a spectral laser diode model," *Opt. Quantum Electron.*, vol. 38, pp. 1019–1027, Sep. 2006.
- [33] J. J. Lim, T. M. Benson, and E. C. Larkins, "Design of wide-emitter single-mode laser diodes," *IEEE J. Quantum Electron.*, vol. 41, no. 4, pp. 506–516, Apr. 2005.
- [34] G. R. Hadley, "Multistep method for wide-angle beam propagation," *Opt. Lett.*, vol. 17, pp. 1743–1745, 1992.
- [35] R. Mackenzie, J. J. Lim, S. Bull, S. Sujecki, and E. C. Larkins, "Inclusion of thermal boundary resistance in the simulation of high-power 980 nm ridge waveguide lasers," *Opt. Quantum Electron.*, vol. 40, no. 5/6, pp. 373–377, Apr. 2008.
- [36] R. Mackenzie, J. J. Lim, S. Bull, S. Sujecki, A. J. Kent, and E. C. Larkins, "The impact of hot-phonons on the performance of dilute nitride edge-emitting quantum well lasers," *J. Phys. Conf. Ser.*, vol. 92, no. 012068, pp. 1–4, 2007.
- [37] J. J. Lim, S. Sujecki, and E. C. Larkins, "The influence of surface effects on the simulation of 1.3  $\mu\text{m}$  InGaAsN edge-emitting lasers," presented at the NUSOD, Singapore, Sep. 11–14, 2006, Paper ThPD1.
- [38] R. B. Darling, "Defect-state occupation, Fermi-level pinning, and illumination effects on free semiconductor surfaces," *Phys. Rev. B*, vol. 43, no. 5, pp. 4071–83, 1991.
- [39] I. Vurgaftman, J. R. Meyer, and L. R. Ram-Mohan, "Band parameters for III–V compound semiconductors and their alloys," *J. Appl. Phys.*, vol. 89, no. 11, pp. 5815–5875, 2001.
- [40] J. J. Lim, R. MacKenzie, S. Sujecki, E. C. Larkins, M. Sadeghi, S. M. Wang, Y. Q. Wei, J. S. Gustavsson, A. Larsson, P. Melanen, P. Sipilä, P. Uusimaa, A. A. George, and P. M. Smowton, "Simulation of DQW GaInNAs laser diodes," *IET Optoelectron.*, vol. 1, no. 6, pp. 259–265, 2007.
- [41] K.-H. Hasler, B. Sumpf, P. Adamiec, F. Bugge, J. Fricke, P. Ressel, H. Wenzel, G. Erbert, and G. Tränkle, "5-W DBR tapered lasers emitting at 1060 nm with a narrow spectral linewidth and a nearly diffraction-limited beam quality," *IEEE Photon. Technol. Lett.*, vol. 20, no. 19, pp. 1648–1650, Oct. 2008.
- [42] B. W. Hakki and L. Paoli, "Gain spectra in GaAs double-heterostructure injection lasers," *J. Appl. Phys.*, vol. 46, no. 3, pp. 1299–1306, 1975.
- [43] D. T. Cassidy, "Technique for measurement of the gain spectra of semiconductor diode lasers," *J. Appl. Phys.*, vol. 56, no. 11, pp. 3096–3099, 1984.
- [44] P. Blood, G. M. Lewis, P. M. Smowton, H. Summers, J. Thomson, and J. Lutti, "Characterization of semiconductor laser gain media by the segmented contact method," *IEEE J. Sel. Topics Quantum Electron.*, vol. 9, no. 5, pp. 1275–1282, Sep/Oct. 2003.
- [45] M. Fukuda, *Reliability and Degradation of Semiconductor Lasers and LEDs*. Boston, MA: Artech House, 1991.
- [46] N. C. Gerhardt, M. R. Hofmann, J. Hader, J. V. Moloney, S. W. Koch, and H. Riechert, "Linewidth enhancement factor and optical gain in (GaIn)(NAs)/GaAs lasers," *Appl. Phys. Lett.*, vol. 84, no. 1, pp. 1–3, 2004.
- [47] R. MacKenzie, J. J. Lim, S. Bull, S. Chao, S. Sujecki, M. Sadeghi, S. M. Wang, A. Larsson, P. Melanen, P. Sipilä, P. Uusimaa, and E. C. Larkins, "Measurement of optical gain, effective group index and linewidth enhancement factor in 1.3  $\mu\text{m}$  dilute nitride double-quantum-well lasers," *IET Optoelectron.*, vol. 1, no. 6, pp. 284–288, 2007.
- [48] S. Bull, A. V. Andrianov, J. G. Wykes, J. J. Lim, S. Sujecki, S. C. Auzanneau, M. Calligaro, M. Lecomte, O. Parillaud, M. Krakowski, and E. C. Larkins, "Quantitative imaging of intracavity spontaneous emission distributions using tapered lasers fabricated with windowed n-contacts," *Proc. Inst. Electr. Eng. Optoelectron.*, vol. 153, no. 1, pp. 2–7, Feb. 2006.
- [49] A. E. Siegman and H. Y. Miller, "Unstable optical resonator loss calculations using the Prony method," *Appl. Opt.*, vol. 9, no. 12, pp. 2729–2736, 1970.
- [50] J. M. G. Tijero, H. Odriozola, L. Borrueal, I. Esquivias, S. Sujecki, and E. C. Larkins, "Enhanced brightness of tapered laser diodes based on

1058 an asymmetric epitaxial design," *IEEE Photon. Technol. Lett.*, vol. 19, 1059 no. 20, pp. 1640–1642, Oct. 2007.

1060 [51] A. Al-Muhanna, L. J. Mawst, D. Botez, D. Z. Garbuzov, R. U. Martinelli, 1061 and J. C. Connolly, "High-power (>10 W) continuous-wave operation 1062 from 100  $\mu\text{m}$  aperture 0.97  $\mu\text{m}$  emitting Al-free diode lasers," *Appl. 1063 Phys. Lett.*, vol. 73, no. 9, pp. 1182–1184, 1998.

1064 [52] M. Krakowski, S. C. Auzanneau, F. Berlie, M. Calligaro, Y. Robert, O. Par- 1065 illaud, and M. Lecomte, "1W high brightness index guided tapered laser 1066 at 980 nm using Al-free active region materials," *Electron. Lett.*, vol. 39, 1067 no. 15, pp. 1122–1123, 2003.

1068 [53] B. Thestrup, M. Chi, and P. M. Petersen, "Lateral mode selection in a 1069 broad area laser diode by self-injection locking with a mirror stripe," 1070 *Proc. SPIE*, vol. 5336, pp. 38–44, 2004.

1071 [54] G. Pauliat, N. Dubreuil, and G. Roosen, "Self-organizing laser cavi- 1072 ties," in *Photorefractive Materials and Their Applications 3: Applications 1073* (Springer Series in Optical Science), P. Günter and J.-P. Huignard, Eds. 1074 New York: Springer-Verlag, 2007, pp. 253–275.

1075 [55] Z. Zhang, G. Pauliat, J. J. Lim, P. J. Bream, N. Dubreuil, A. J. Kent, 1076 E. C. Larkins, and S. Sujecki, "Numerical modeling of high-power self- 1077 organizing external cavity lasers," *Opt. Quantum Electron.*, to be pub- 1078 lished.

1079 [56] G. L. Bourdet, I. Hassiaoui, R. McBride, J. F. Monjardin, H. Baker, 1080 N. Michel, and M. Krakowski, "High-power, low-divergence, linear ar- 1081 ray of quasi-diffraction-limited beams supplied by tapered diodes," *Appl. 1082 Opt.*, vol. 46, no. 25, pp. 6297–6301, 2007.

1083 [57] D. Paboeuf, G. Lucas-Leclin, P. Georges, N. Michel, M. Krakowski, 1084 J. J. Lim, S. Sujecki, and E. C. Larkins, "Narrow-line coherently-combined 1085 tapered laser diodes in a Talbot external cavity with a volume Bragg grat- 1086 ing," *Appl. Phys. Lett.*, vol. 93, pp. 211102-1–211102-3, 2008.



1087  
1088  
1089  
1090  
1091  
1092  
1093  
1094  
1095  
1096  
1097  
1098

**Jun Jun Lim** (S'01–M'04) was born in Batu Pahat, Malaysia, in 1978. He received the B.Eng. degree (with first-class honors) in electronic engineering and the Ph.D. degree from the University of Nottingham, Nottingham, U.K., in 1999 and 2003, respectively.

Since 2004, he has been a Research Fellow at the University of Nottingham, where he was involved in several projects on the modeling of high-speed and high-brightness laser diodes. His current research interests include the simulation, analysis, and design of optoelectronic devices.

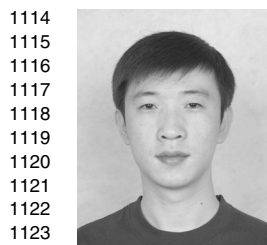


1100  
1101  
1102  
1103  
1104  
1105  
1106  
1107  
1108  
1109  
1110  
1111  
1112  
1113

**Slawomir Sujecki** was born in Grojec, Poland, in 1969. He received the M.Sc. and Ph.D. degrees in electronic engineering from Warsaw University of Technology, Warsaw, Poland, in 1993 and 1997, respectively.

During 1994–1995, he was a Deutscher Akademischer Austauschdienst Fellow with the Technische Universität Berlin. During 1996–1998, he was a British Council Fellow and then a Royal Society/Wolfson Foundation Fellow at the University of Nottingham, Nottingham, U.K., where he joined the

Department of Electrical and Electronic Engineering in April 2001. He started lecturing at Kielce University of Technology, Poland, in 1998. He joined the National Institute of Telecommunications, Poland, in 1999.



1114  
1115  
1116  
1117  
1118  
1119  
1120  
1121  
1122  
1123

**Lei Lang** (S'07) was born in Shijiazhuang, China, in 1981. He received the B.Eng. degree in electronic information engineering from Hebei University of Technology, Tianjin, China, in 2004, and the M.Sc. degree in electronic communications and computer engineering in 2005 from the University of Nottingham, Nottingham, U.K., where he is currently working toward the Ph.D. degree in electrical and electronic engineering.



**Zhichao Zhang** (S'01–M'05) received the B.Eng. 1124 and M.Sc. degrees in electrical and electronic engi- 1125 neering from Shandong University, Jinan, China, in 1126 1987 and 1990, respectively. He is currently working 1127 toward the Ph.D. degree in electrical and electronic 1128 engineering at the University of Nottingham, Not- 1129 tingham, U.K. 1130 1131

**David Paboeuf** was born in Nantes, France, in 1984. He received the Engi- 1132 neering degree from the Ecole Supérieure d'Optique, Orsay, France, and the 1133 Master's degree in optics and photonics from the University Paris Sud, Orsay, 1134 France, in 2006. He is currently working toward the Ph.D. at the Laboratoire 1135 Charles Fabry de l'Institut d'Optique, Palaiseau, France, on the development of 1136 external cavities for brightness improvement of laser diodes. 1137 1138



**Gilles Pauliat** received the Ph.D. degree from the 1139 University Paris Sud, Orsay, France, in 1986. 1140

He was a Postdoctoral Researcher in the Quantum 1141 Electronic Laboratory, Federal Polytechnic School, 1142 Zurich, for one year. He joined the Centre National de 1143 la Recherche Scientifique, Palaiseau, France, where 1144 he is currently the Head of the Matériaux non 1145 Linéaires et Applications Research Group, Labora- 1146 toire Charles Fabry de l'Institut d'Optique. His cur- 1147 rent research interests include high-density data stor- 1148 age with holographic memories and self-organizing 1149 laser cavities. 1150

Dr. Pauliat is a member of the Board of Directors of the European Optical Society. 1151 1152 1153

**Gaëlle Lucas-Leclin** was born in Guérande, France. She received the M.S. 1154 degree in optics from the Ecole Supérieure d'Optique, Orsay, France, in 1994, 1155 and the Ph.D. degree from the University Paris XI, Orsay, in 1998. 1156

Since 1998, she has been an Assistant Professor at the Institut d'Optique 1157 Graduate School, Centre National de la Recherche Scientifique (CNRS), Uni- 1158 versity Paris Sud, Palaiseau, France, where she is with the Laboratoire Charles 1159 Fabry de l'Institut d'Optique, and is in charge of the semiconductor physics and 1160 semiconductor sources lectures. Her current research interests include extended 1161 cavity laser diodes and vertical external cavity semiconductor lasers. 1162 1163



**Patrick Georges** was born in Metz, France, in 1962. 1164 He received the Engineering degree from the Ecole 1165 Supérieure d'Optique, Orsay, France, in 1985, and 1166 the Ph.D. degree in 1989 on colliding pulses mode 1167 locked dye lasers at different wavelengths and pulse 1168 compression. 1169

He is currently a Senior Scientist at the Cen- 1170 tre National de la Recherche Scientifique (CNRS), 1171 Palaiseau, France, where he is with the Institut 1172 d'Optique, and leads the Lasers and Biophoton- 1173 ics Group, Laboratoire Charles Fabry de l'Institut 1174

1175 d'Optique. His current research interests include diode-pumped solid-state  
1176 lasers, new laser materials, picosecond and femtosecond lasers, high-brightness  
1177 laser diodes, fiber amplifier systems, and applications of picosecond or fem-  
1178 tosecond lasers in biophotonics (time-resolved fluorescence spectroscopy, two-  
1179 photon microscopy).

1180 Dr. Georges is a Fellow of the Optical Society of America.  
1181

1182 **Roderick C. I. MacKenzie** received the M.Eng. and Ph.D. degrees in electronic  
1183 engineering from the University of Nottingham, Nottingham, U.K., in 2004 and  
1184 2008, respectively.

1185 He was engaged in the measurement and simulation of 1.3- $\mu\text{m}$  dilute ni-  
1186 tride laser diodes, focusing specifically on self-heating and its impact on de-  
1187 vice performance. He is currently with the University of Nottingham. His cur-  
1188 rent research interests include measurement of device gain and thermographic  
1189 imagery.  
1190

1191 **Philip Bream** received the M.Eng. degree (with first-class honors) in electronic  
1192 engineering and the Ph.D. degree from the University of Nottingham, Notting-  
1193 ham, U.K., in 2002 and 2006, respectively.

1194 He was engaged in research on nonequilibrium carrier dynamics and gain  
1195 in semiconductor quantum wells (QWs). He is currently with the University of  
1196 Nottingham.  
1197



1198 **Stephen Bull** (S'01–M'04) received the M.Eng. de-  
1199 gree (with first-class honors) in electronic engineer-  
1200 ing with German and the Ph.D. degree from the Uni-  
1201 versity of Nottingham, Nottingham, U.K., in 2001  
1202 and 2004, respectively.

1203 He is currently a Postdoctoral Research Fellow at  
1204 the University of Nottingham. His current research  
1205 interests include spectroscopic imaging techniques  
1206 for the characterization of laser diodes, including ex-  
1207 ternal cavity lasers, the validation of simulation tools  
1208 using these techniques, and the degradation dynam-  
1209 ics of high-power laser bars.  
1210



1211 **Karl-Heinz Hasler** was born in Ludwigslust, Ger-  
1212 many, in 1952. He received the Dipl.-Phys. degree  
1213 from Humboldt University, Berlin, Germany, in 1978.

1214 From 1978 to 1991, he was with the semicon-  
1215 ductor industry, where he was involved in the de-  
1216 velopment of LEDs, near-infrared response (NIR)  
1217 detectors, and laser diodes. From 1992 to 2000, he  
1218 was with the Astrophysikalisches Institut Potsdam  
1219 (AIP), where he was involved in the field of magne-  
1220 tohydrodynamics and helioseismology. Since 2000,  
1221 he has been with the Ferdinand-Braun-Institut für  
1222 Höchstfrequenztechnik, Berlin, where he is engaged in the development of  
1223 high-power, high-brightness semiconductor lasers.  
1224



1225 **Bernd Sumpf** was born in Berlin, Germany, in 1958. 1225  
1226 He received the Diploma in physics and the Ph.D. 1226  
1227 degree from Humboldt-Universität Berlin, Berlin, in 1227  
1228 1981 and 1987, respectively. 1228

1229 He was engaged in research on lead salt diode 1229  
1230 lasers for spectroscopic applications. From 1993 till 1230  
1231 1997, he was with the Technische Universität Berlin, 1231  
1232 where he was engaged in research on high-resolution 1232  
1233 spectroscopy and difference-frequency generation. In 1233  
1234 1997, he received the postdoctoral lecture qualifica- 1234  
1235 tion. Since 2000, he has been with the Ferdinand- 1235  
1236 Braun-Institut für Höchstfrequenztechnik, Berlin, where he is involved in the 1236  
1237 field of high-power and high-brightness diode lasers. 1237  
1238

1239 **Hans Wenzel** received the Diploma and Doctoral degrees in physics from 1239  
1240 Humboldt University, Berlin, Germany, in 1986 and 1991, respectively. 1240

1241 He was engaged in research on electrooptical modeling of semiconductor 1241  
1242 lasers. From 1991 to 1994, he was involved in a research project on the 3- 1242  
1243 D simulation of DFB lasers. In 1994, he joined the Ferdinand-Braun-Institut 1243  
1244 für Höchstfrequenztechnik, Berlin, where he is engaged in the development of 1244  
1245 high-brightness semiconductor lasers. His current research interests include the 1245  
1246 analysis, modeling, and simulation of optoelectronic devices. 1246  
1247



1248 **Götz Erbert** (M'95) received the Diploma in physics 1248  
1249 from Humboldt University, Berlin, Germany, in 1973, 1249  
1250 and the Doctoral degree in physics from the Academy 1250  
1251 of Sciences of the German Democratic Republic 1251  
1252 (GDR), in 1990. 1252

1253 From 1973 to 1991, he was with the Academy of 1253  
1254 Sciences, where he was first engaged in the field of 1254  
1255 integrated optics and dynamic holographic gratings 1255  
1256 in semiconductors, and later in semiconductor lasers. 1256  
1257 In 1992, he joined the Ferdinand-Braun-Institut für 1257  
1258 Höchstfrequenztechnik, Berlin, where he has been 1258  
1259 engaged in the optoelectronic activities since 1996. He is also involved in re- 1259  
1260 search on high-power semiconductor lasers based on GaAs using strained-layer 1260  
1261 quantum-well active regions in the wavelength range from 650 to 1200 nm. 1261  
1262

1263 **Birgitte Thestrup** received the Ph.D. degree in physics from the University of 1263  
1264 Copenhagen, Copenhagen, Denmark, in 1999. 1264

1265 She is currently a Senior Scientist in the Department of Photonics Engineer- 1265  
1266 ing, Technical University of Denmark, Roskilde, Denmark. From 2001 to 2007, 1266  
1267 she was with the Diode Laser Group, Optics and Plasma Research Department, 1267  
1268 Risoe National Laboratory, Denmark, where she also worked on laser-induced 1268  
1269 plasmas. She is the author or coauthor of more than 30 papers and one book. 1269  
1270 She holds two patents. Her current research interests include external cavity 1270  
1271 diode laser systems for industrial and medical applications, and high-quality 1271  
1272 and energy-efficient solid-state lighting systems for specific applications. 1272  
1273

1274 **Paul Michael Petersen** received the M.Sc. degree in engineering and the Ph.D. 1274  
1275 degree in physics from the Technical University of Denmark (DTU), Roskilde, 1275  
1276 Denmark, in 1983 and 1986, respectively. 1276

1277 He has 15 years of research experience in laser physics, nonlinear optics, and 1277  
1278 optical measurement techniques, and has headed several collaborative research 1278  
1279 projects within laser physics. He is currently the Head of light sources and 1279  
1280 industrial sensors in the Department of Photonics Engineering, DTU. He is also 1280  
1281 an Adjunct Professor of optics at Niels Bohr Institute, Copenhagen University, 1281  
1282 Copenhagen, Denmark. He is the Head of the Center for Biomedical Optics and 1282  
1283 New Laser Systems. He has authored or coauthored more than 100 scientific 1283  
1284 publications and nine patents. He has 20 years of teaching experience in optics, 1284  
1285 quantum optics, laser technique, and nonlinear optics. 1285  
1286

1287 **Nicolas Michel**, photograph and biography not available at the time of  
1288 publication.  
1289

1290 **Michel Krakowski**, photograph and biography not available at the time of  
1291 publication.  
1292



**Eric C. Larkins** received the B.S.E.E. degree from 1293  
Cornell University, Ithaca, NY, in 1980, and the 1294  
M.S.E.E. degree and the Ph.D. degree in electrical 1295  
engineering from Stanford University, Stanford, CA, 1296  
in 1985 and 1991, respectively. 1297

In 1994, joined the Department of Electrical and 1298  
Electronic Engineering, University of Nottingham, 1299  
Nottingham, U.K., where he became a Professor of 1300  
optoelectronics in 2002. From 1991 to 1994, he was a 1301  
Visiting Scientist at the Fraunhofer Institut für Ange- 1302  
wandte Festkörperphysik, Freiburg, Germany. His 1303

current research interests include laser diodes, and functional and nanopho- 1304  
tonic devices. 1305  
1306

## QUERIES

- 1308 Q1: Author: Please provide the IEEE membership details (membership grades and years in which these were obtained), if any,  
1309 for all the authors except J. J. Lim, L. Lang, Z. Zhang, S. Bull, and G. Erbert.
- 1310 Q2: Author: Please check the funding information in the first footnote. Is it Ok as edited?
- 1311 Q3: Author: A table has been referred to in this sentence, whereas the same is not provided. Please check.
- 1312 Q4: Author: Is the edit OK?
- 1313 Q5: Author: Please check Ref. [54] if it is OK as typeset.
- 1314 Q6: Author: Please update Ref. [55] if possible.
- 1315 Q7: Author: Please check the IEEE membership details of Z. Zhang for correctness.
- 1316 Q8: Author: Please check the affiliations of G. Lucas-Leclin and P. Georges in their biographies. Are they OK as typeset?
- 1317 Q9: Author: Please provide the university name from where P. Georges received the Ph.D. degree.
- 1318 Q10: Author: Please specify what does “with German” indicate in the biography of S. Bull.
- 1319 Q11: Author: Please specify if the postdoctoral lecture qualification refers to an academic degree received by B. Sumpf.
- 1320 Q12: Author: Please provide the location (city and country names) of the Academy of Sciences of the German Democratic  
1321 Republic (GDR).
- 1322 Q13: Author: Please specify if the Center for Biomedical Optics and New Laser Systems is a subdivision of Copenhagen  
1323 University.